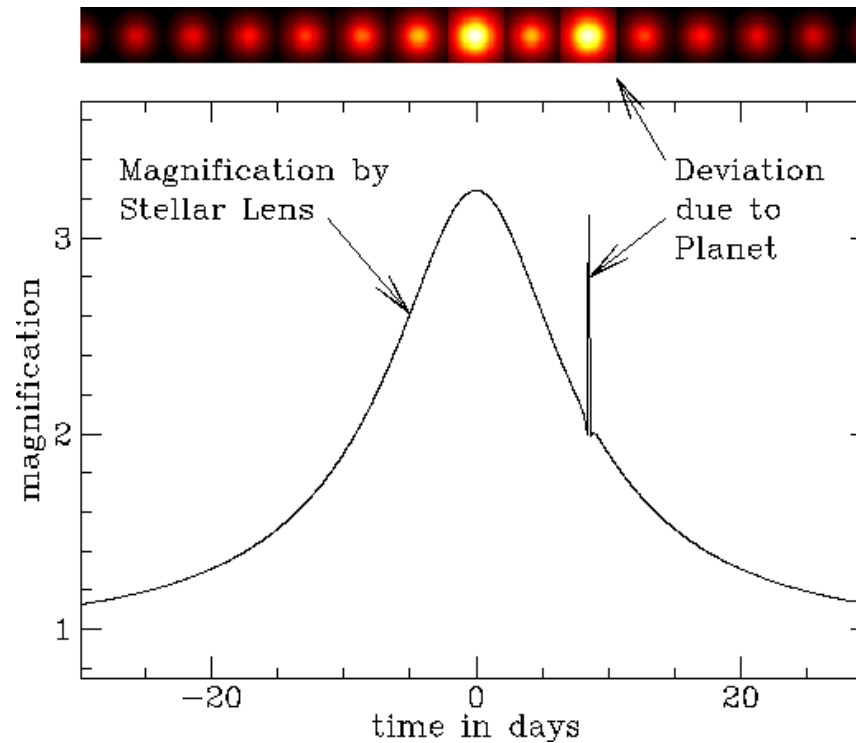


# Higher Order Microlensing Effects I & II

David Bennett  
University of Notre Dame



# Talk Outline

- Parallax
  - Importance – mass measurements
  - Types – orbital, terrestrial, and satellite
  - degeneracies
  - Xallarap vs. orbital parallax
  - Geocentric vs. Heliocentric
  - Binary and planetary events can have larger parallax signals
- Orbital motion
  - parameterization:  $v_x$ ,  $v_y$ ,  $T$
  - Kepler constraints – minimum velocities
  - Motion of caustics limits the constraints on parallax

# Talk Outline (2)

- Promise and Curse of High Magnification
  - Sensitive to planets in a wide range of positions
  - Also distant or close stellar binaries
  - Implies multiplanet sensitivity
  - But signals can overlap
- Additional lens mass
  - 3+ mass lens equation
  - Likely in high-mag events
  - Consider both additional star or planet
  - High mag events – 3<sup>rd</sup> mass may be more than just a small perturbation
  - Extremely high-mag events – additional mass at different distance
    - 2 + 1 lens mass equation not solved

# Talk Outline (3)

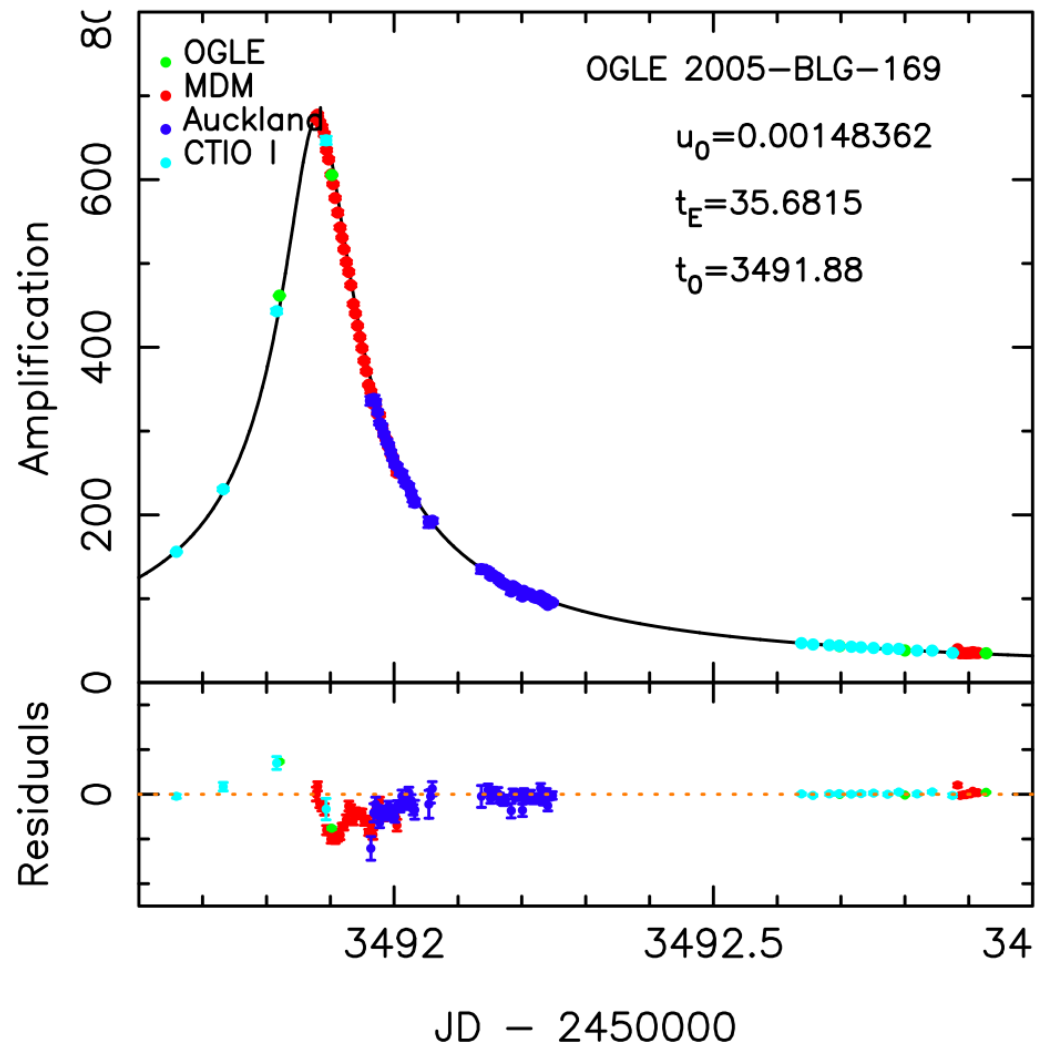
- Additional Source
- Modeling strategy
- Calculation of light curves
  - Various techniques: points source, ray-shooting, contour
  - Optimal method point source + ray shooting
    - 2nd order method for limb darkened source
- Examples
  - OGLE-2006-BLG-109
  - MOA-266
  - OGLE-07-349
  - MOA-10-117
  - OGLE-08-270

# Modeling & Photometry Interact

- Identification of planetary candidates requires good photometry
- Modeling helps to identify photometry issues
- Improved photometry often needed for a convincing discovery
- higher order effects are often subtle and sensitive to systematic photometry errors
- History of the OGLE-2005-BLG-169 event

# OGLE-2005-BLG-169Lb Identification

- 1 July, 2005 Bond produces DIA photometry for  $\mu$ FUN data and reports signal in MDM data, and that Rattenbury suspects  $q \sim 10^{-5}$  models
- Andy Gould and I were initially skeptical about this event
- Nich Rattenbury and Ian Bond are more optimistic and convince me to look at the event again



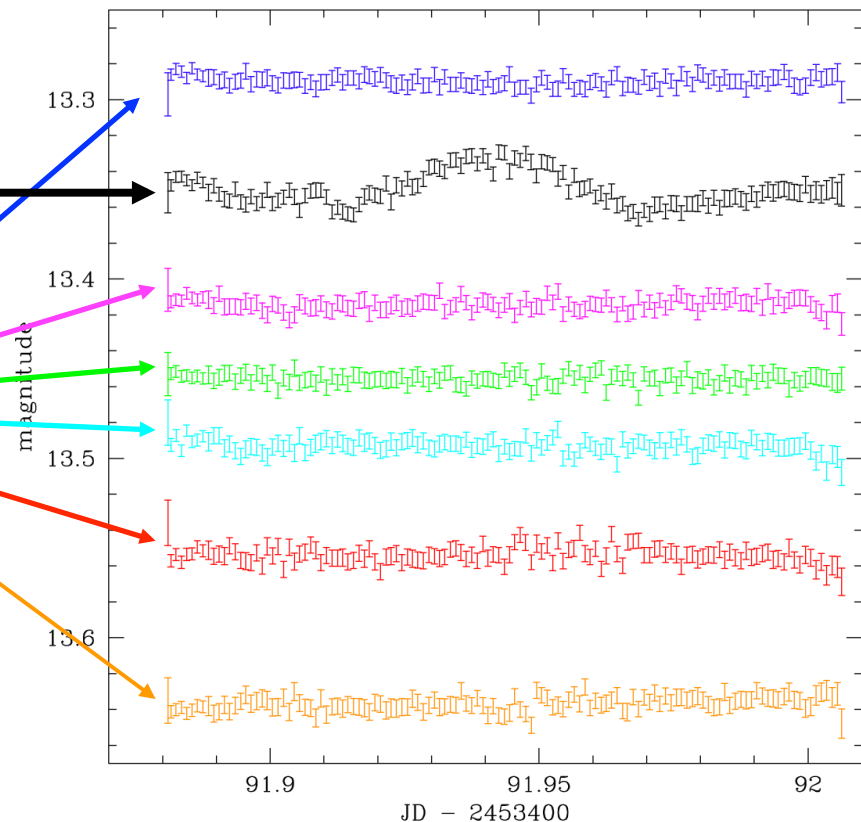
# OGLE-2005-BLG-169Lb Early Modeling

- Nov., 2005, DPB runs analysis again and finds that point-source  $q \sim 10^{-5}$  models are preferred over point-source stellar binaries, as Ian and Nick had previously indicated
- The signal was almost entirely due to MDM data and had a very low amplitude of only a few per cent
- Careful tests of the photometric precision were requested

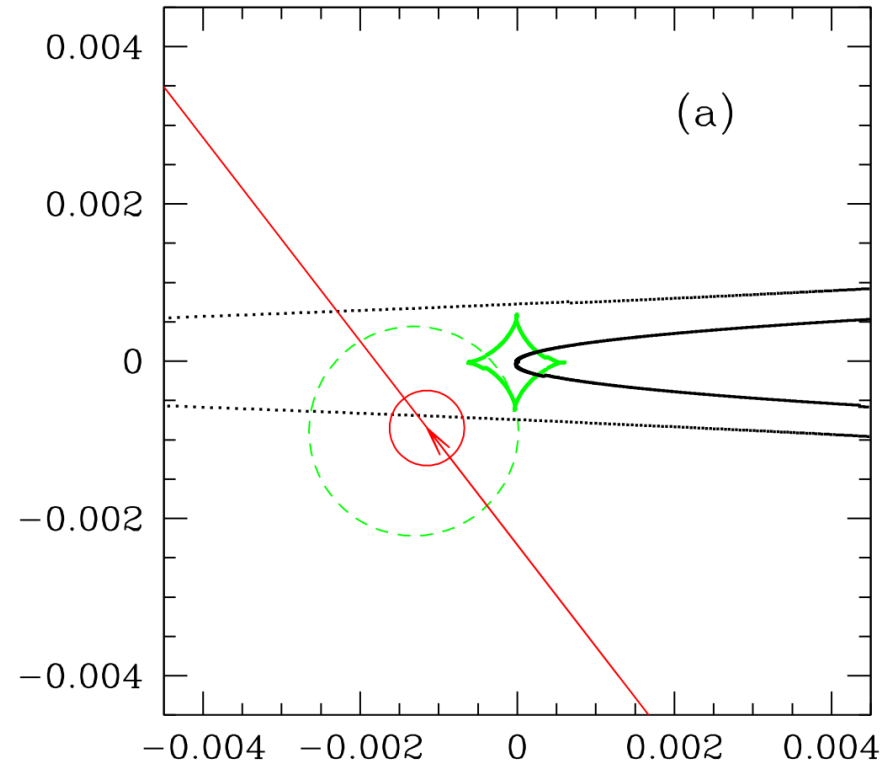
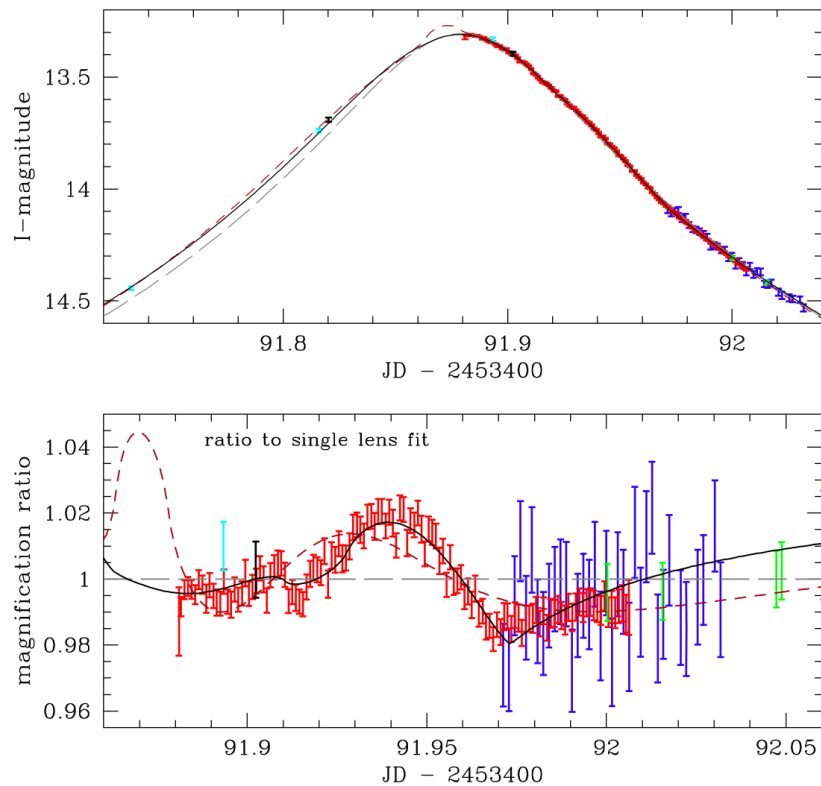
Deviation of OGLE-05-169 from  
standard single-lens model

Constant stars of similar  
brightness

Photometry was reprocessed with  
the OGLE pipeline and passed  
many photometry tests.

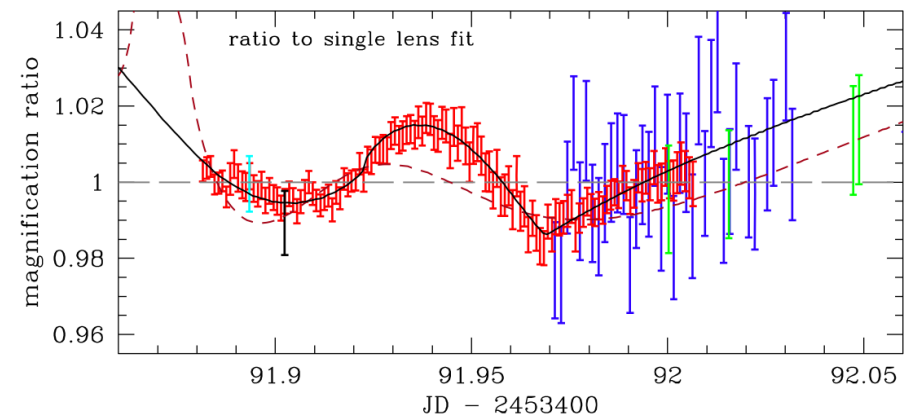
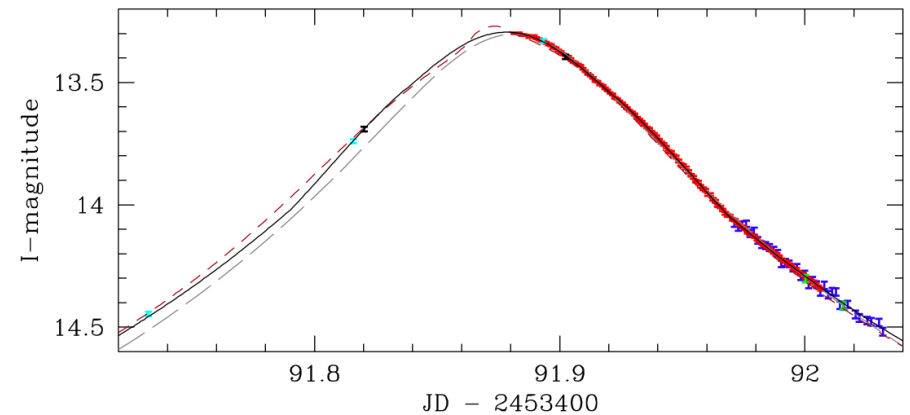
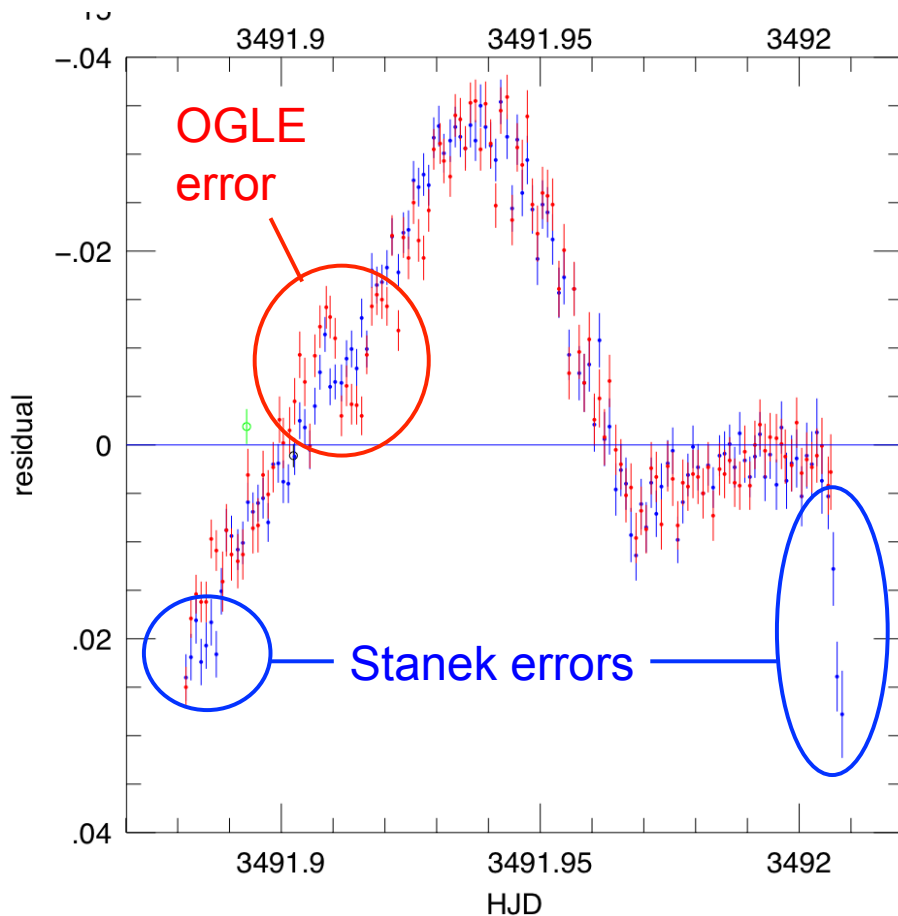


# OGLE-2005-BLG-169 Photometry Tests



Low-mass planet of  $q \sim 2 \times 10^{-5}$  ( $\sim 3$  Earth-masses) appears to be required, but the features in the MDM data are not exactly matched by the model. In particular, the sharp feature at  $t = 91.91$  can be only partially accounted for by a very weak caustic entry. [Note: caustic crossing can give very weak signals!]

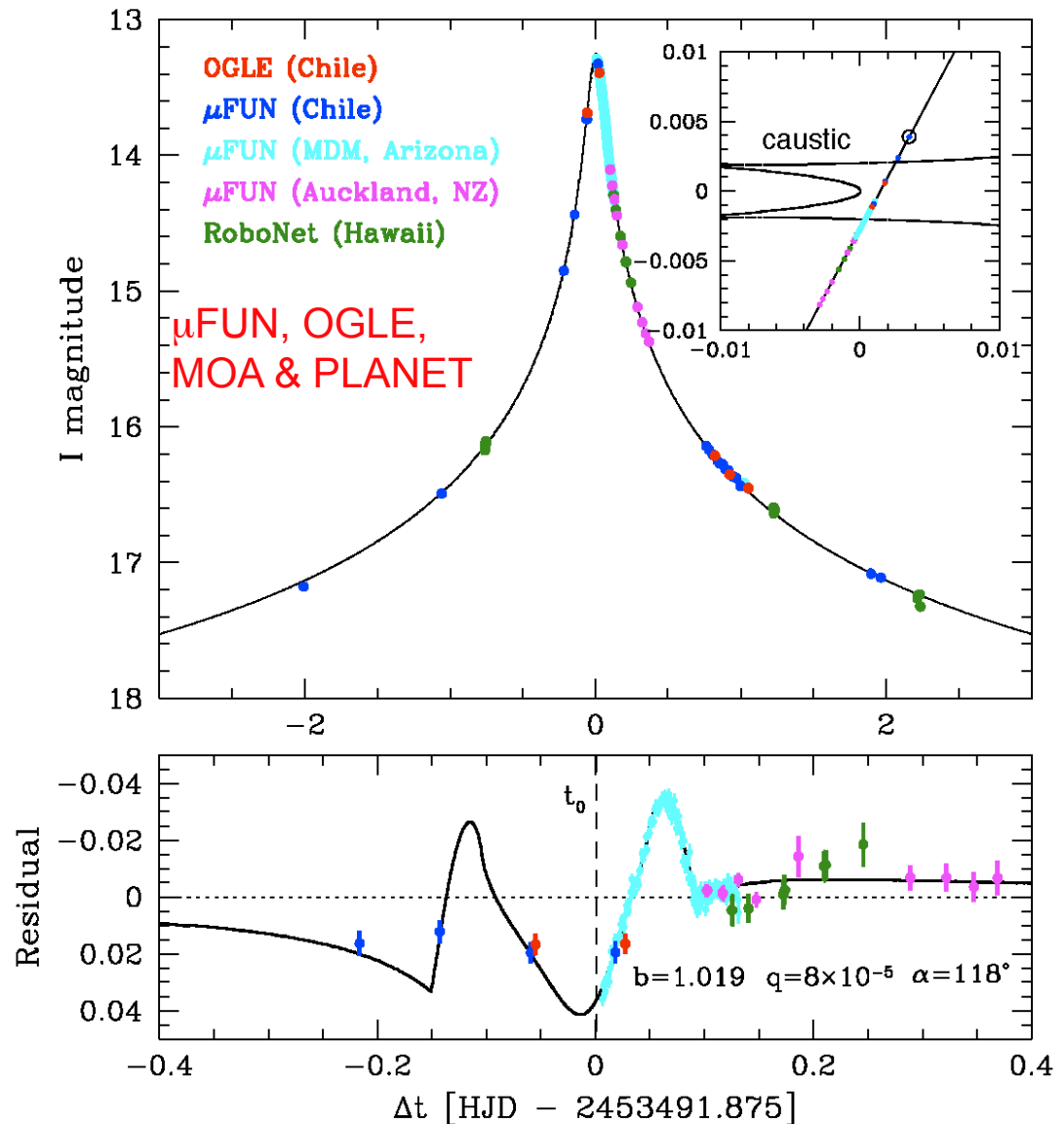
# OGLE-2005-BLG-169Lb: Oops!



Comparison of OGLE Pipeline photometry to Staneck DIA photometry revealed systematic photometry errors in both. The feature at  $t = 91.91$  disappeared from the OGLE Pipeline photometry when the fit radius was increased, so this was an error related to seeing, but other images with worse seeing did not show such problems. The best fit mass ratio becomes  $q \sim 8 \times 10^{-5}$  ( $\sim 13$  Earth-masses).

# OGLE-2005-BLG-169Lb

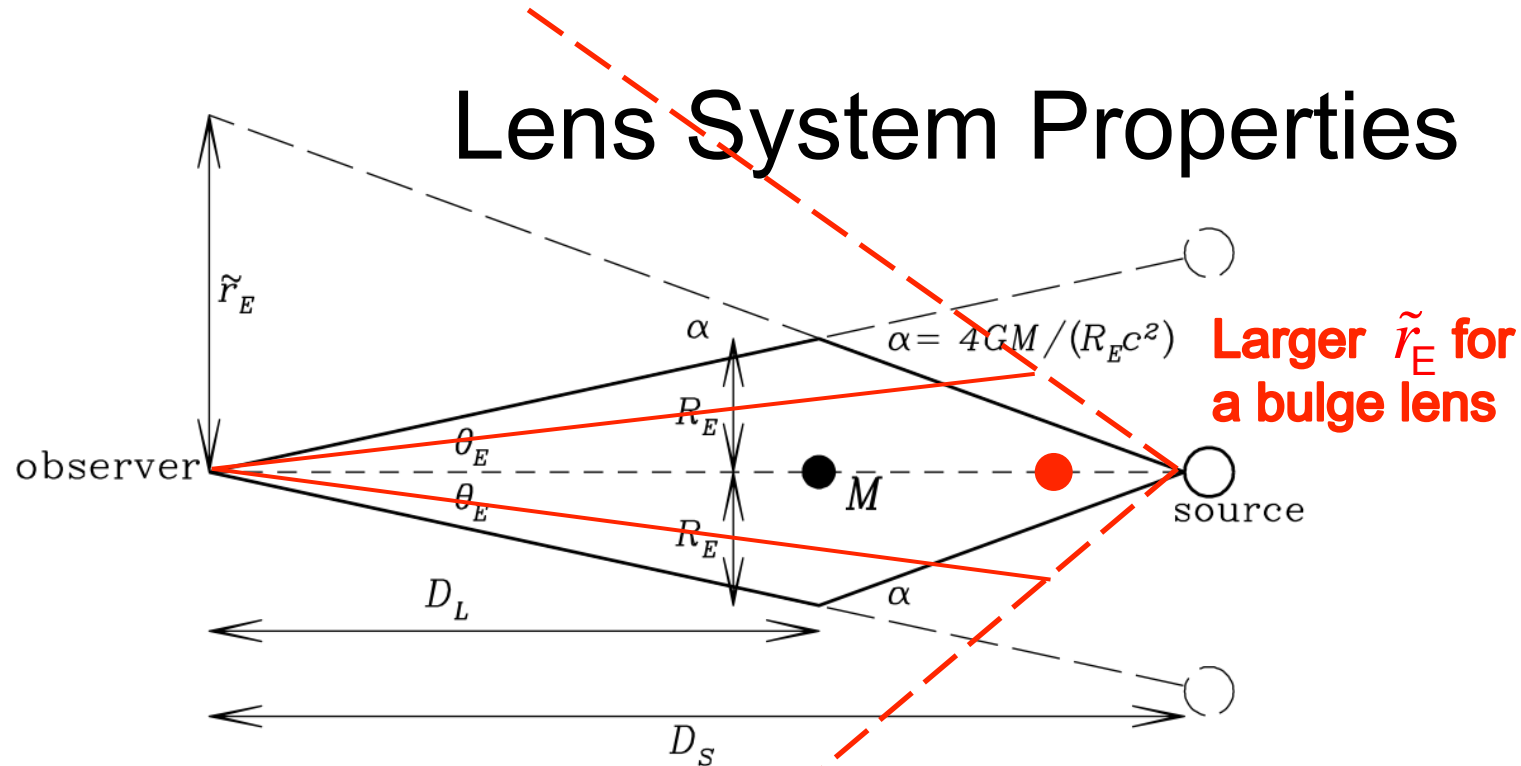
- Detection of a  $\sim 13 M_{\oplus}$  planet in a high magnification microlensing event
- Caustic crossing signal is obvious when light curve is divided by a single lens curve.
- Detection efficiency for  $\sim 10 M_{\oplus}$  planets is  $\ll$  than for Jupiter-mass planets
  - 2/4 microlensing planets are super-Earths ( $\sim 10 M_{\oplus}$ )
  - Super-Earths are much more common than Jupiters at 1-5 AU
  - $\sim 37\%$  of stars have super-Earths at 1.5-4.5 AU ( $> 16\%$  at 90% confidence)



# Lens System Properties

- For a single lens event, 3 parameters (lens mass, distance, and velocity) are constrained by the Einstein radius crossing time,  $t_E$
- There are two ways to improve upon this with light curve data:
  - Determine the angular Einstein radius :  $\theta_E = \theta_* t_E / t_* = t_E \mu_{\text{rel}}$  where  $\theta_*$  is the angular radius of the star and  $\mu_{\text{rel}}$  is the relative lens-source proper motion
  - Measure the projected Einstein radius,  $\tilde{r}_E$ , with the microlensing parallax effect (due to Earth's orbital motion).

# Lens System Properties



- Einstein radius :  $\theta_E = \theta_* t_E / t_*$  and projected Einstein radius,  $\tilde{r}_E$ 
  - $\theta_*$  = the angular radius of the star
  - $\tilde{r}_E$  from the microlensing parallax effect (due to Earth's orbital motion).

$$R_E = \theta_E D_L, \text{ so } \alpha = \frac{\tilde{r}_E}{D_L} = \frac{4GM}{c^2 \theta_E D_L}. \text{ Hence } M = \frac{c^2}{4G} \theta_E \tilde{r}_E$$

# Finite Source Effects & Microlensing Parallax Yield Lens System Mass

- If only  $\theta_E$  or  $\tilde{r}_E$  is measured, then we have a mass-distance relation.
- Such a relation can be solved if we detect the lens star and use a mass-luminosity relation
  - This requires HST or ground-based adaptive optics
- With  $\theta_E$ ,  $\tilde{r}_E$ , and lens star brightness, we have more constraints than parameters

mass-distance relations:

$$M_L = \frac{c^2}{4G} \theta_E^2 \frac{D_S D_L}{D_S - D_L}$$

$$M_L = \frac{c^2}{4G} \tilde{r}_E^2 \frac{D_S - D_L}{D_S D_L}$$

$$M_L = \frac{c^2}{4G} \tilde{r}_E \theta_E$$

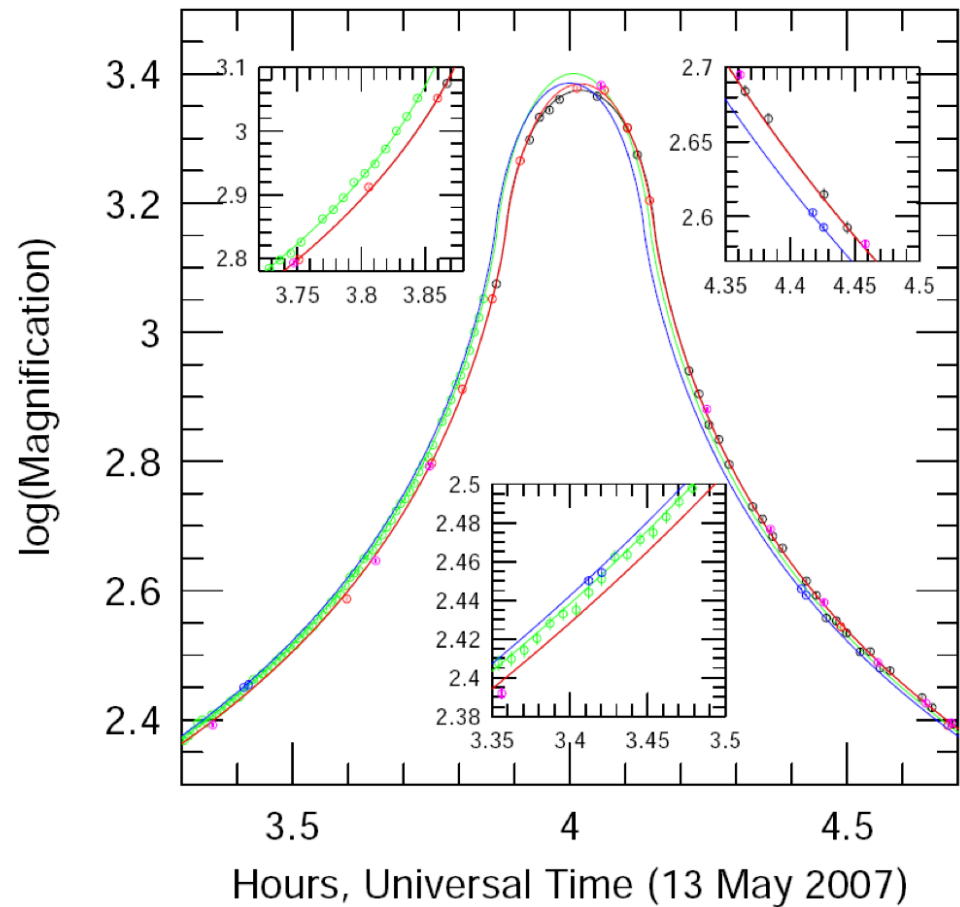
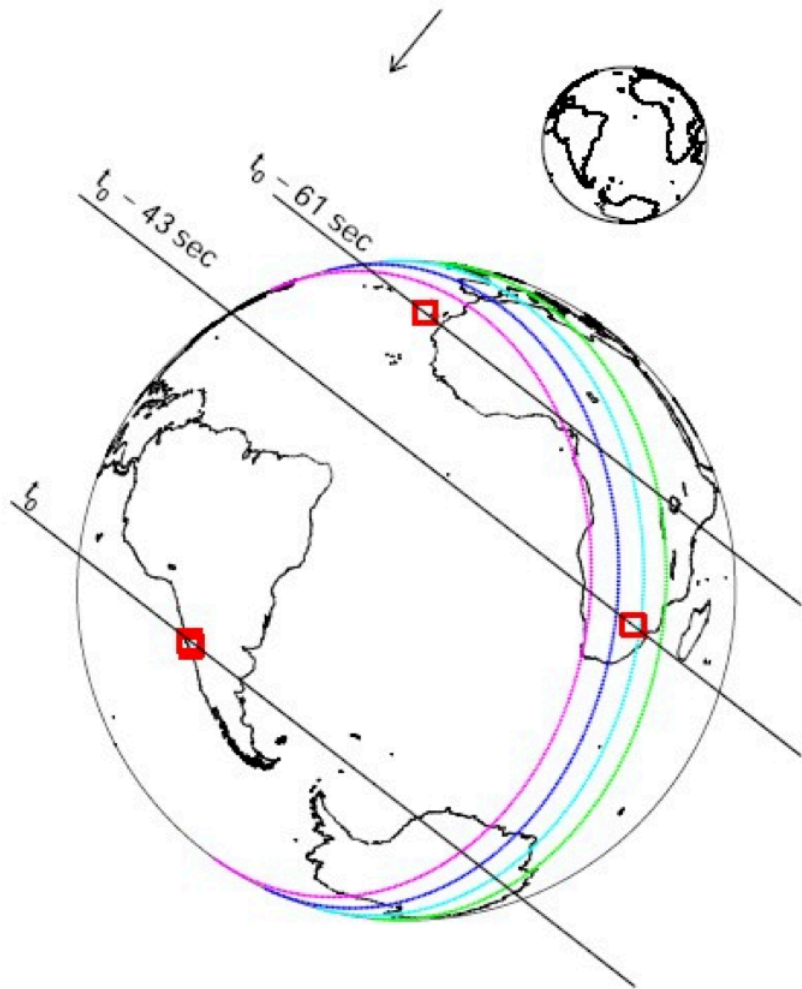
# 3 Ways to Measure Microlensing Parallax

- Terrestrial - from different locations on the Earth
  - Requires very high magnification - rapid change in brightness
  - Measured for OGLE-2007-BLG-224 - disk brown dwarf
- Orbital motion of the Earth
  - Requires a long Einstein radius crossing time,  $t_E \geq 100$  days
  - Measurable for some lenses in the Galactic disk, but not in the Galactic bulge
- From a Satellite far from Earth
  - Solar System missions provide “opportunities”
    - Cassini (late 1990’s)
    - Deep Impact 2004 (proposal)
  - OGLE-2005-SMC-1 measured by Spitzer
  - MOA-2009-BLG-266 - first planetary microlensing event with extra-terrestrial observations - by EPOXI (formerly Deep Impact) in Oct., 2009.

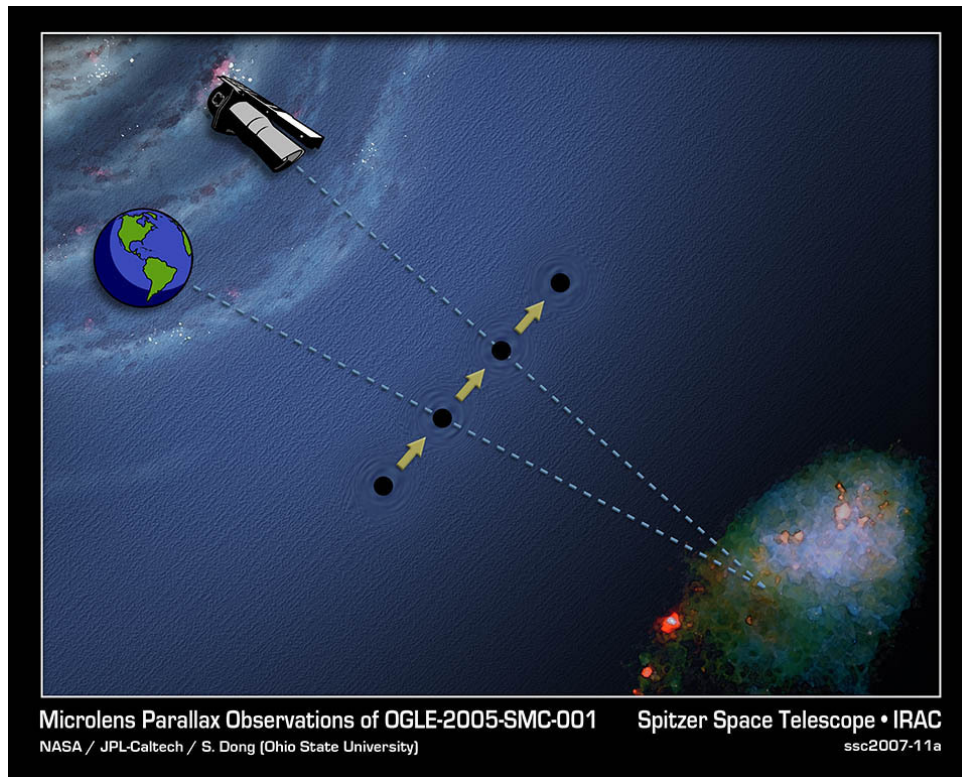
# Terrestrial Microlensing Parallax

OGLE-2007-BLG-224

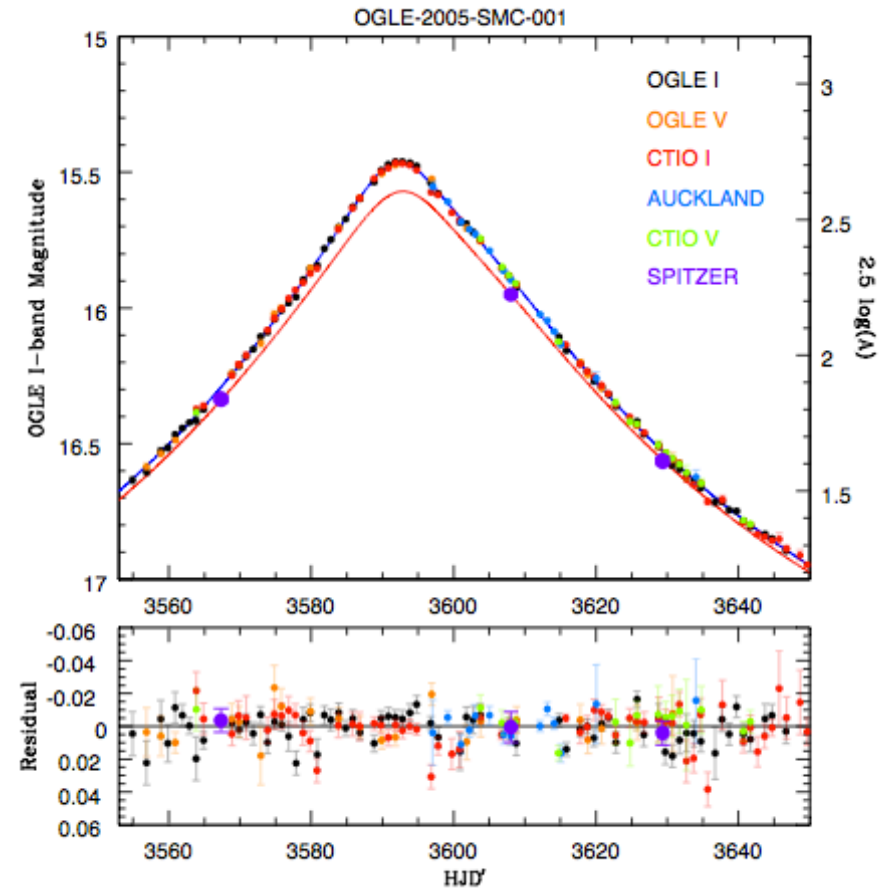
Canaries South Africa Chile



# Space-Based Microlensing Parallax



Dong, S., et al., 2007, ApJ, 664, 862

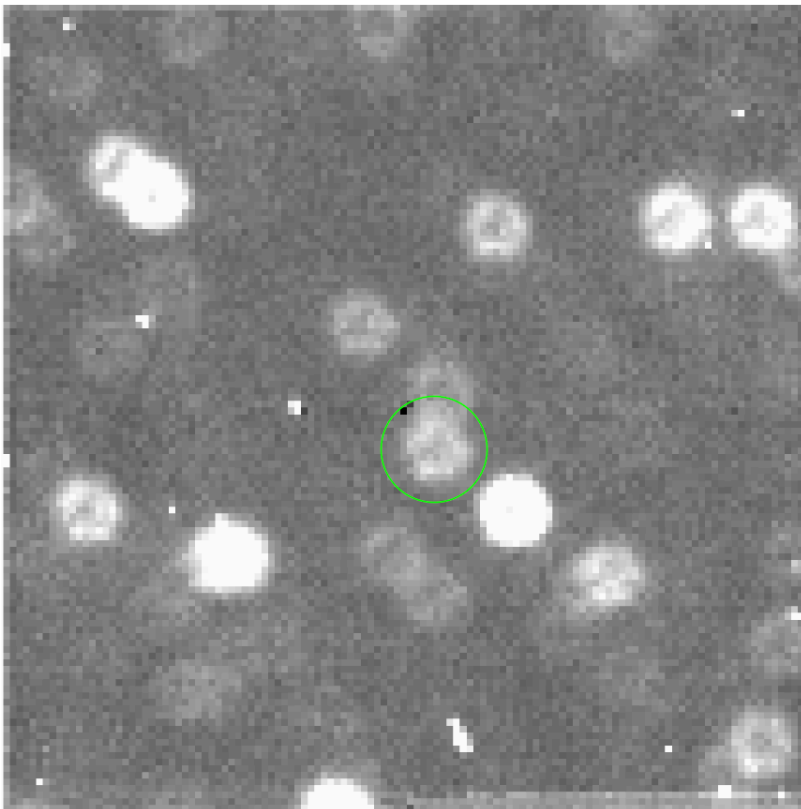
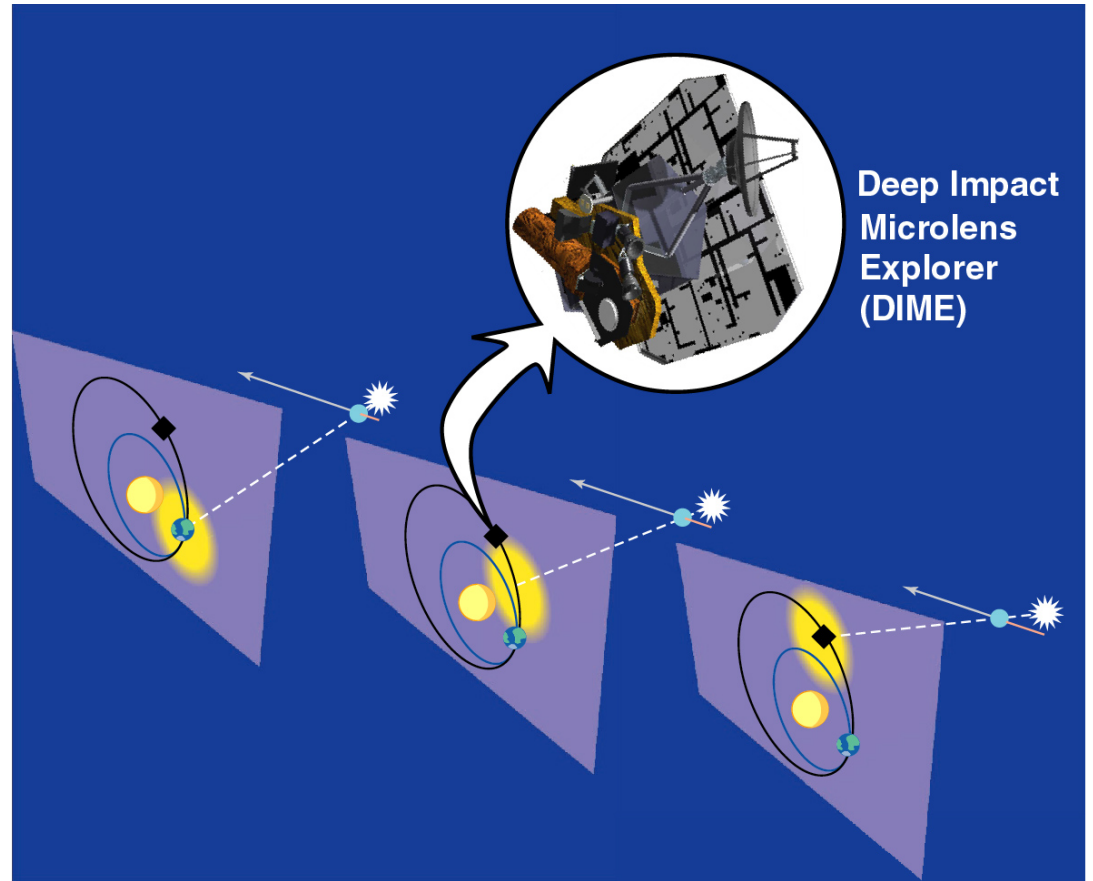


Space-based parallax from Spitzer in Earth-trailing orbit

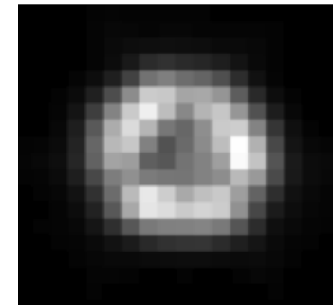
# Space-Based Microlensing Parallax

Deep Impact - now EPOXI is in a position to measure this effect.

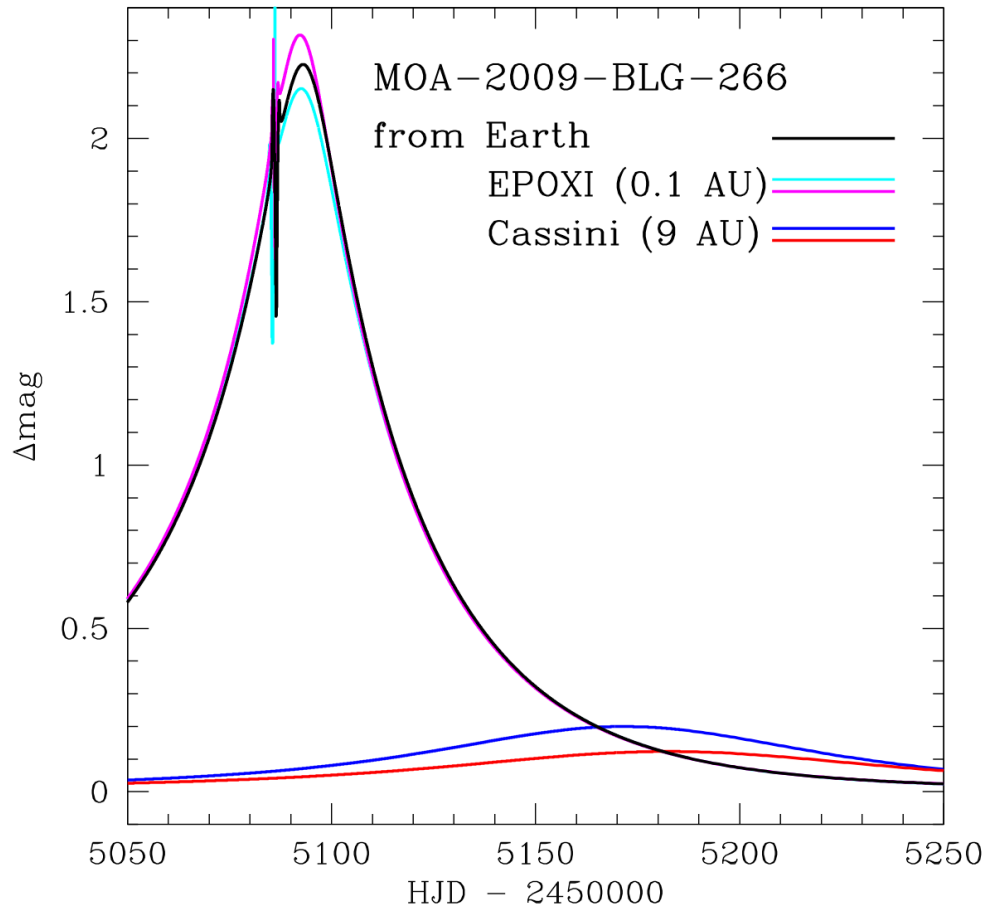
2009: Geometric exoplanet and host star mass measurements with DI



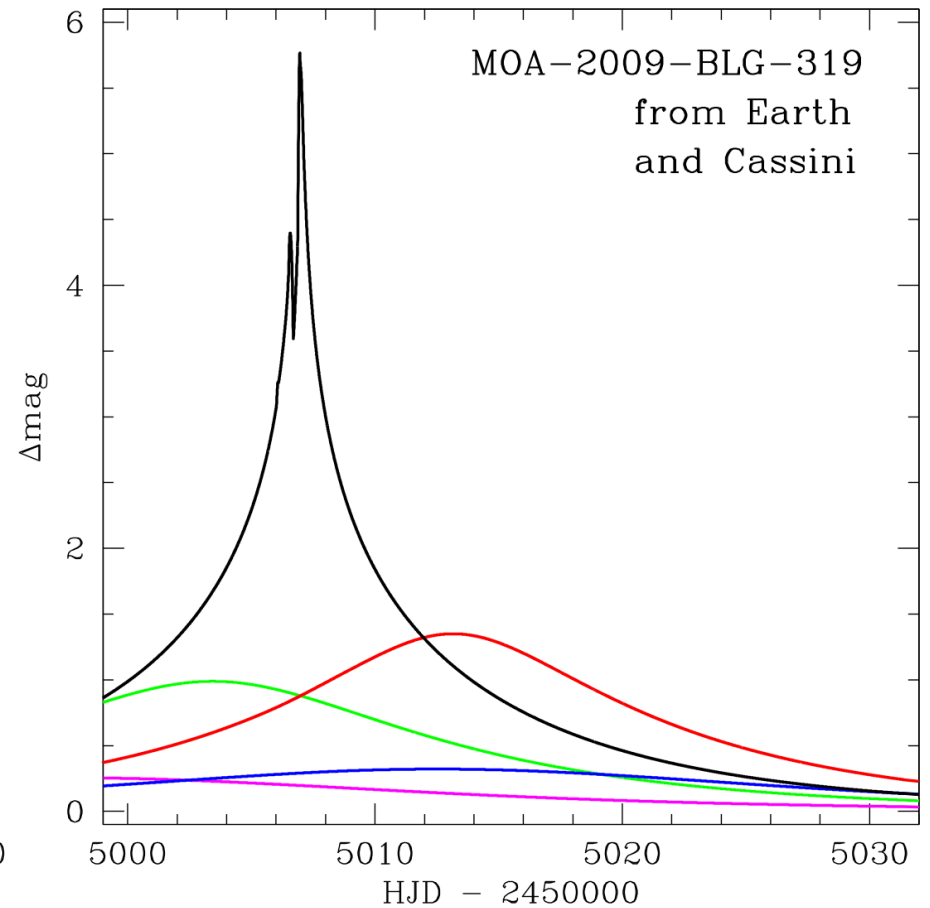
EPOXI PSF!



# Satellite Observations of Exoplanet Microlensing events

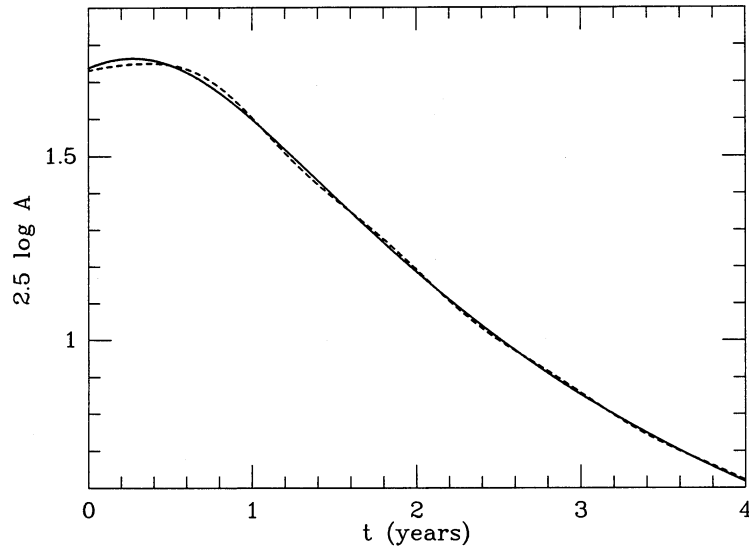


Galactic disk lens system  
(long)

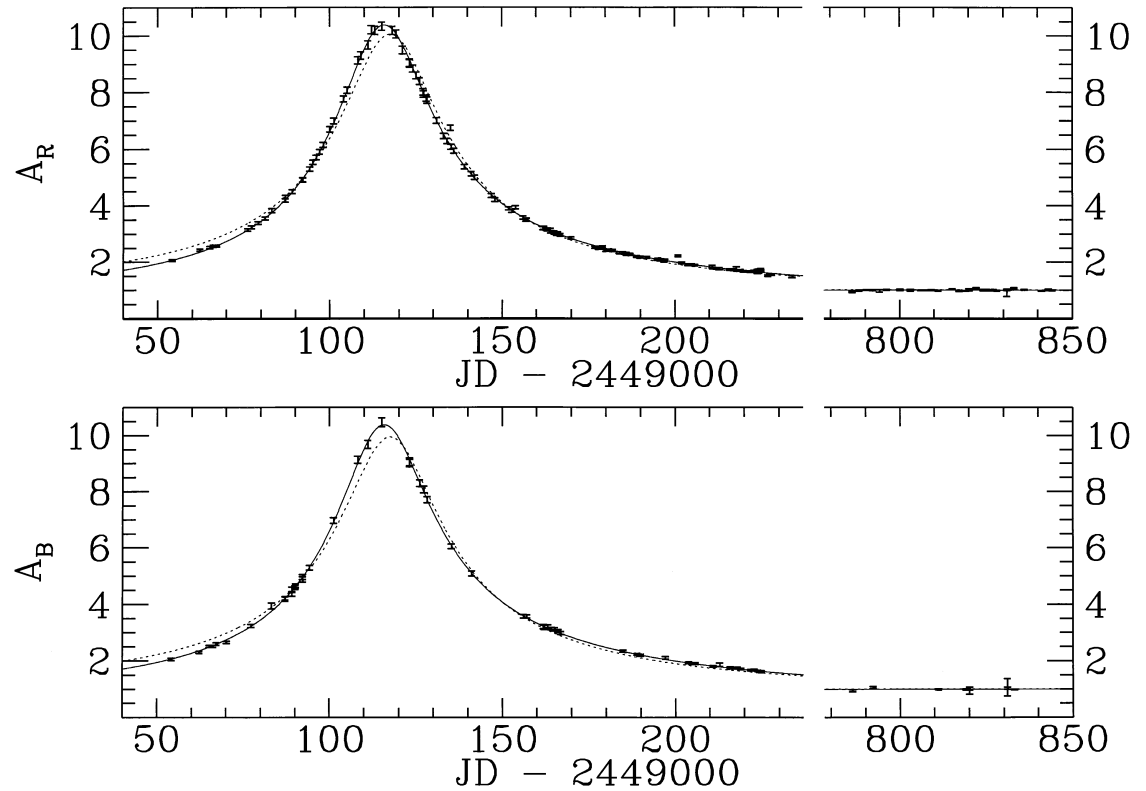


Galactic bulge lens system  
(short)

# Orbital Microlensing Parallax

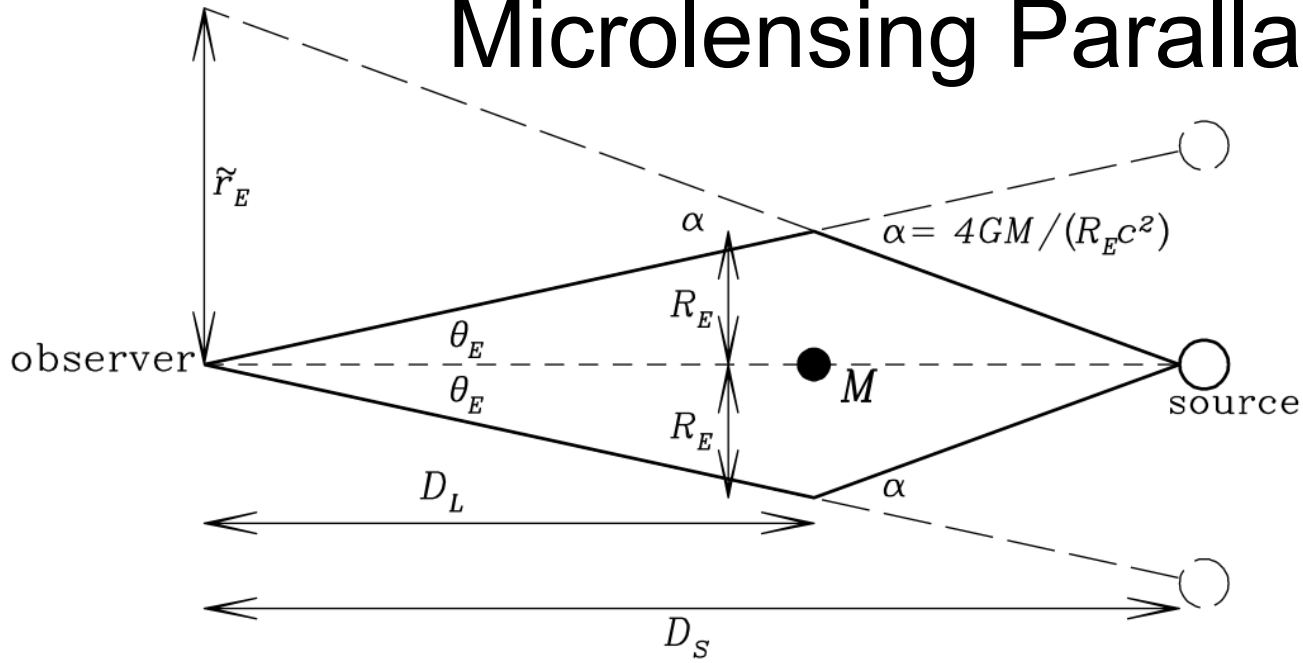


Gould (1992)  $10^3 M_{\odot}$  LMC  
Microlensing event  
(dashed curve)



Alcock et al. (1995) 1<sup>st</sup> observed parallax  
event: MACHO-104-C (solid curve)

# Micro lensing Parallax Parameters

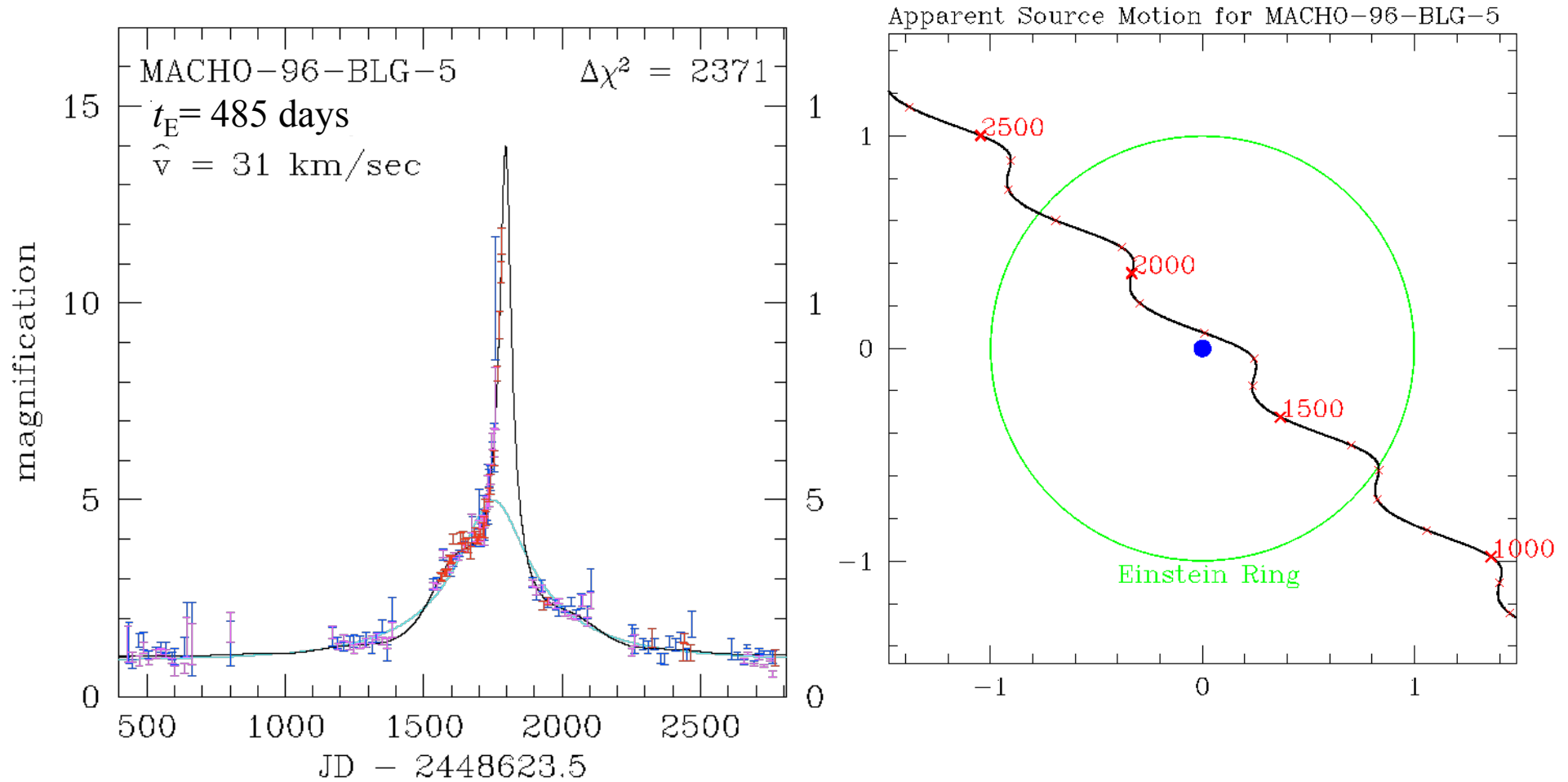


- projected Einstein radius,  $\tilde{r}_E$ 
    - conceptually simple
  - parallax vector,  $\boldsymbol{\pi}_E = (1\text{AU})/\tilde{r}_E$ 
    - convenient for modeling, as  $\pi_E \rightarrow 0$  when parallax vanishes
  - projected (source-lens) velocity,  $\hat{\boldsymbol{v}} = \tilde{r}_E / t_E$ 
    - depends on velocities and distance – independent of mass
- 2-d vectors:  $\hat{\boldsymbol{v}} \parallel \boldsymbol{\pi}_E \parallel \tilde{\boldsymbol{r}}_E$

# Parallax Coordinate Systems

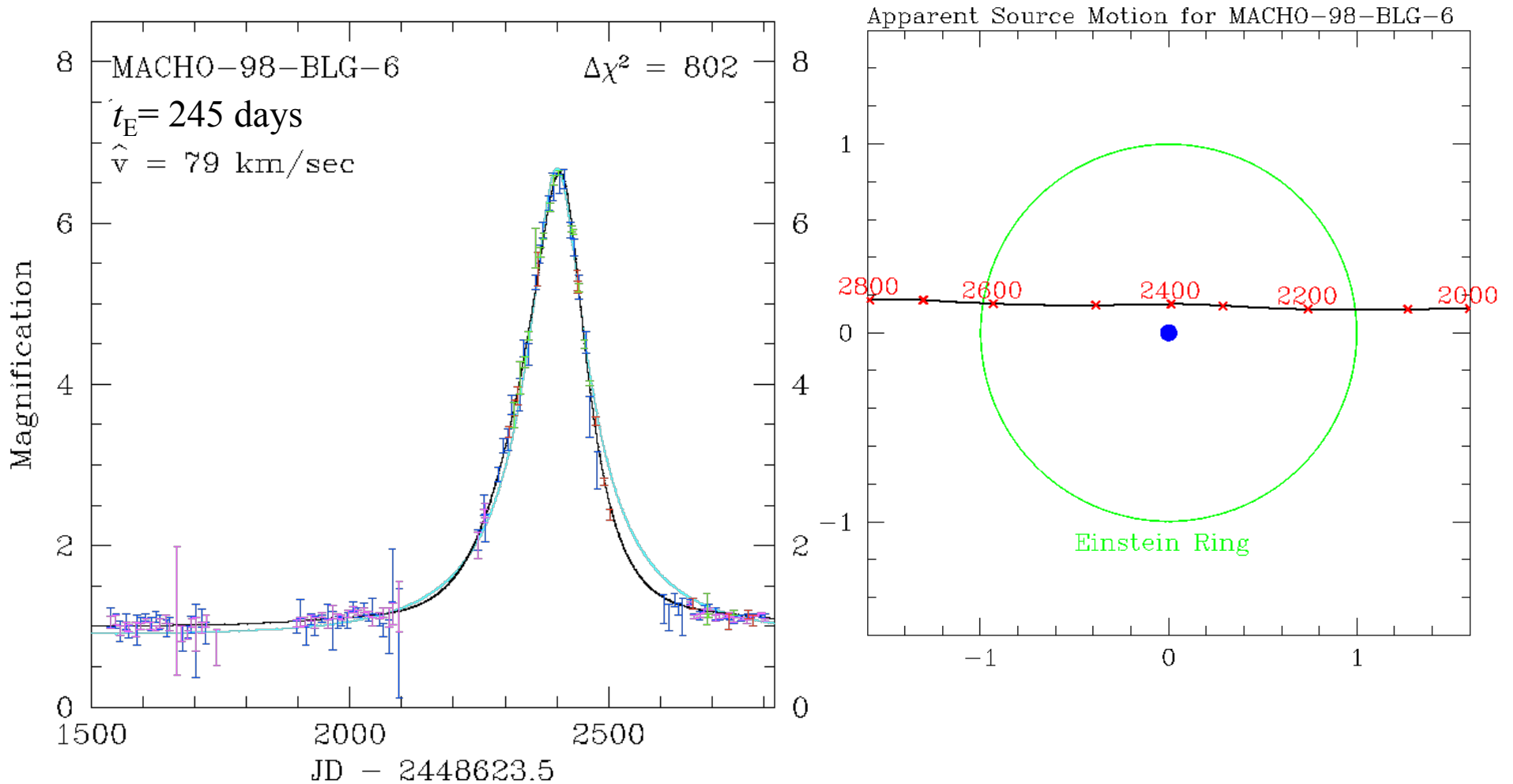
- Heliocentric
  - conceptually simple
  - useful for comparison with direct relative proper motion measurements
  - when  $\hat{v} \sim 30$  km/s, the parameters  $t_E$ ,  $t_0$ , and  $u_0$  can change substantially between the parallax on non-parallax fits – and they may have large, but correlated uncertainties
- Geocentric
  - a inertial frame moving instantaneously with the Earth at a time,  $t_{\text{fix}}$
  - parameters are similar to non-parallax models without the additional, correlated uncertainties
  - lens-source relative proper motion in this frame is not very useful, since the Earth follows the Solar motion over long timescales

# Orbital Microlensing Parallax



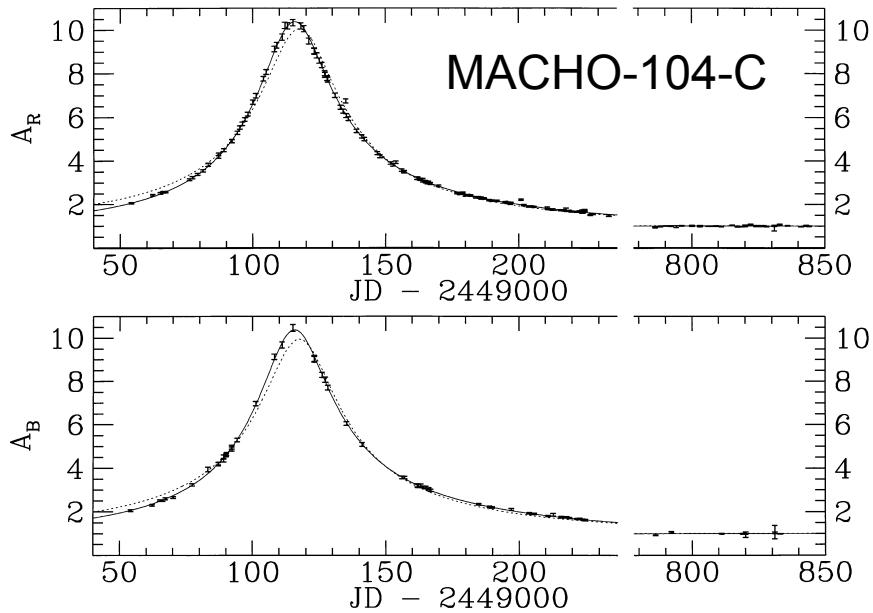
$\hat{v} \sim 30$  km/s implies large light curve variations

# Orbital Microlensing Parallax

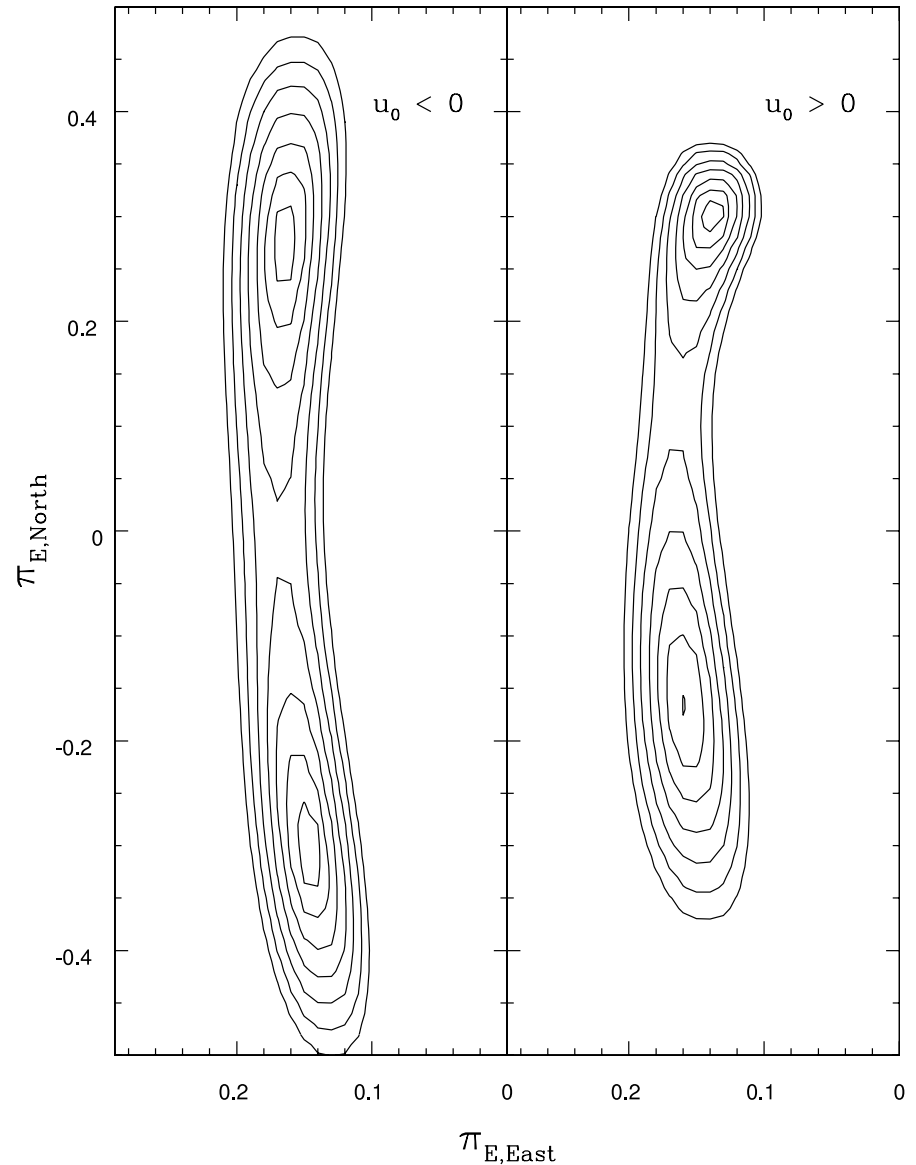


$\pi_E \sim \pi_{E,E}$  - i.e. lens-source relative velocity is nearly E-W

# Orbital Parallax Degeneracies



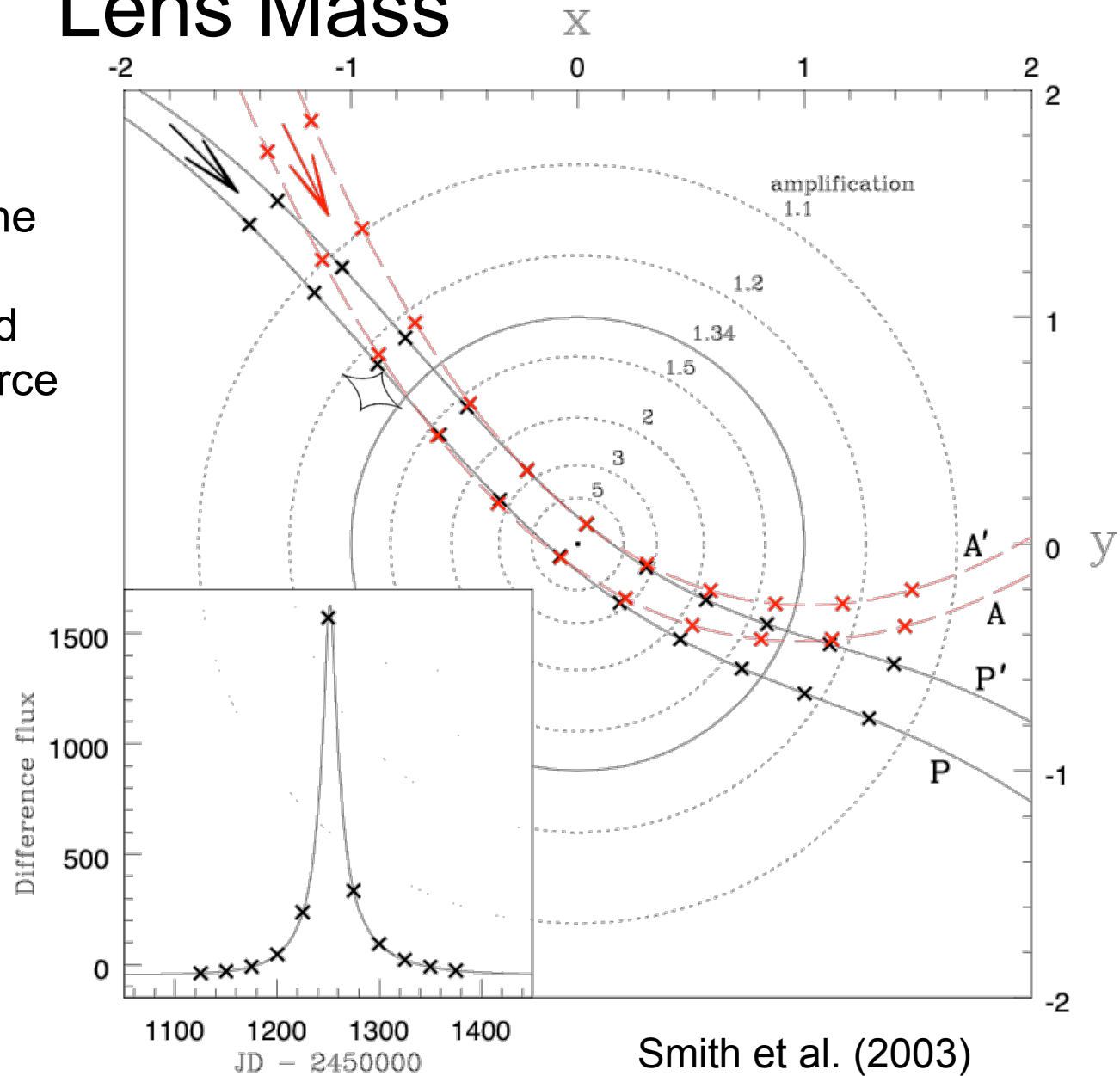
- One directions (usually N-S) is more poorly constrained than the other
  - N-S component of Earth's acceleration is small
  - if  $t_E \ll 1$  year, acceleration direction doesn't change much during event
- orientation of the lens system can be reflected with respect to the Earth-Sun system: takes  $u_0 \leftrightarrow -u_0$  and  $\theta \leftrightarrow -\theta$  (or  $\alpha \leftrightarrow -\alpha$ )



Smith et al. (2003); Gould (2004)

# Uncertainty Reduced by Additional Lens Mass

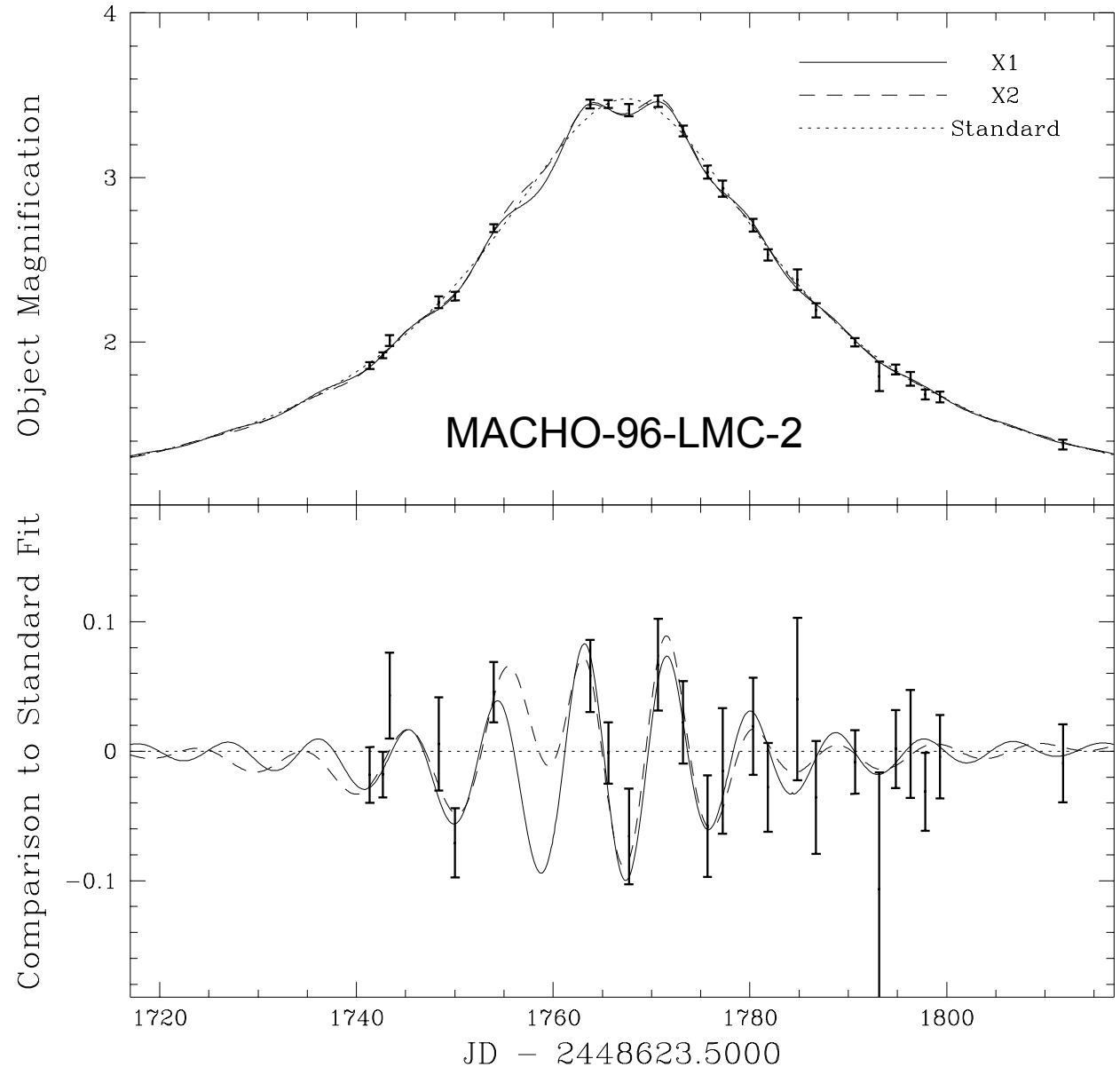
With a 2<sup>nd</sup> mass, the magnification depends on the 2-d position of the source not just the radial position.



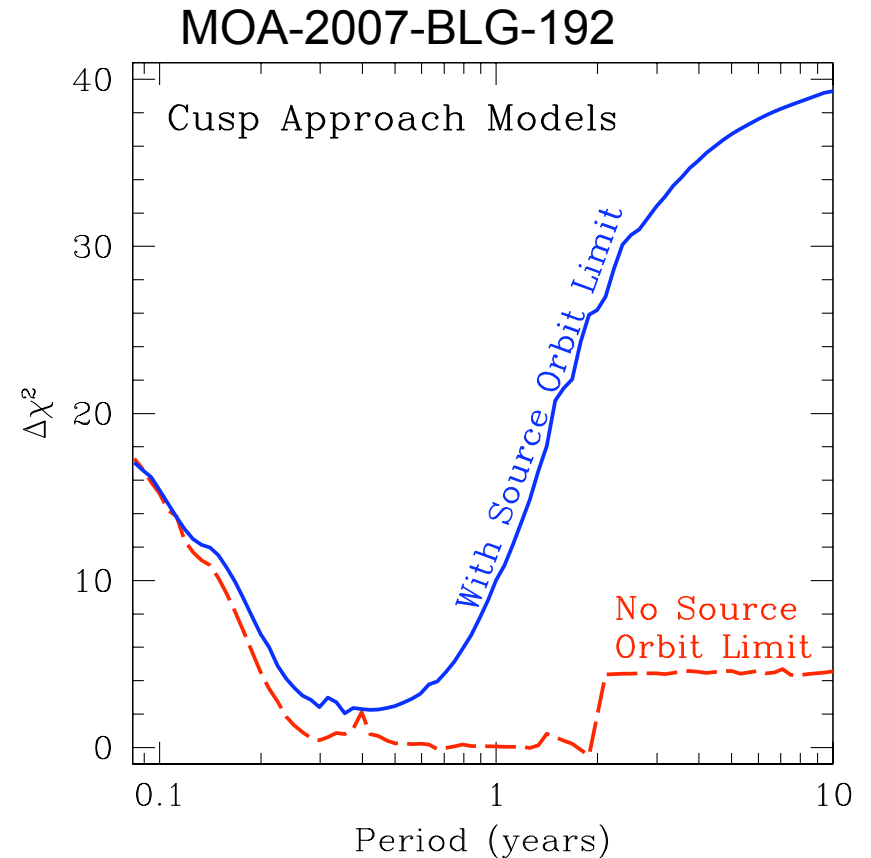
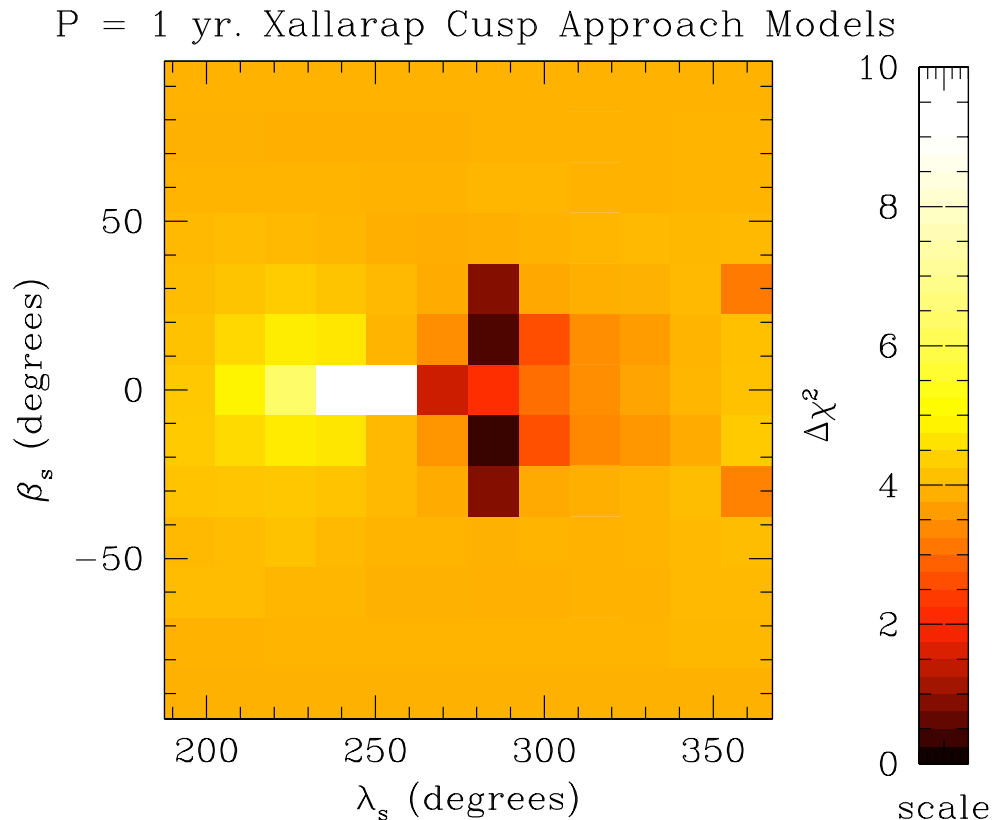
# Parallax vs. Xallarap

If the source has a binary companion, then the orbital motion of the source can affect the light curve.

Xallarap can always mimic orbital parallax, but it is somewhat unlikely to have a binary companion with an orbital period of 1-1000 days.



# Ruling out Xallarap



Does the best fit xallarap model match the parameters of the Earth's orbit?

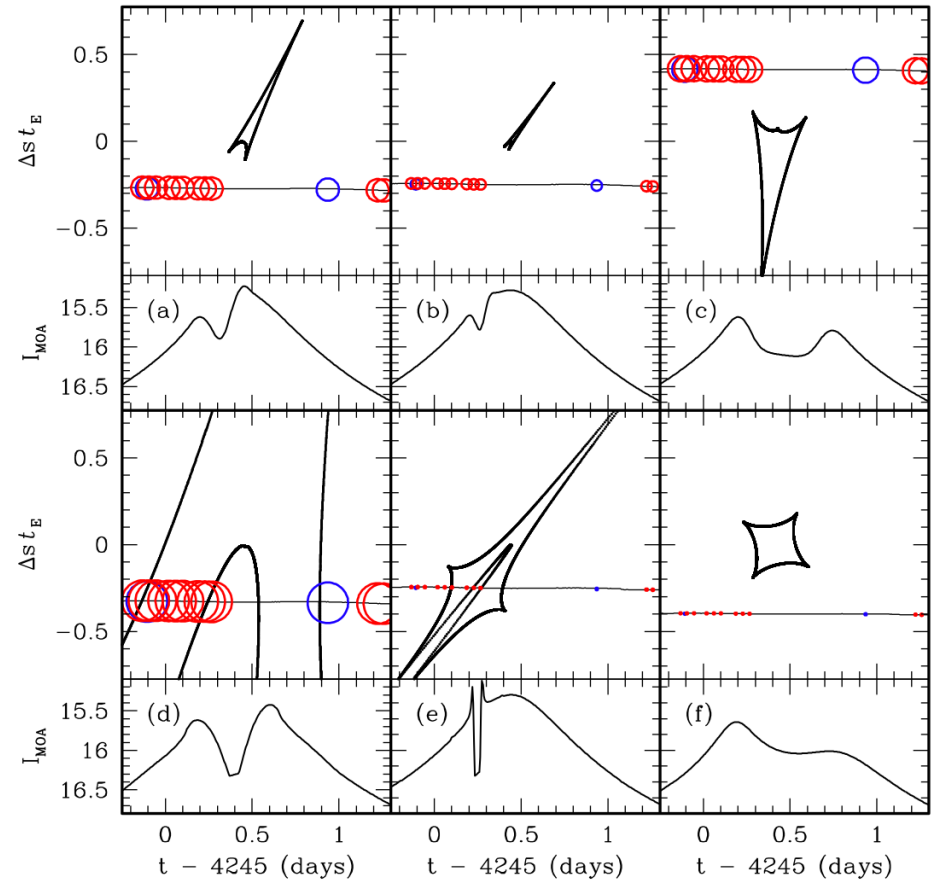
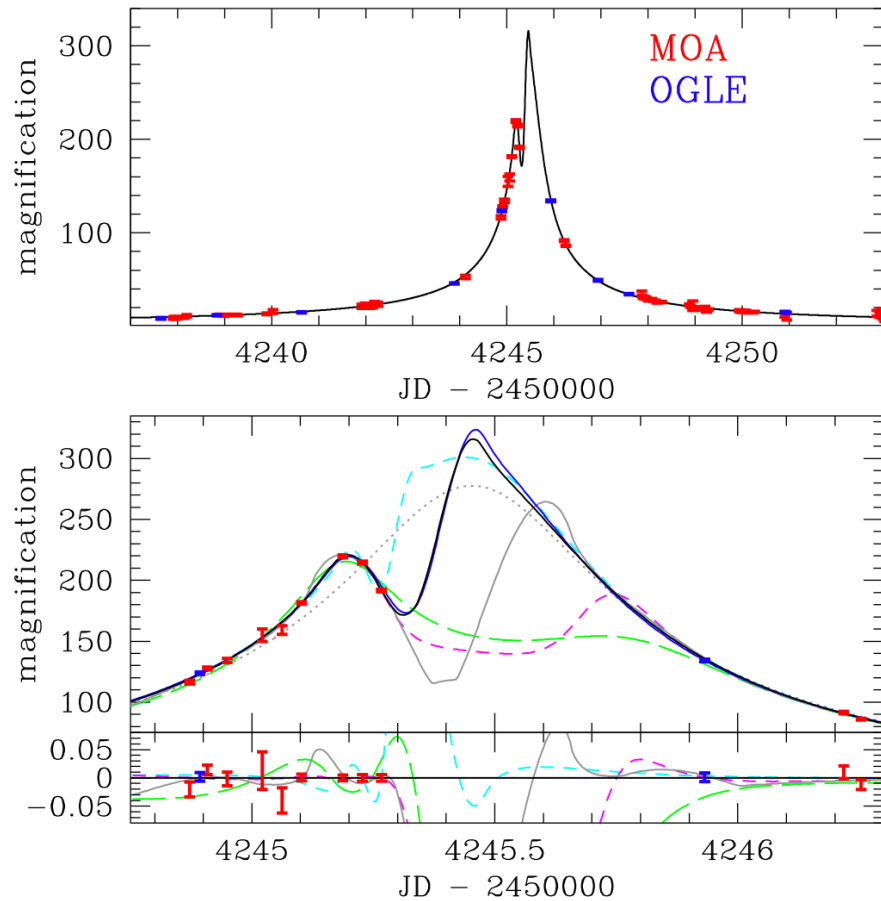
Xallarap can't mimic terrestrial parallax.

Because  $\theta_E$  is routinely measured, we know the Einstein radius projected to the position of the source, so we can use Kepler's 3<sup>rd</sup> law to set a limit on the orbital semi-major axis.

# MOA-2007-BLG-192

a high magnification event not predicted due to bad weather

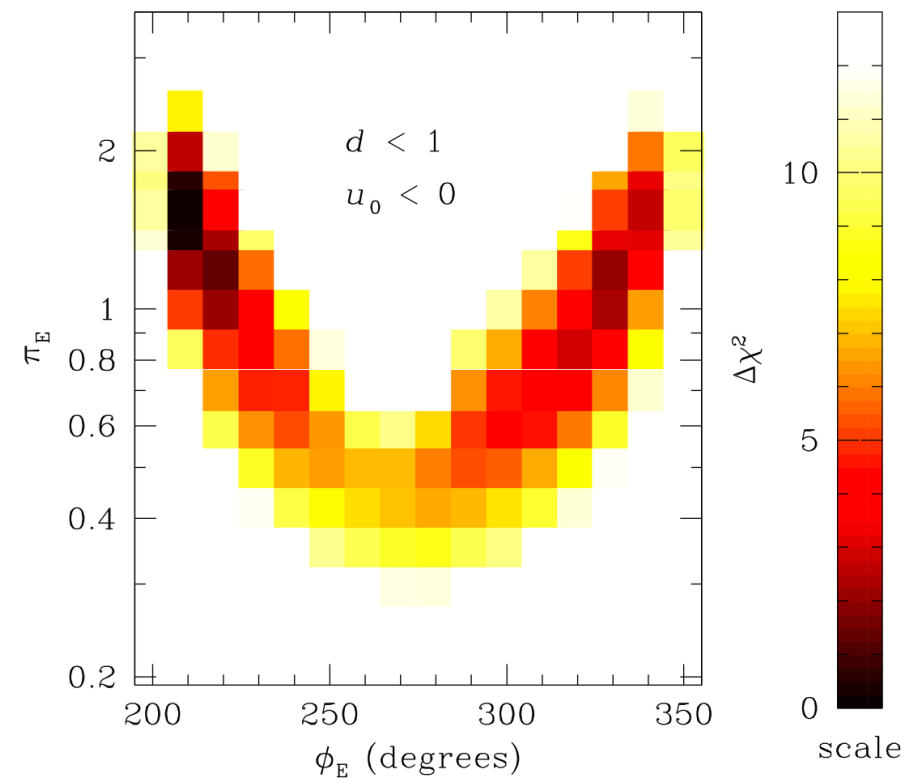
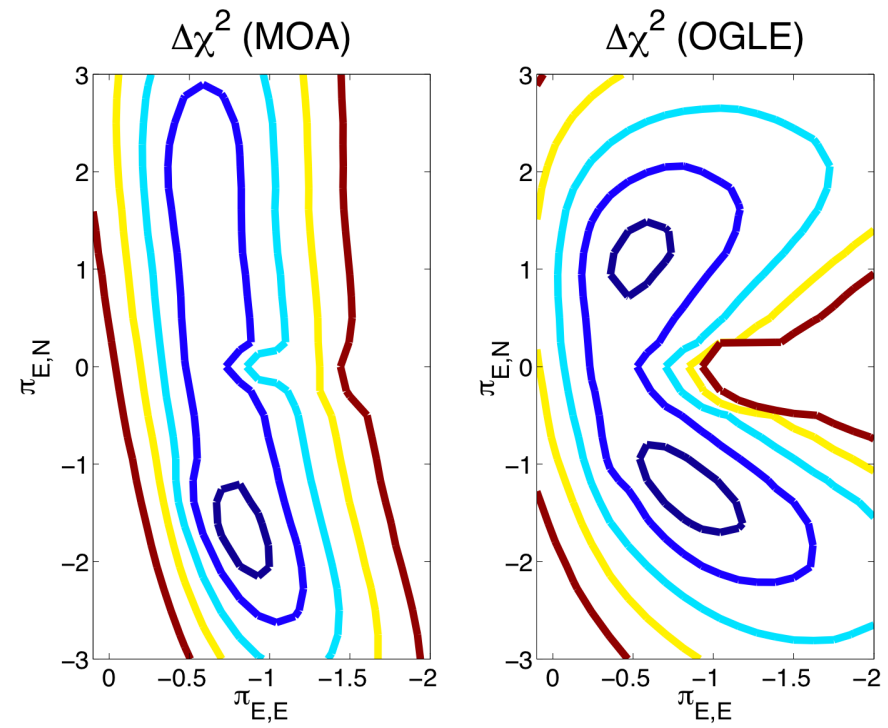
$q \approx 10^{-4}$   $d = 0.9R_E$  or  $1.1R_E$ . Different models can fit the data, but all have similar parameters.



Bennett et al. (2008)

# MOA-2007-BLG-192 Microlensing Parallax

$\pi_E = \frac{1}{\tilde{r}_E}$  is more convenient than  $\tilde{r}_E$  for modeling



$\Delta\chi^2$  contours for MOA and OGLE data. Contours are plotted at  $\Delta\chi^2 = 1, 4, 9, 16, 25$  (calculations by Yvette Perrott, Auckland U.)

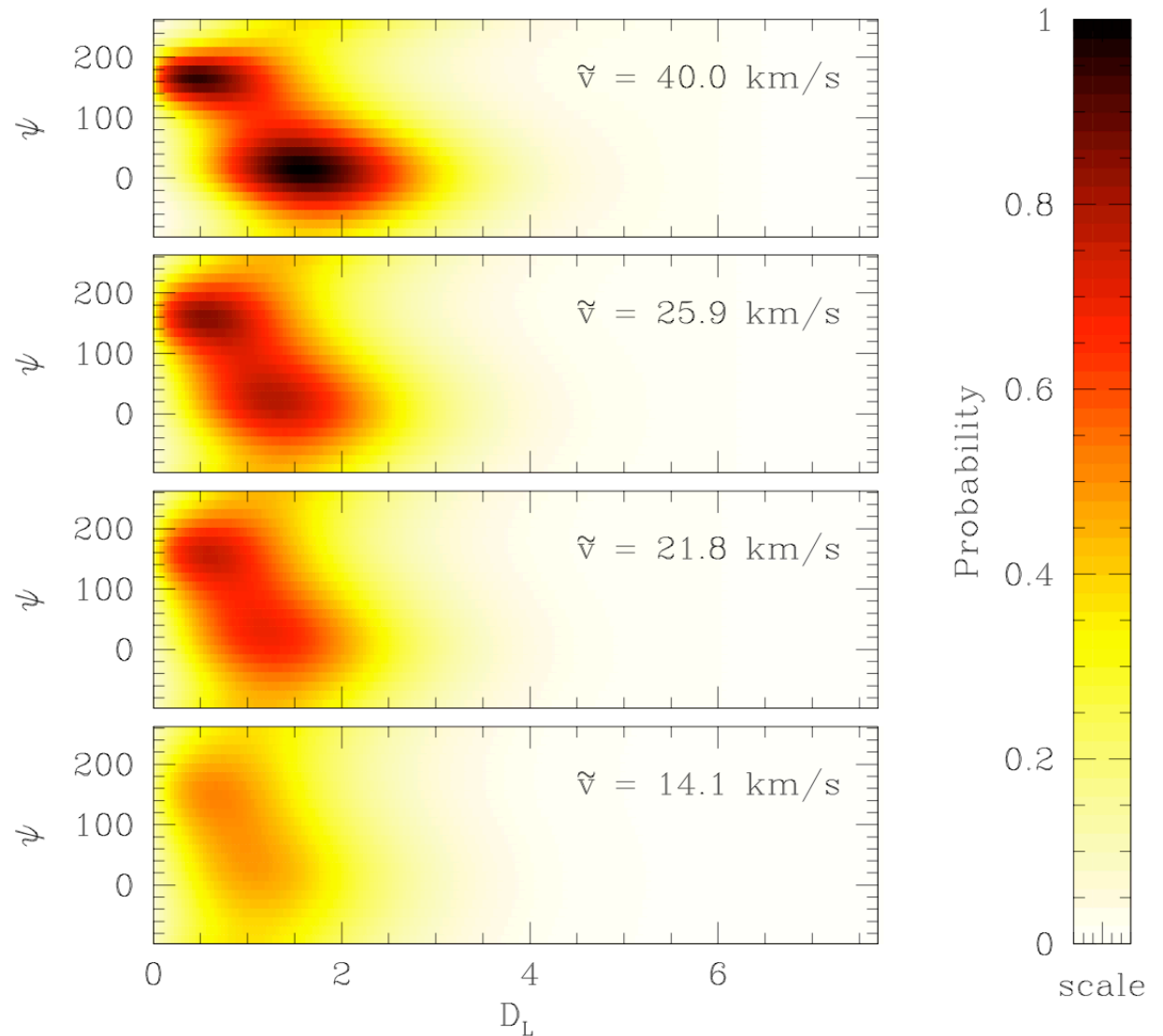
Combined MOA and OGLE  $\Delta\chi^2$  values now in polar coordinates.

# Microensing Parallax Implications for MOA-2007-BLG-192

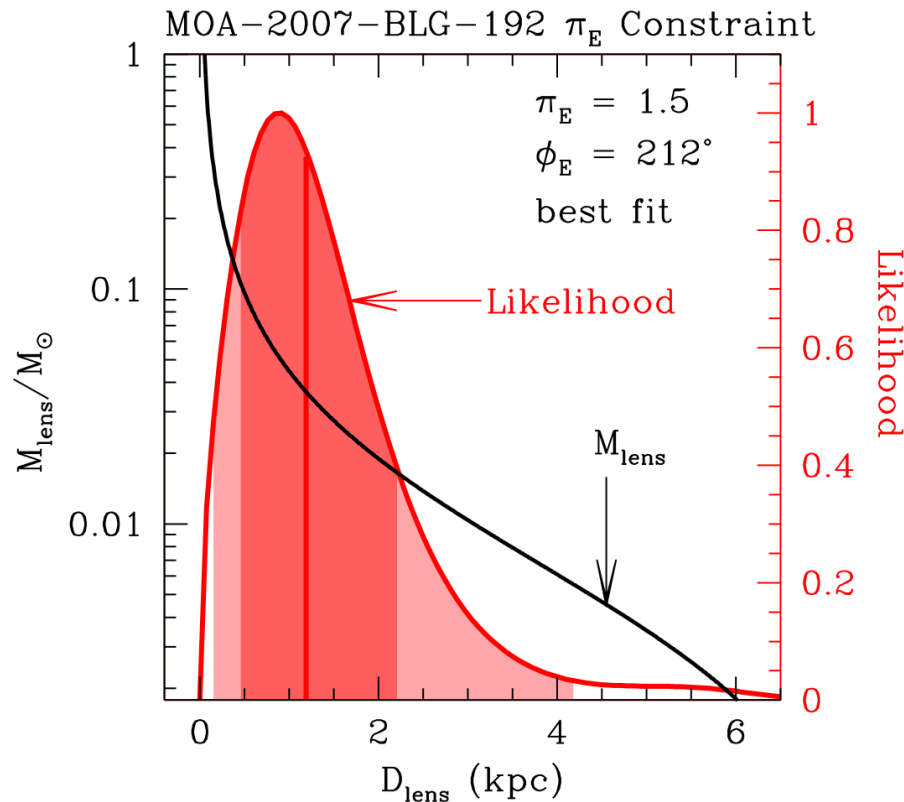
$\tilde{v} = \hat{v}$  probability distribution based on Galactic. A function of a 2-d velocity vector and distance.

Measurement of lens-source proper motion will determine

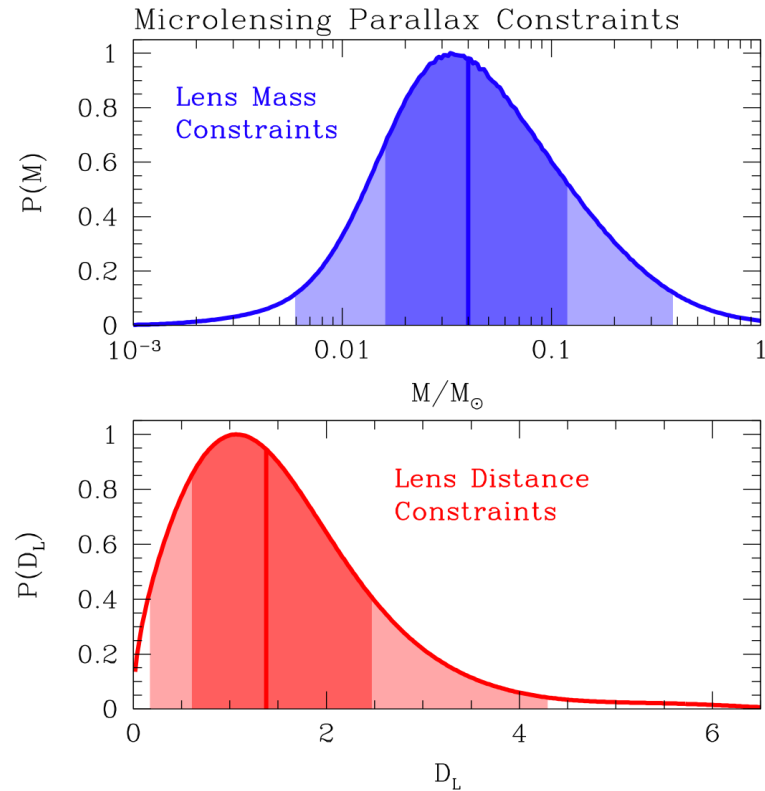
$$\tilde{v} = \hat{v}$$



# Microensing Parallax Implications for MOA-2007-BLG-192



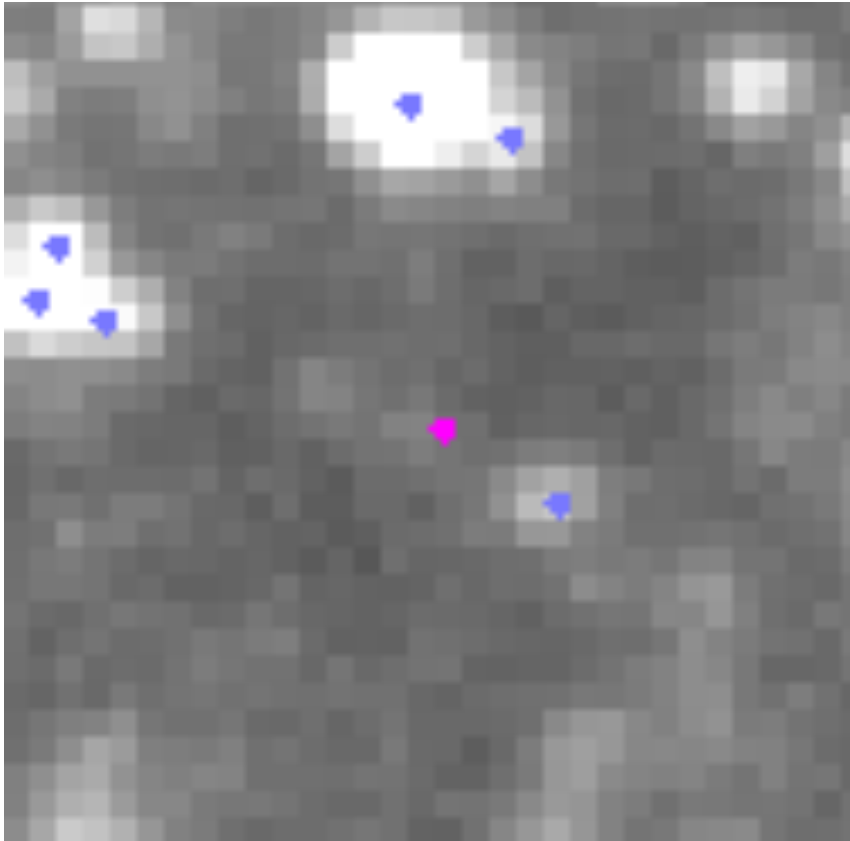
Mass-distance relation and probability of function of distance for best fit model.



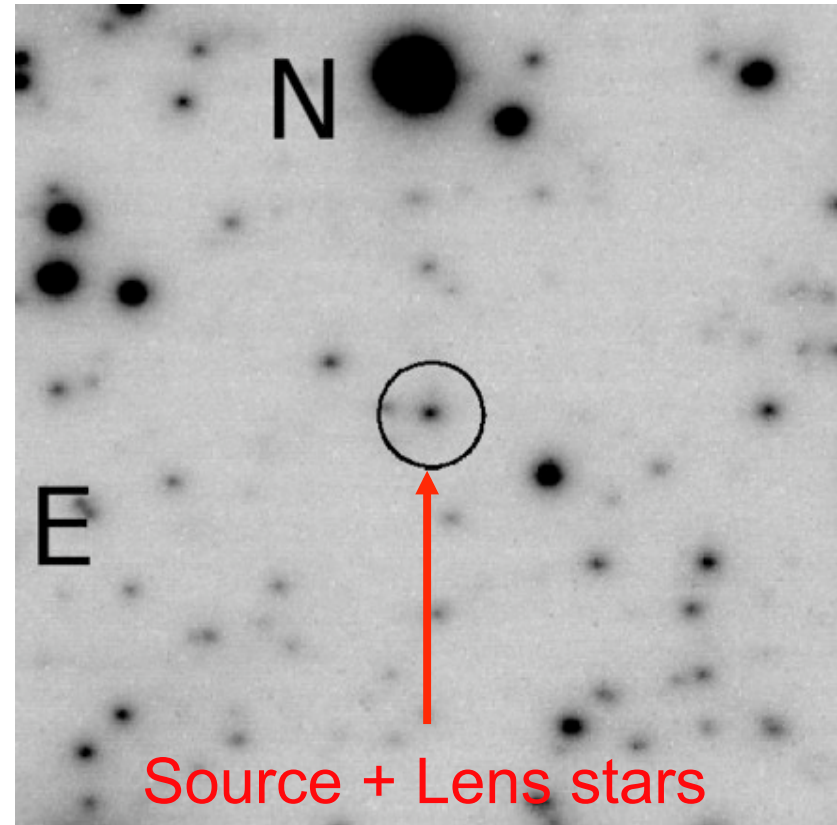
Average over all parallax models consistent with the data:

$$M_* = 0.040^{+0.080}_{-0.015} M_\odot$$

# VLT Adaptive Optics Images of MOA-2007-BLG-192



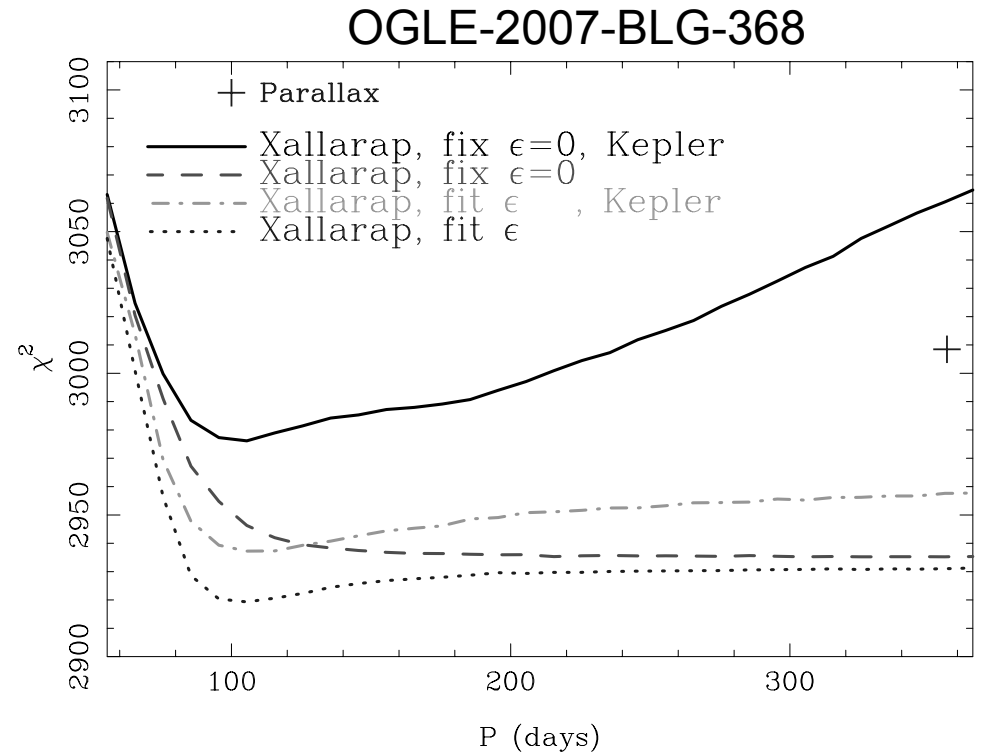
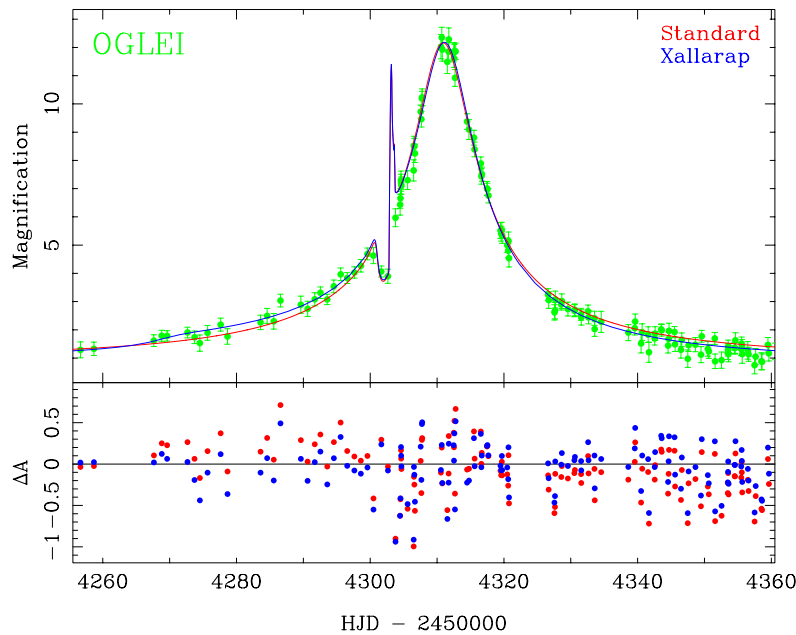
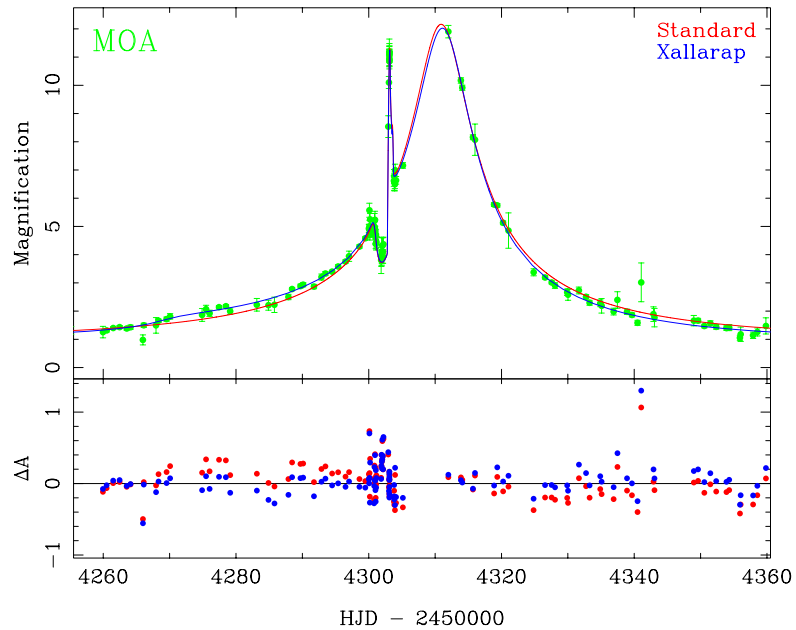
OGLE, I-band, 0.75'' seeing



VLT, AO, J-band, 0.15'' seeing

Preliminary AO photometry indicates that the lens is not brighter than the source in the J-band.

# Ruling in Xallarap



Xallarap model provides a much better fit than parallax with  $\Delta\chi^2 \sim 70$

Xallarap signal seen in MOA and OGLE data independently.

Sumi et al. (2010)

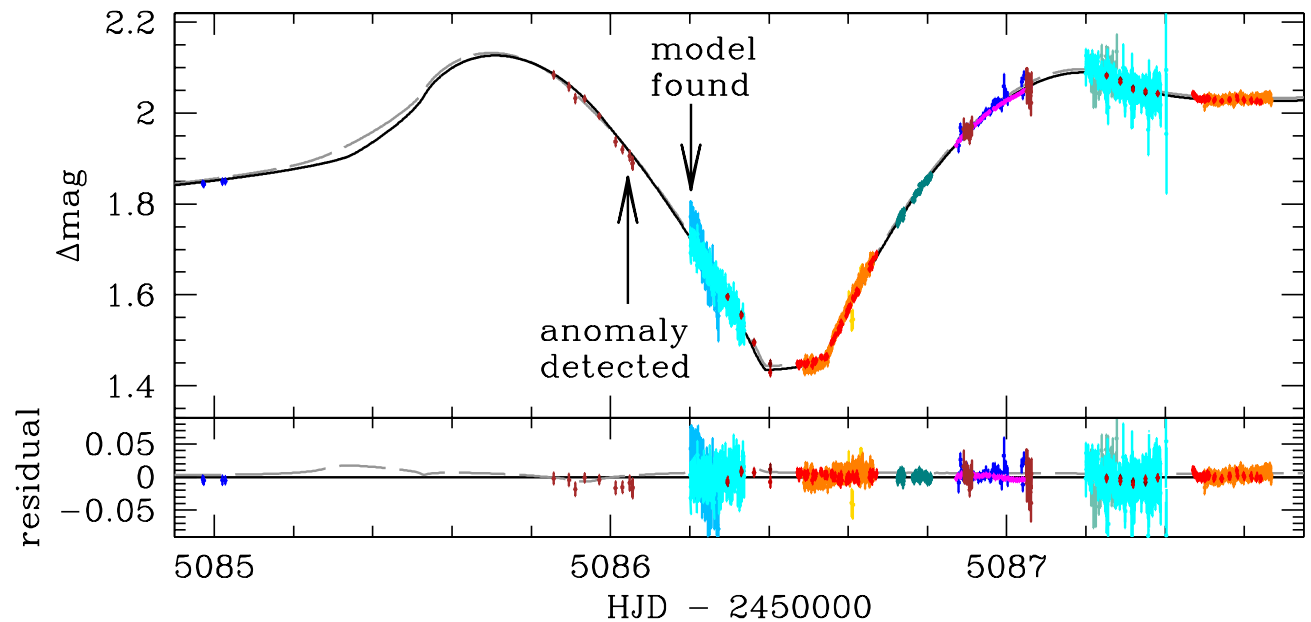
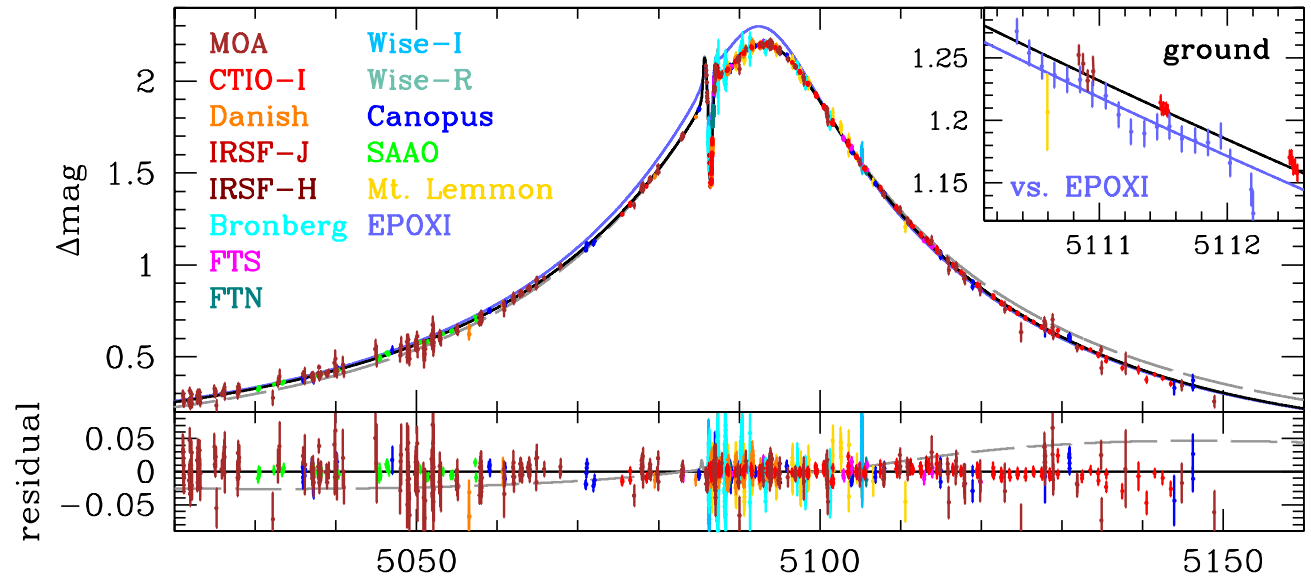
# Example: MOA-2009-BLG-266Lb

MOA survey  
discovery (Muraki et  
al. 2011)

Peak on 18 Sep.  
2009, when Earth's  
acceleration is  
nearly perpendicular  
to line of sight.

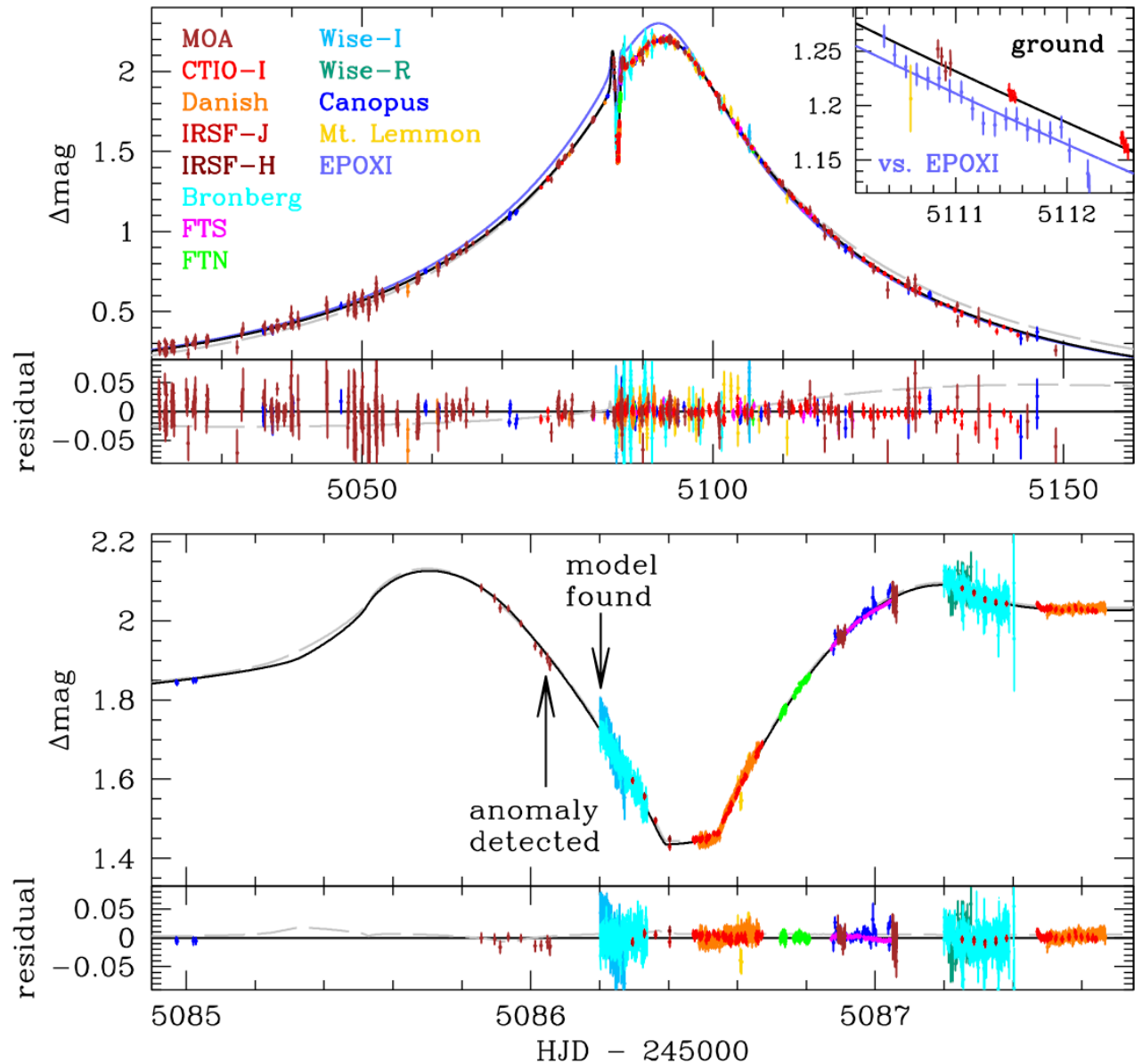
Parallax signal  
detected with  
 $\Delta\chi^2 = 2789.3$

First cold Neptune  
with a measured  
mass.



# Survey Discovery: MOA-2009-BLG-266

- Planet discovered by MOA on Sept. 11, 2009
- Lowest mass planet at  $> 0.05$  AU with a mass measurement  $\sim 10M_{\oplus}$  at  $\sim 3$  AU
- Deep Impact (now EPOXI Spacecraft observations contribute
- If extended mission is approved, regular microlensing parallaxes even for bulge events

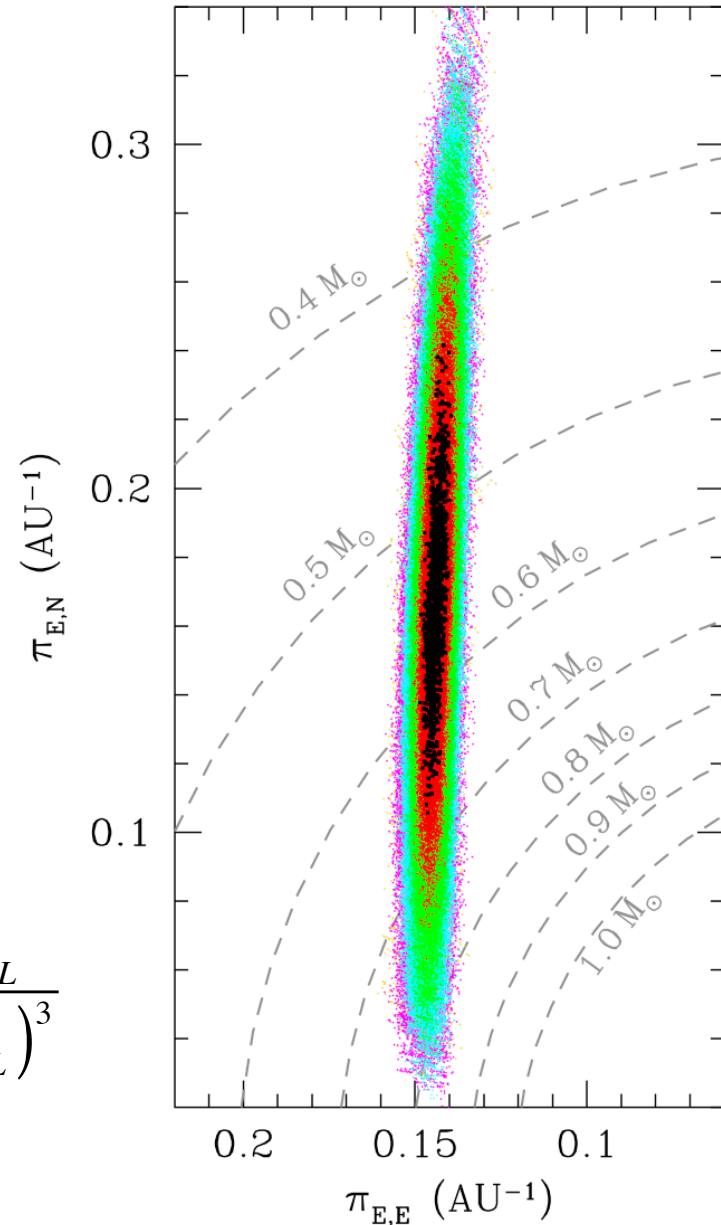


# Example: MOA-2009-BLG-266Lb

- for a static lens system, the  $u_0 > 0$  model is preferred over  $u_0 < 0$  by  $\Delta\chi^2 = 13.4$ . Other parameters differ:  
 $q(u_0 > 0) = 5.4 \times 10^{-5}$   
 $q(u_0 < 0) = 5.8 \times 10^{-5}$
- But, planet must orbit its host star
- Orbital motion improves  $\chi^2$  by  $\Delta\chi^2 = 3.2$  (for 2 fewer d.o.f.) - not significant
- Difference between  $u_0 > 0$  and  $u_0 < 0$  solutions drops to  $\Delta\chi^2 = 6.3$
- Orbital motion removes systematic difference in other parameters
- Orbital parameters limited by requiring planet to be bound:

$$\dot{s}_x^2 + \dot{s}_y^2 \leq \frac{2GM_L}{d_\perp R_E^2} = \frac{2GM_L}{s(\theta_E D_L)^3}$$

(Dong et al. 2009)



# Orbital Motion in Planetary Microlensing

- All star+planet events must have orbital motion
  - Can be minimized with a long separation along the line of sight, but this is unlikely
- Typical orbital period is  $\sim 8$  years
- Or  $10^{-3}R_E$  per day
- For fixed  $\theta_E$ , orbital motion (in  $R_E$  units) is minimized for  $D_L = \frac{2}{3}D_S$ , maximized for  $D_L \rightarrow 0$  and  $D_L \rightarrow D_S$ 
  - $D_L \rightarrow 0$  implies very low-mass lens system and large parallax signal
  - $D_L \rightarrow D_S$  implies very massive lens system
- Most easily detected in events with long duration planetary signals
  - Massive planets
  - $s \sim 1$ , connected or “resonant” caustic
    - Radial motion of such caustics is larger
- If planetary signal has a duration of  $N$  days, then orbital motion is almost certainly important if light curve changes significantly when the planet position is changed by  $N(10^{-3}R_E)$

# Orbital Motion Modeling

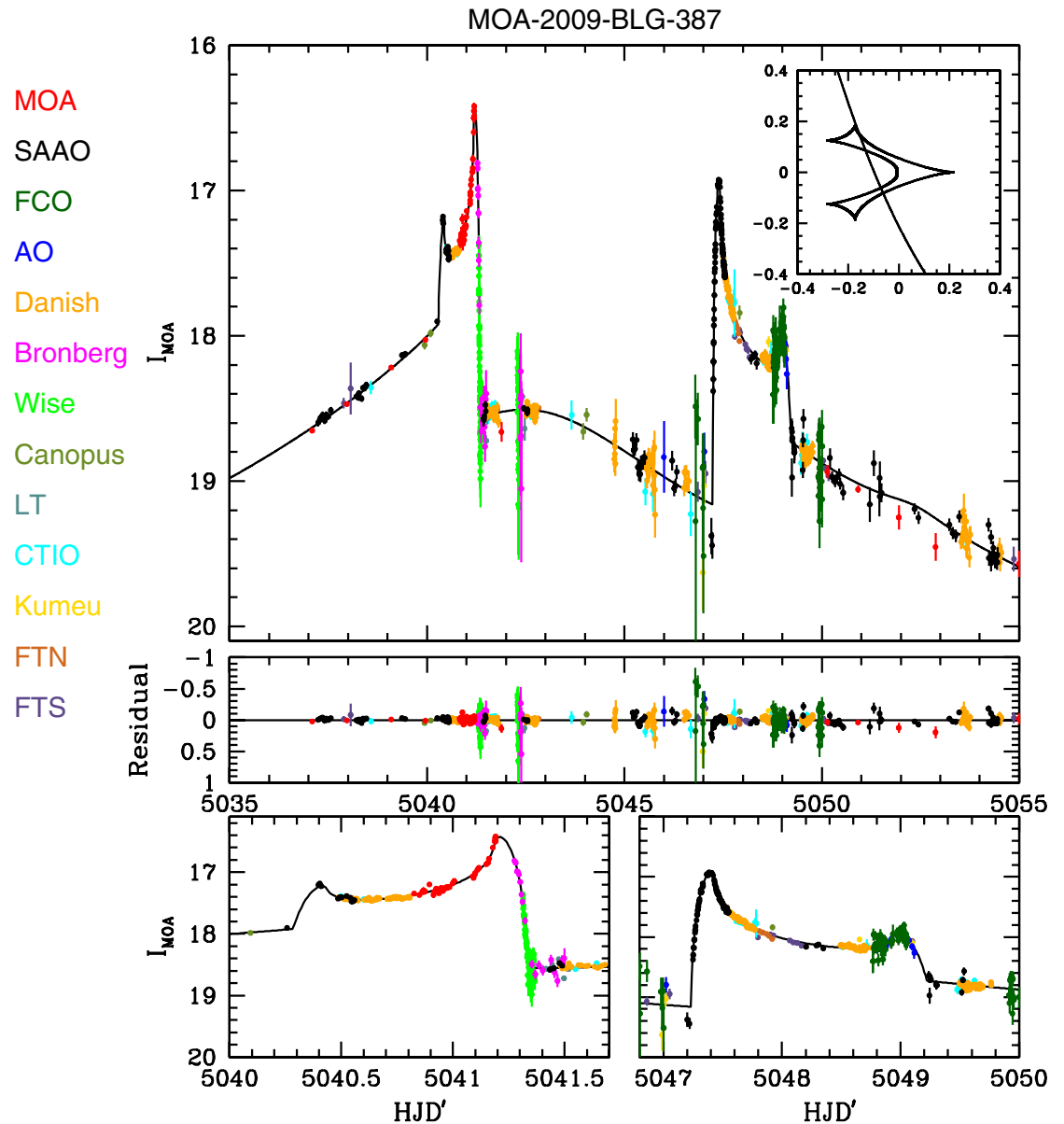
- We sample only a small portion of the light curve
- So, we first consider lowest order terms:
  - 0<sup>th</sup> order: 2-d positions:  $s = s_x, s_y = 0$  (0<sup>th</sup> order separation defines  $x$ -axis)
  - 1<sup>st</sup> order: 2-d velocities:  $\dot{s}_x, \dot{s}_y$
  - 2<sup>nd</sup> order: 1-d acceleration:  $\ddot{s}_x$ , acceleration only toward the host
  - higher order terms are unlikely to be important for a planetary event (but could be important with stellar binaries)
- 5 parameters are enough to describe a circular orbit (with a center at the origin)
  - 2 parameters to describe the orbital plane (passing through the origin)
  - the radius, phase, and period of the orbit
  - A circular orbit is described by 5 parameters
- Thus, a circular orbit can be described by  $s_x, \dot{s}_x, \dot{s}_y$ , and the orbital period,  $T$
- If we know the planetary mass (from measurements of  $\theta_E$  and  $\pi_E$ )

# Orbital Motion as a Nuisance: MOA-2009-BLG-387

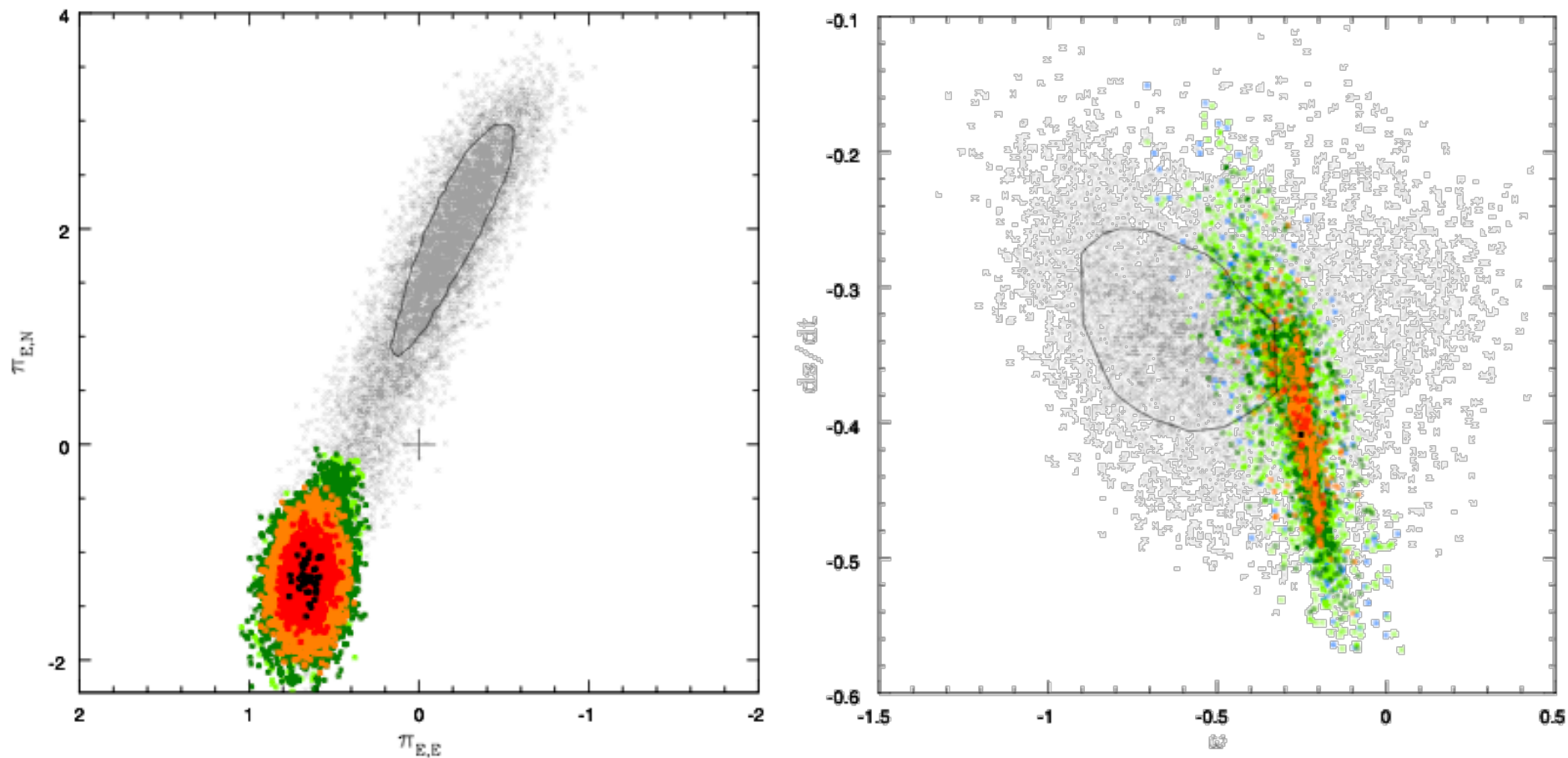
4 caustic crossings in 10 days for very massive planet ( $q \sim 0.013$ ) at  $s \sim 0.91$ ,  $t_E \sim 40$  days.

Sensitive to both orbital motion and parallax.

Batista et al. (2011)



# Orbital Motion as a Nuisance: MOA-2009-BLG-387



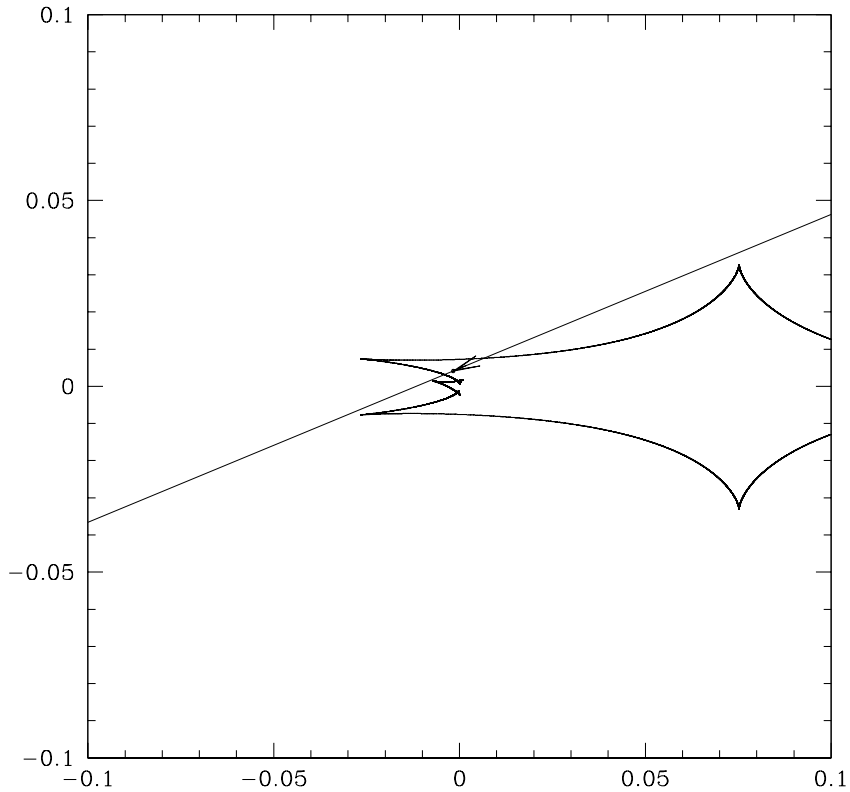
Parallax-only and orbital motion only models in color; Joint parallax + orbital motion in grey. If lens system was static, we could get a precise parallax value and precise lens masses...

# Example of Complicated Planetary Event

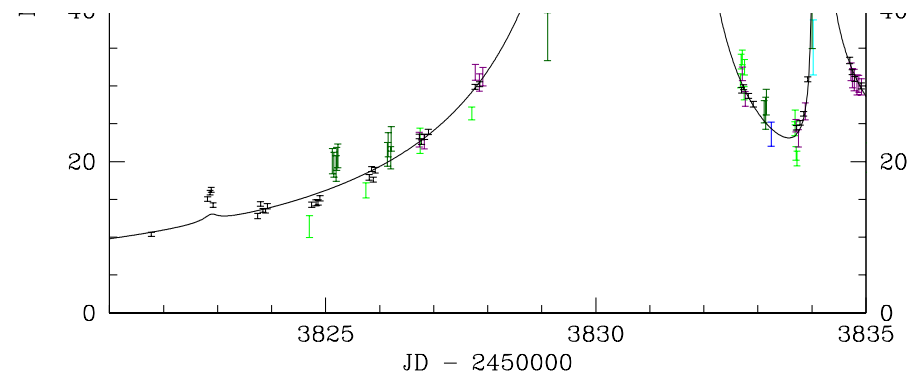
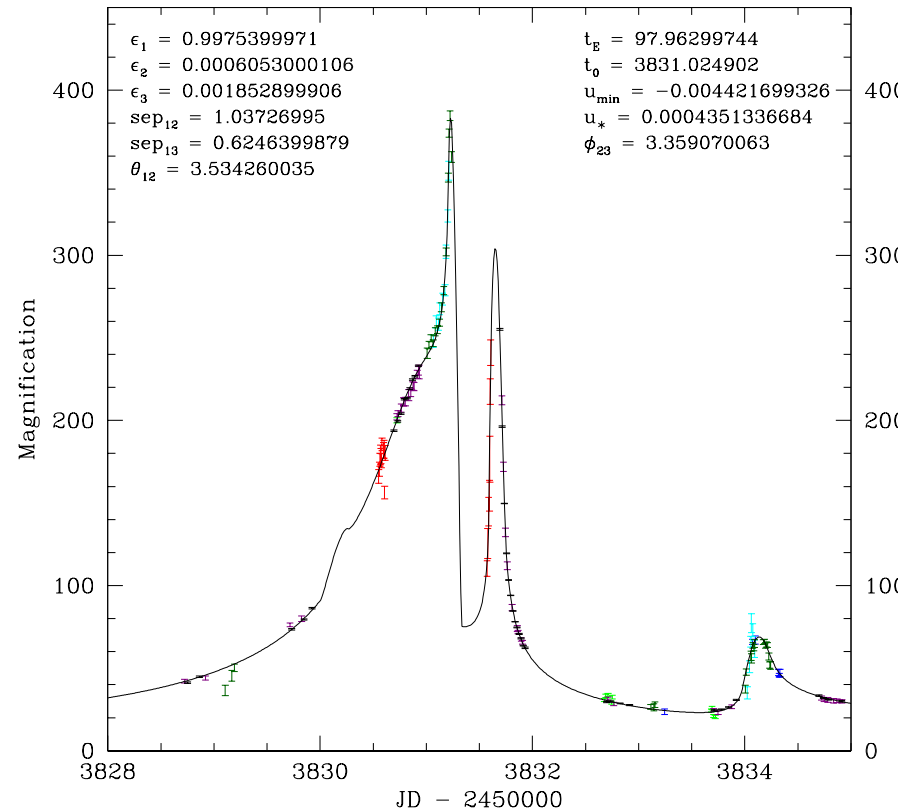
- OGLE-2006-BLG-109
- Includes 2-planets, orbital motion of a planet near the Einstein radius and microlensing parallax
- Follow-up observations see the host star

Gaudi et al. (2008); Bennett et al. (2010)

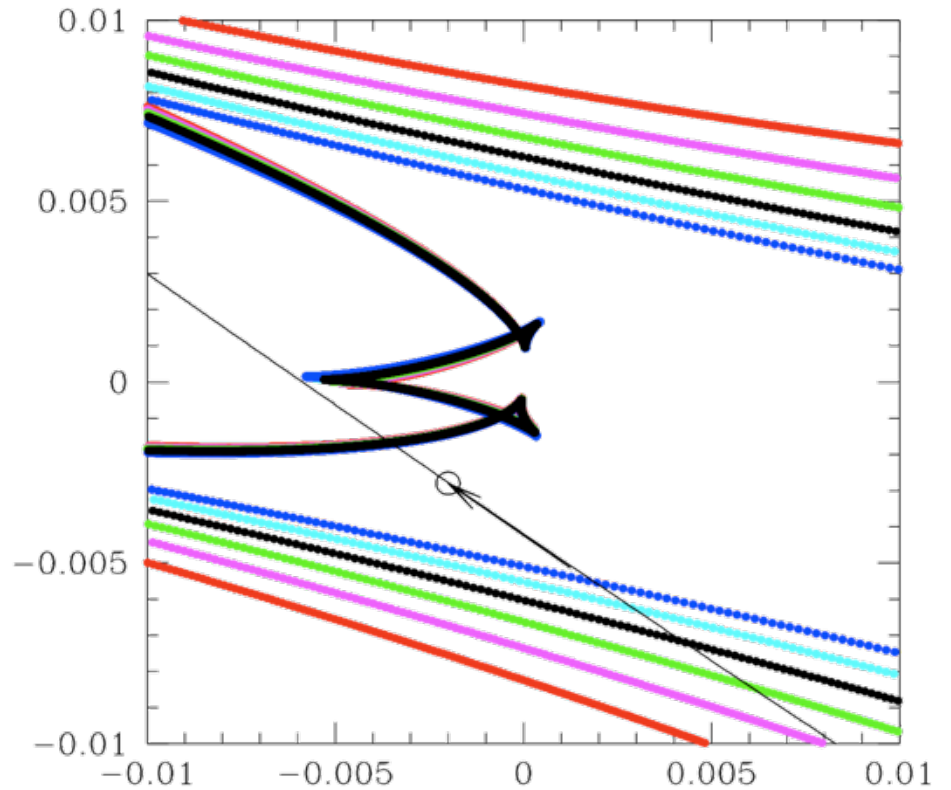
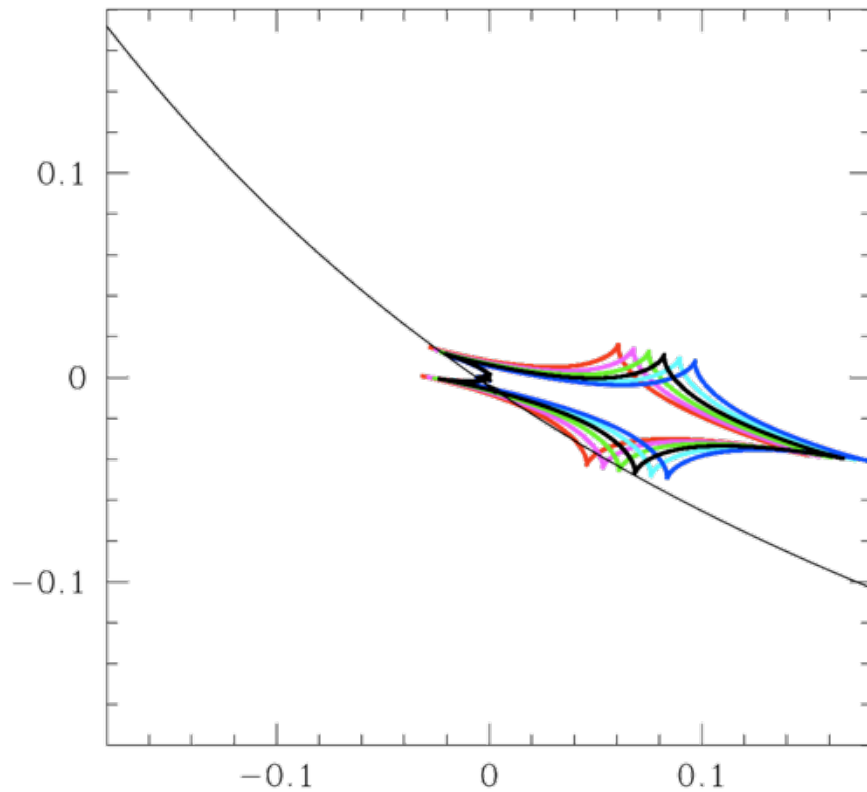
# Static Solution for OGLE-2006-BLG-109



Without orbital motion, the source misses the early caustic crossing.  
 With 11 days between cusp approach and peak, we can expect  $\sim 0.01 R_E$  of radial caustic motion during the planetary deviation



# OGLE-2006-BLG-109Lb,c Caustics

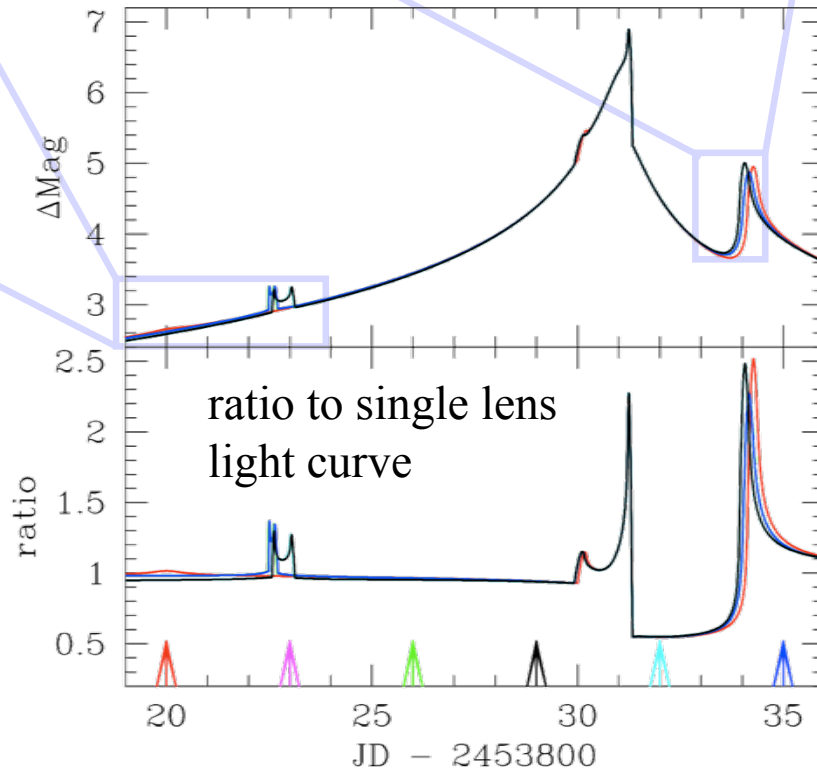
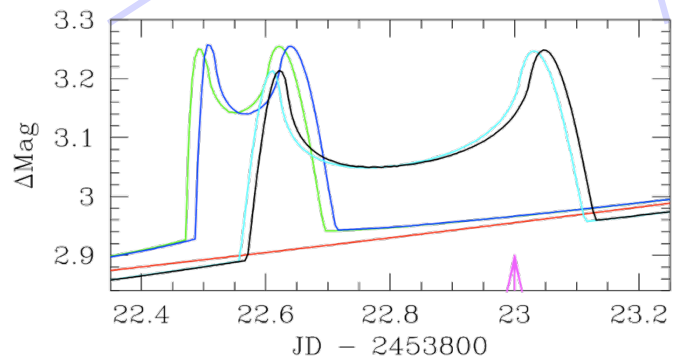
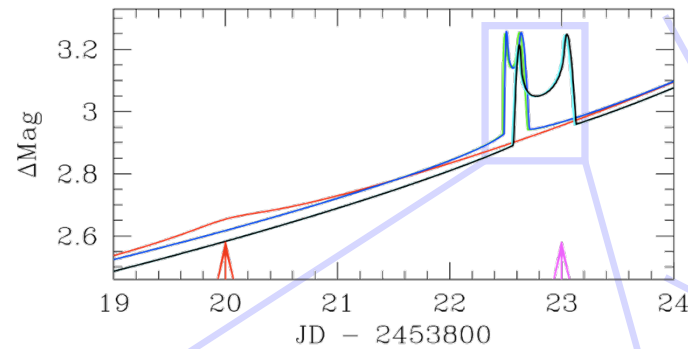
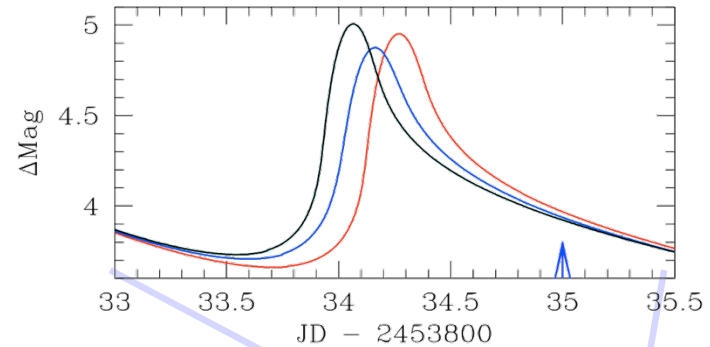


- Curved source trajectory due to Earth's orbital motion: microlensing parallax
- Caustic curves plotted at 3-day intervals
- 0.2% of 14-yr orbit completed during planetary event
- Model includes planet-star relative velocity and acceleration

# Effect of Parallax & Orbital Motion

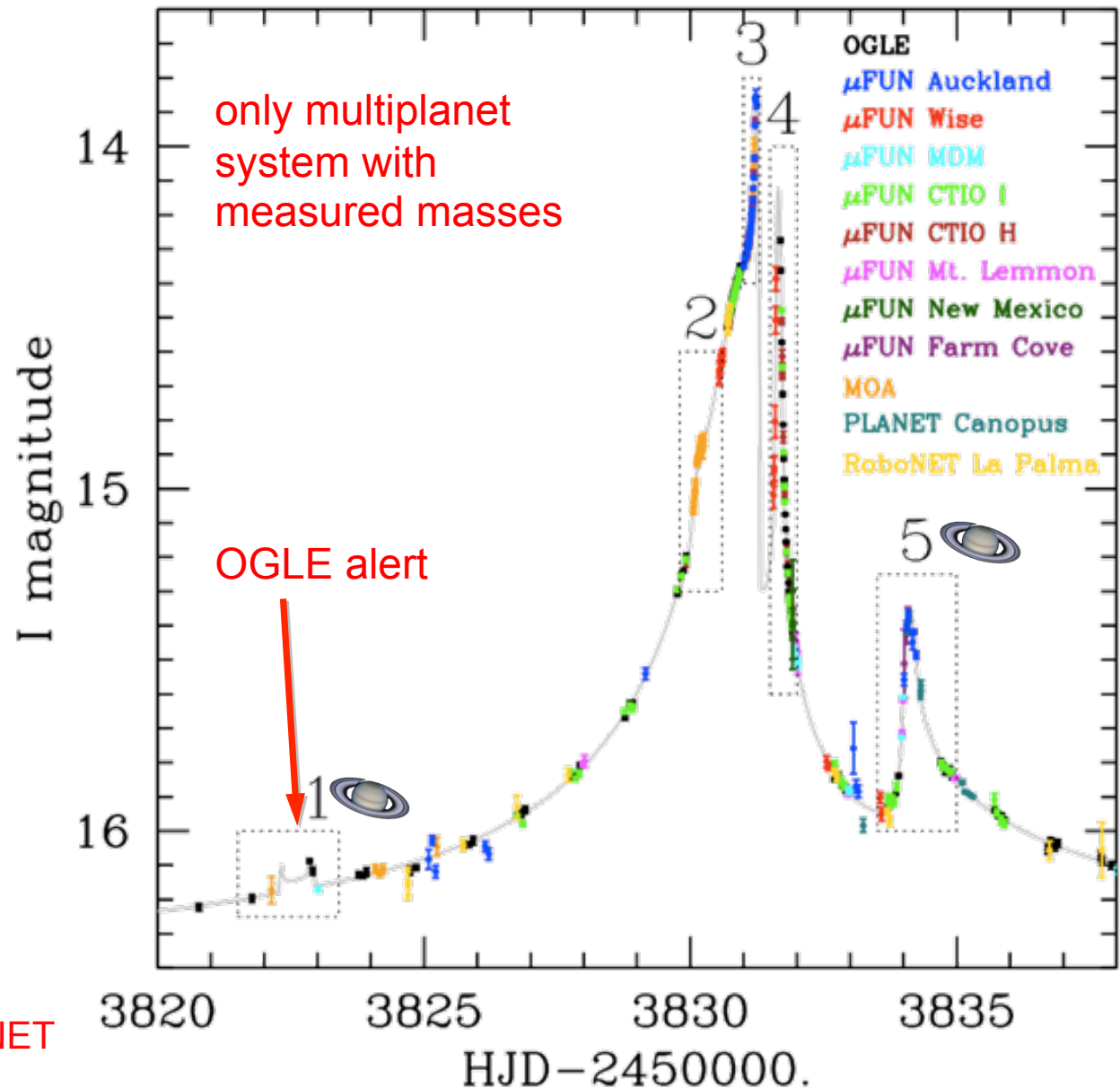
- **black** curve is the full model
- **red** curve: neither orbital motion nor parallax.
- **blue** curve: orbital motion, but no parallax
- **green** curve: constant velocity approx.
- **cyan** curve: parallax and the constant velocity approx.

Binary model similar to OGLE-06-109



# Double-Planet Event: OGLE-2006-BLG-109

- 5 distinct planetary light curve features
- OGLE alerted 1<sup>st</sup> feature as potential planetary signal
- High magnification
- Feature #4 requires an additional planet
- Planetary signals visible for 11 days
- Features #1 & #5 require the orbital motion of the Saturn-mass planet

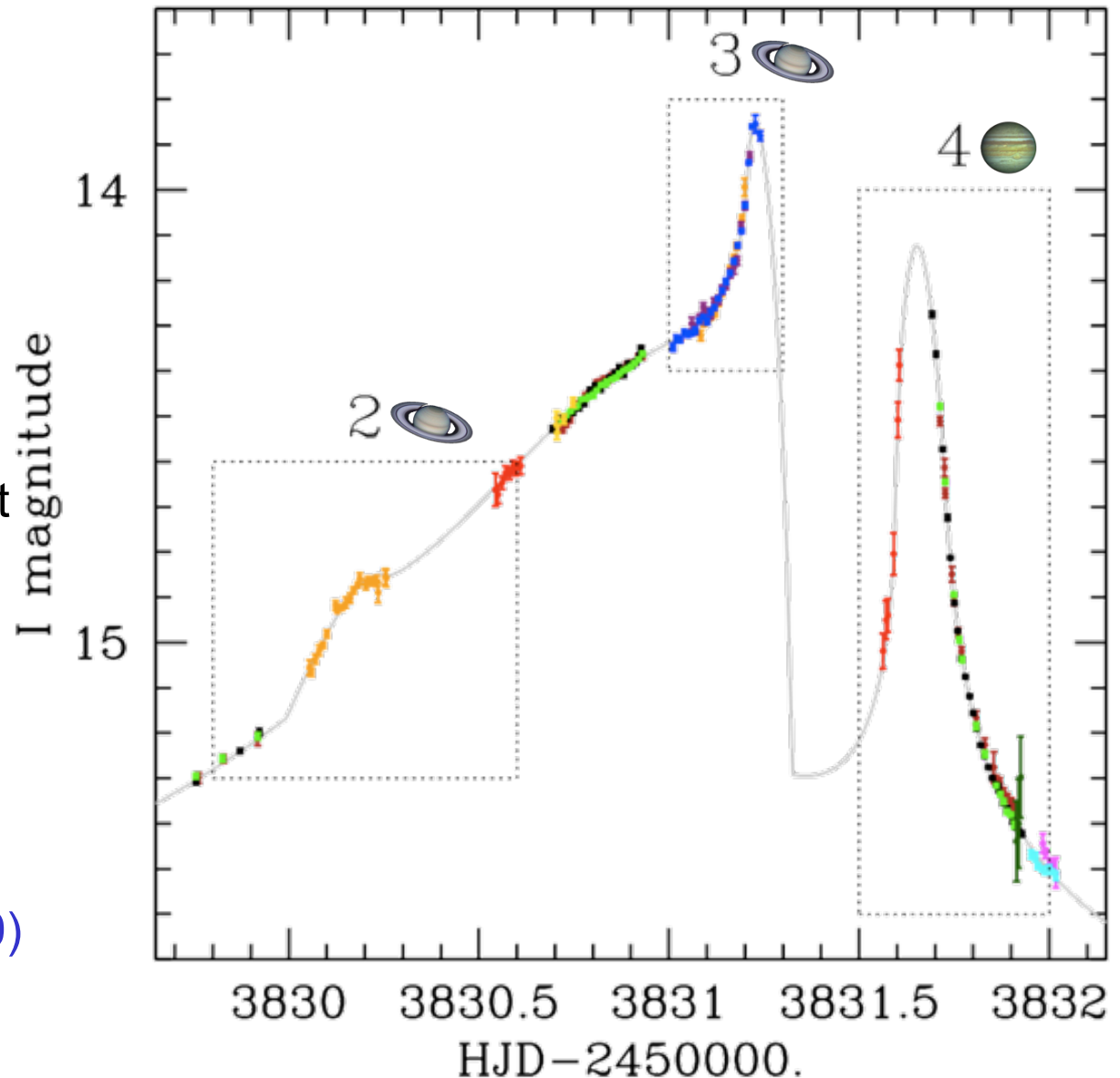


μFUN, OGLE, MOA & PLANET

# OGLE-2006-BLG-109 Light Curve Detail

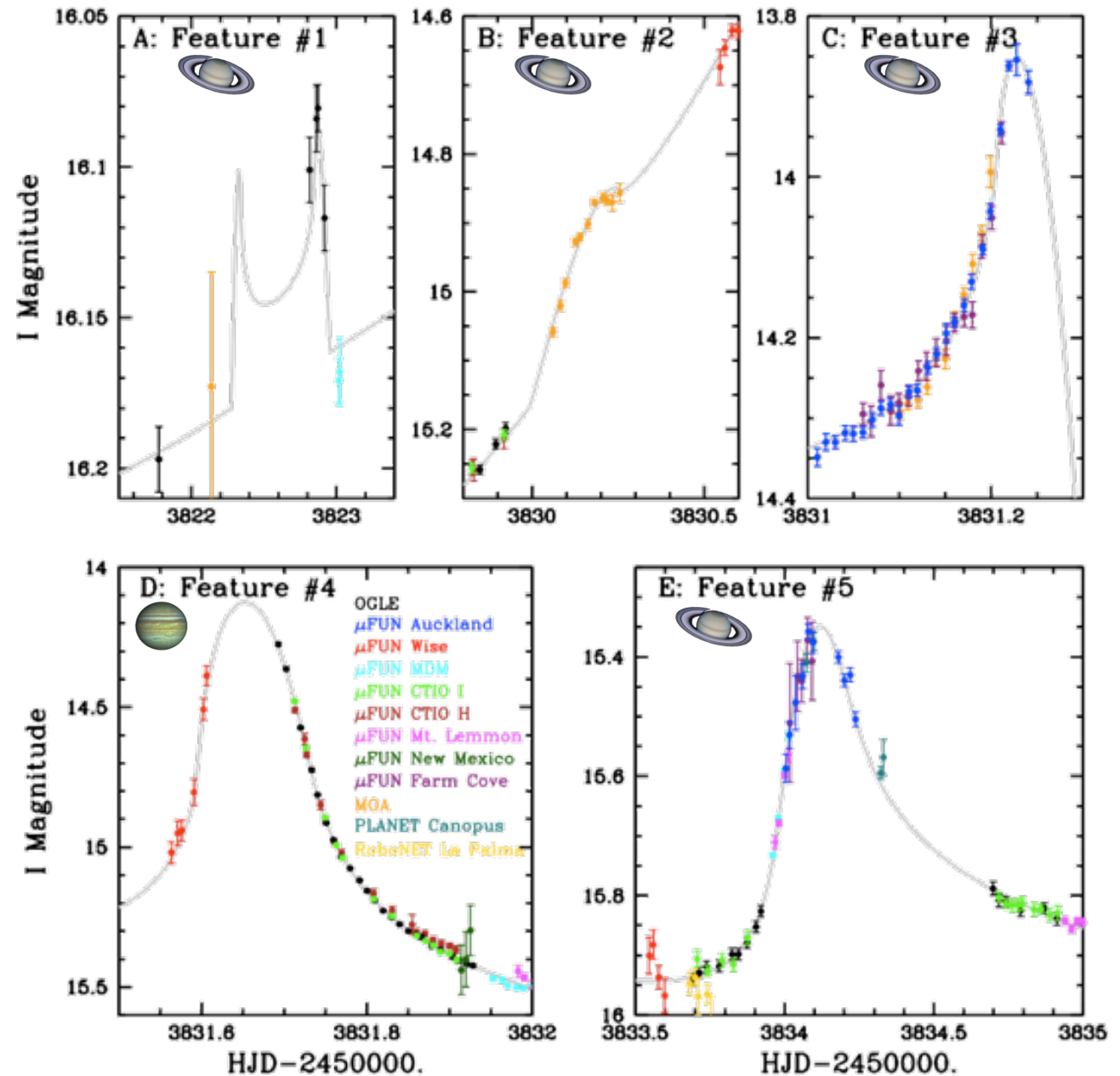
- OGLE alert on feature #1 as a potential planetary feature
- $\mu$ FUN (Gaudi) obtained a model approximately predicting features #3 & #5 prior to the peak
- But feature #4 was not predicted - because it is due to the Jupiter - not the Saturn

Gaudi et al (2008)  
Bennett et al (2010)

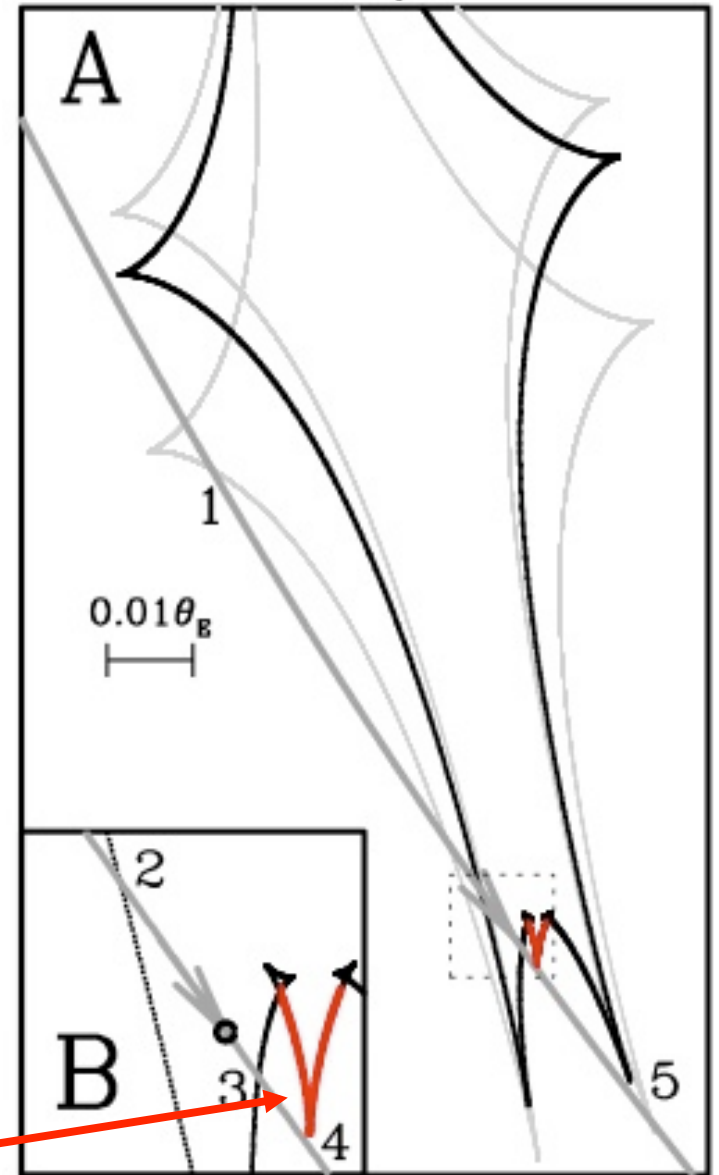
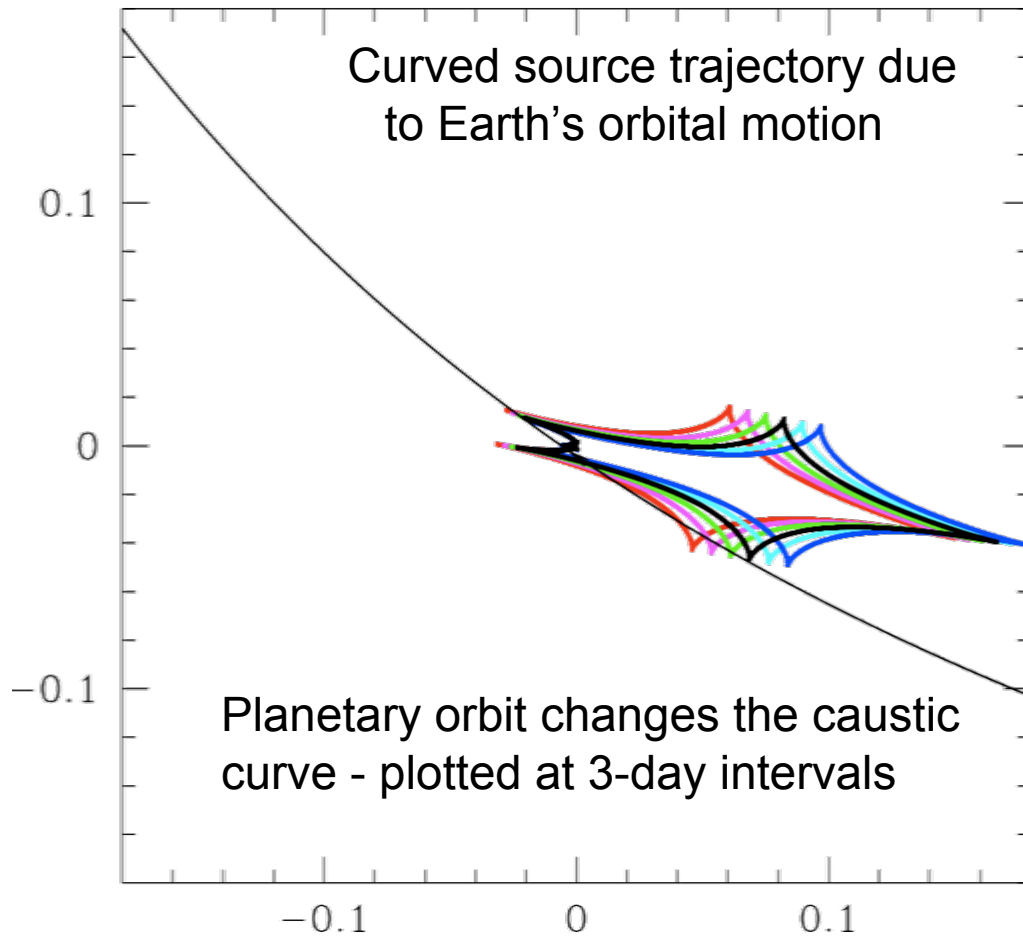


# OGLE-2006-BLG-109 Light Curve Features

- The basic 2-planet nature of the event was identified during the event,
- But the final model required inclusion of orbital motion, microlensing parallax and computational improvements (by Bennett).

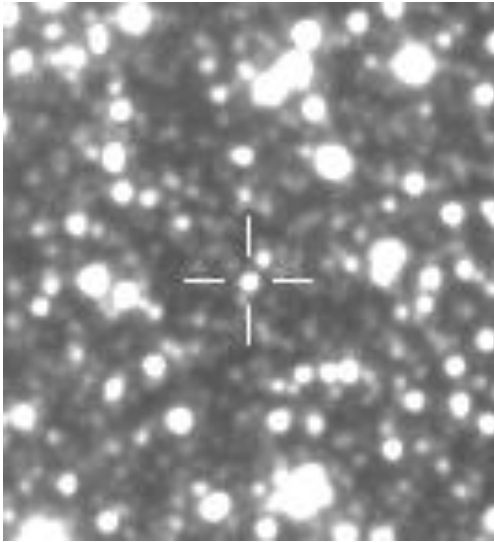


# OGLE-2006-BLG-109Lb,c Caustics

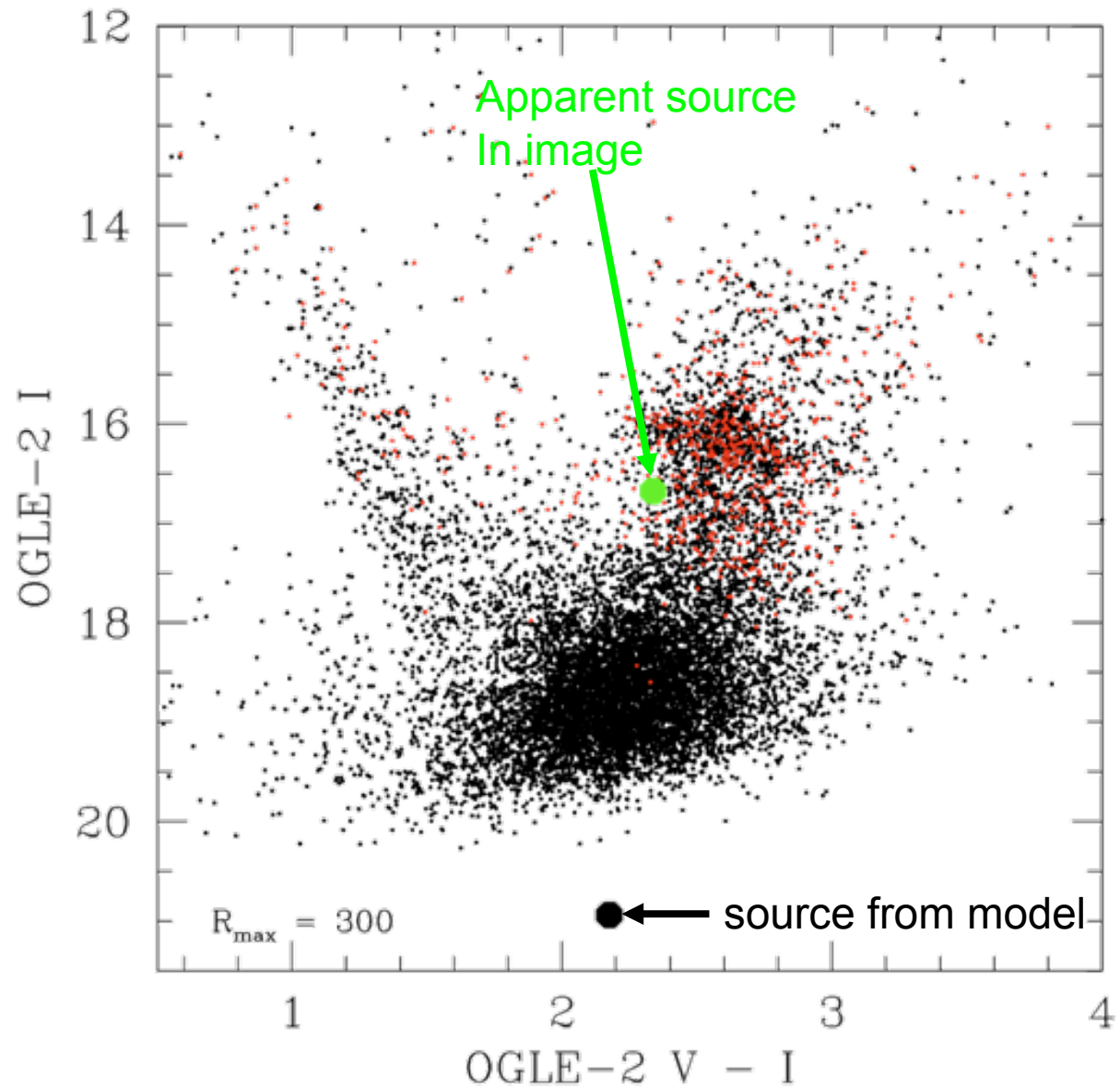


Feature due to Jupiter

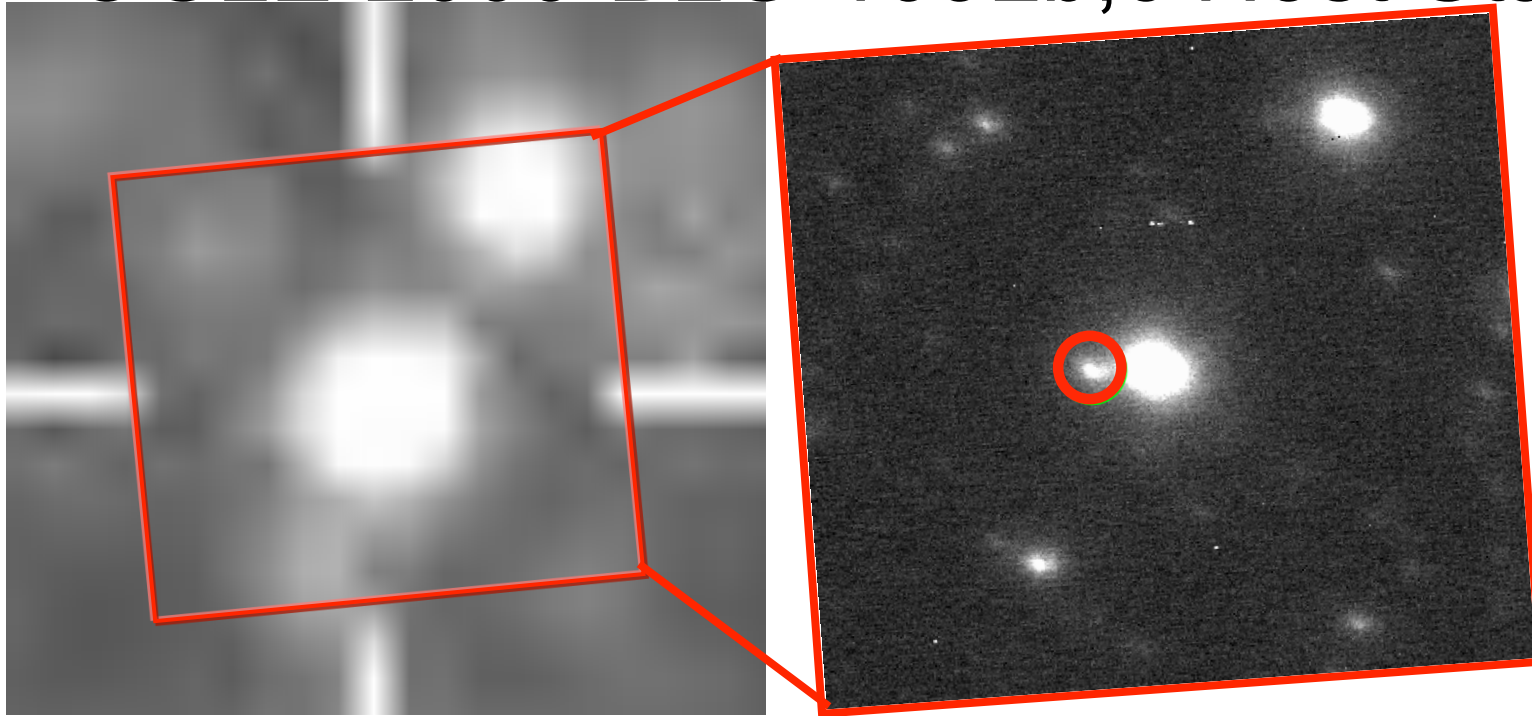
# OGLE-2006-BLG-109 Source Star



The model indicates that the source is much fainter than the apparent star at the position of the source. Could the brighter star be the lens star?



# OGLE-2006-BLG-109Lb,c Host Star



- OGLE images show that the source is offset from the bright star by 350 mas
- B. Macintosh: Keck AO images resolve lens+source stars from the brighter star.
- But, source+lens blend is 6 $\times$  brighter than the source (from CTIO H-band light curve), so the lens star is 5 $\times$  brighter than source.
  - H-band observations of the light curve are critical because the lens and source are not resolved
- Planet host (lens) star magnitude  $H \approx 17.17$ 
  - JHK observations will help to constrain the extinction toward the lens star

# Only Multiplanet System with Measured Masses

Host star mass:  $M_L = 0.52_{-0.07}^{+0.18} M_\odot$  from light curve model.

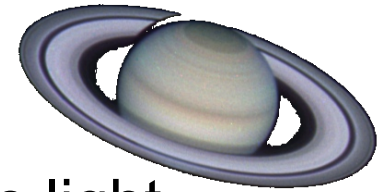
- Apply lens brightness constraint:  $H_L \approx 17.17$ .
- Correcting for extinction:  $H_{L0} = 16.93 \pm 0.25$ 
  - Extinction correction is based on  $H_L - K_L$  color
  - Error bar includes both extinction and photometric uncertainties
- Lens system distance:  $D_L = 1.54 \pm 0.13$  kpc

Host star mass:  $M_L = 0.51 \pm 0.05 M_\odot$  from light curve and lens H-magnitude.

Other parameter values:

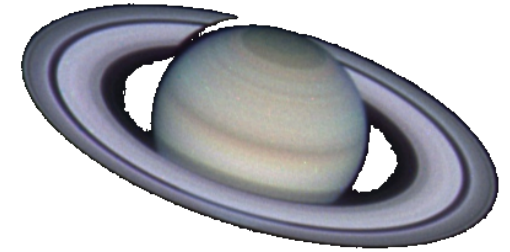
- “Jupiter” mass:  $m_b = 0.73 \pm 0.06 M_{\text{Jup}}$   
semi-major axis:  $a_b = 2.3 \pm 0.5 \text{ AU}$
- “Saturn” mass:  $m_c = 0.27 \pm 0.03 M_{\text{Jup}} = 0.90 M_{\text{Sat}}$   
semi-major axis:  $a_c = 4.5_{-1.0}^{+2.2} \text{ AU}$
- “Saturn” orbital velocity:  $v_t = 9.5 \pm 0.5 \text{ km/sec}$   
eccentricity:  $\varepsilon = 0.15_{-0.10}^{+0.17}$   
inclination:  $i = 63 \pm 6^\circ$

# Orbital Motion Modeling

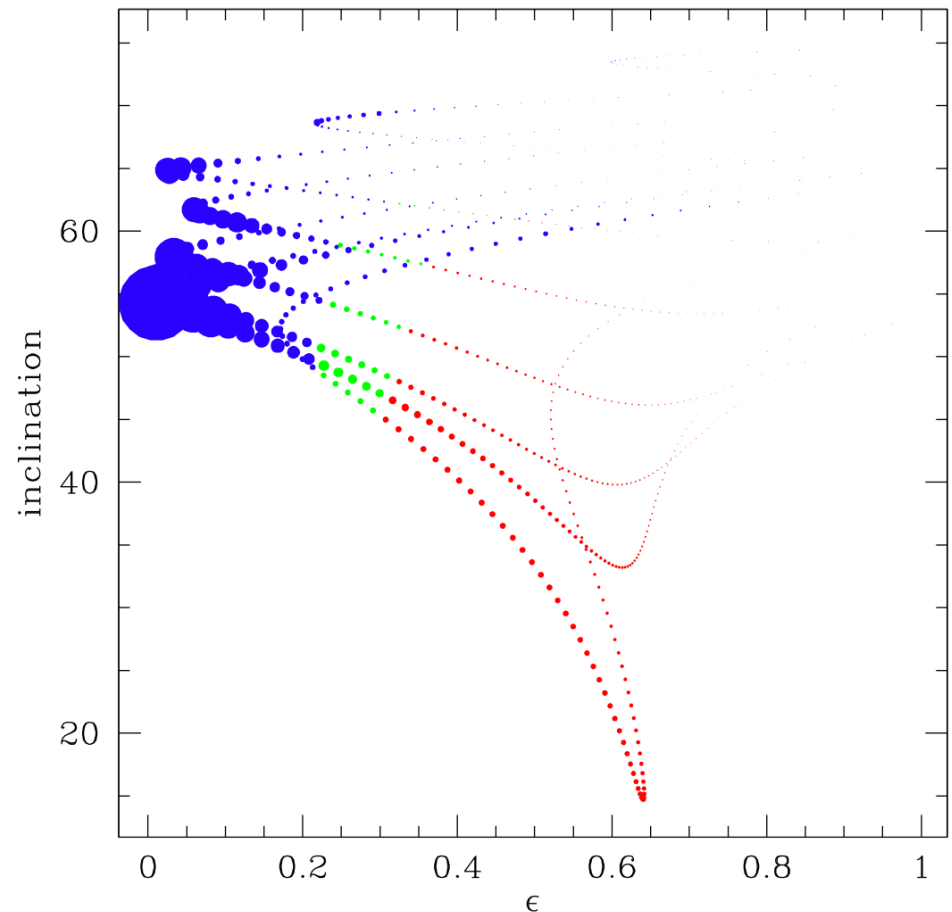


- 4 orbital parameters are well determined from the light curve
  - 2-d positions and velocities
  - Slight dependence on distance to the source star when converting to physical from Einstein Radii units
- Masses of the host star and planets are determined directly from the light curve
  - So a full orbit is described by 6 parameters (3 relative positions & 3 relative velocities)
  - A circular orbit is described by 5 parameters
- Models assume planetary circular motion
  - 2-d positions and velocities are well determined
  - Orbital period is constrained, but not fixed by the light curve
  - The orbital period parameter can be interpreted as acceleration or 3-d Star-Saturn distance (via  $a = GM/r^2$ )
- Details in Bennett et al (2010)

# Full Orbit Determination for OGLE-2006-BLG-109Lc

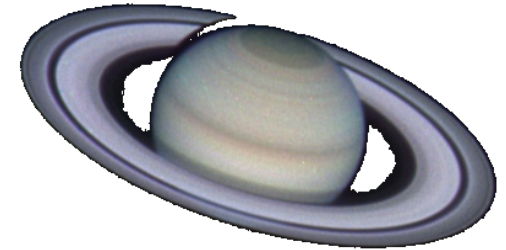


- Series of fits with fixed orbital acceleration (weight with fit  $\chi^2$ )
- Each fit corresponds to a 1-parameter family of orbits parameterized by  $v_z$ 
  - unless  $\frac{1}{2}(v_x^2 + v_y^2) - \frac{GM}{r} > 0$
- Assume the Jupiter orbits in the same plane and reject solutions **crossing** the Jupiter orbit or that are **Hill-unstable**
- Weight by prior probability of orbital parameters
  - planet is unlikely to be near periastron if  $\epsilon \gg 0$



Families of solutions corresponding to best models at various values of  $a$ .

# Full Orbit Determination for OGLE-2006-BLG-109Lc



- Full calculation using Markov chains run at fixed acceleration.
- Include only Hill-stable orbits
- results:

$$M_{LA} = 0.51 \pm 0.05 M_{\odot}$$

$$M_{Lc} = 0.27 \pm 0.03 M_J$$

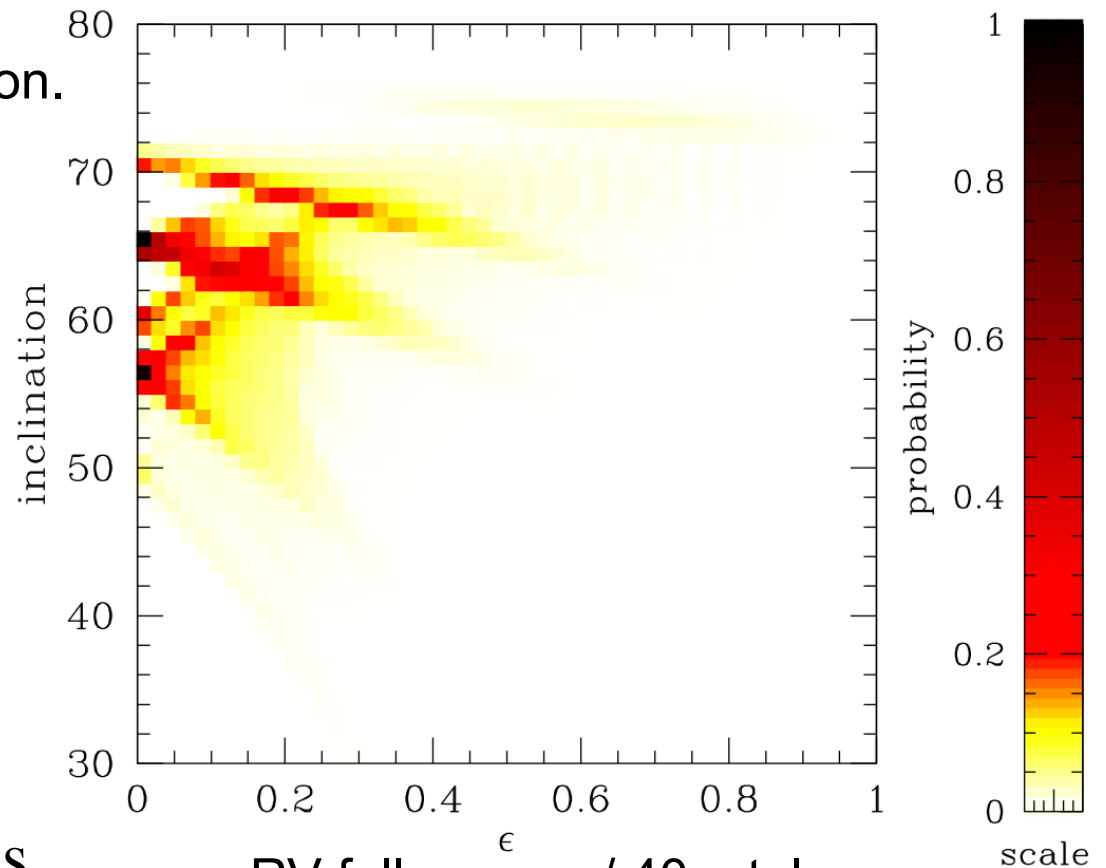
$$M_{Lb} = 0.73 \pm 0.07 M_J$$

$$a_{Lc} = 4.5^{+2.2}_{-1.0} \text{ AU}$$

$$a_{Lb} = 2.3 \pm 0.5 \text{ AU}$$

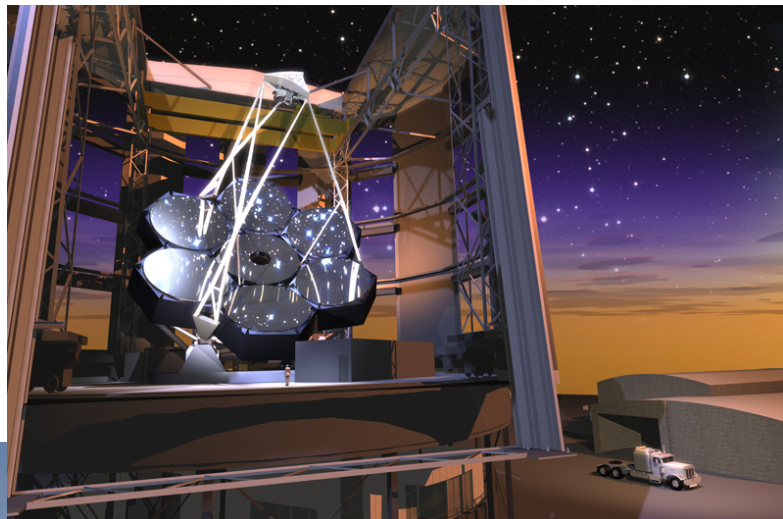
$$\text{inclination} = 64^{+4}_{-7} \text{ degrees}$$

$$\varepsilon = 0.15^{+0.17}_{-0.10}$$



- RV follow-up w/ 40m telescope  
-K = 19 m/sec (H = 17.2)

# Future Doppler Radial Velocity Confirmation



GMT - 22m aperture  
1<sup>st</sup> light in 2017



E-ELT – 42m aperture  
1<sup>st</sup> light in 2017



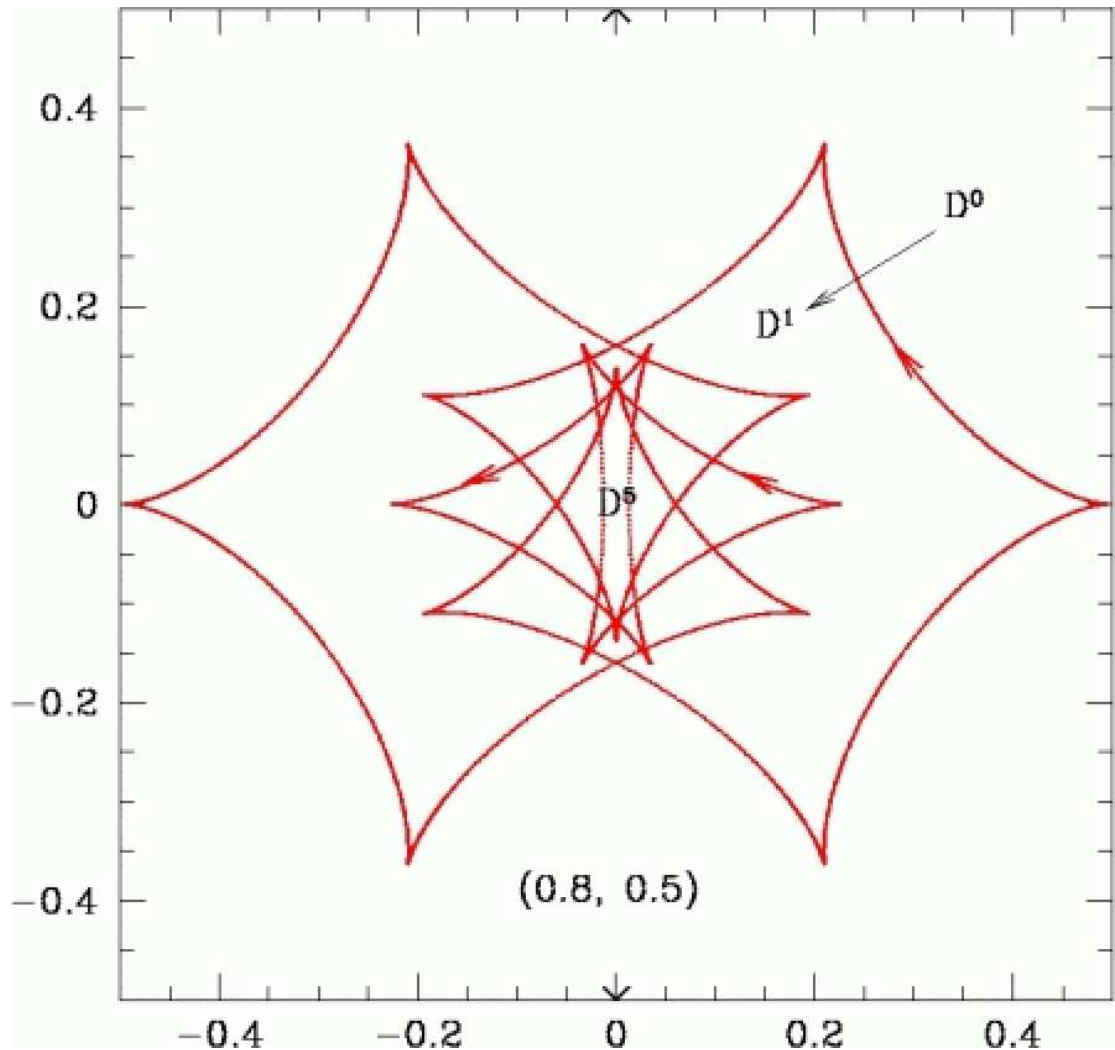
TMT – 30m aperture  
1<sup>st</sup> light in 2017

A high throughput, high resolution spectrograph on a 22-40m aperture telescope can measure the 19 m/s RV signal

# Lens Systems With $> 2$ Masses

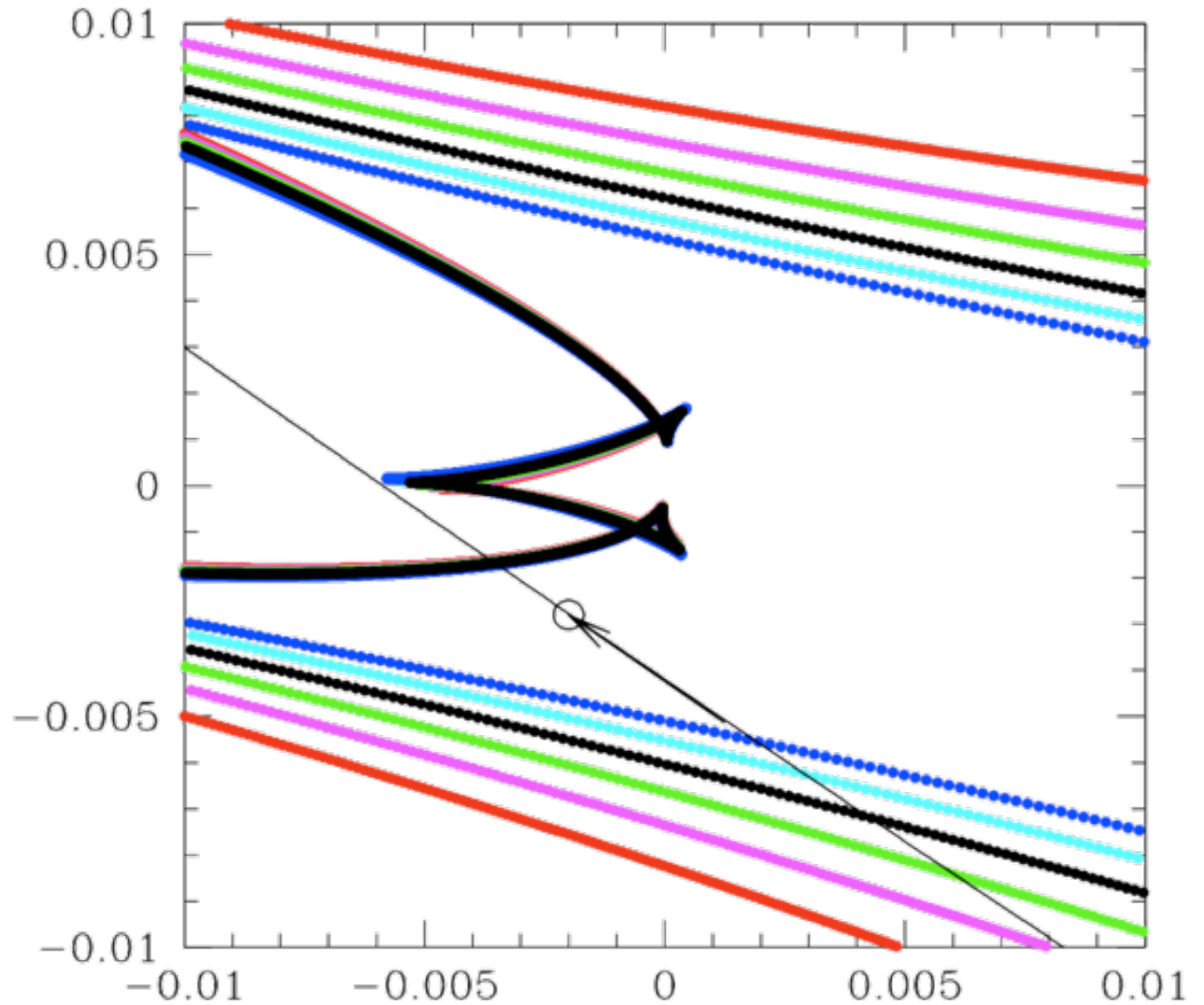
Systems like the 4 equal mass lens system with caustic structure shown at right, can be quite different from binary lenses. This system can will go from 5  $\rightarrow$  7  $\rightarrow$  9  $\rightarrow$  11  $\rightarrow$  13  $\rightarrow$  15 images if the source travels from region  $D^0$  to  $D^5$ .

But, such a configuration is very unlikely for a stable, bound system.

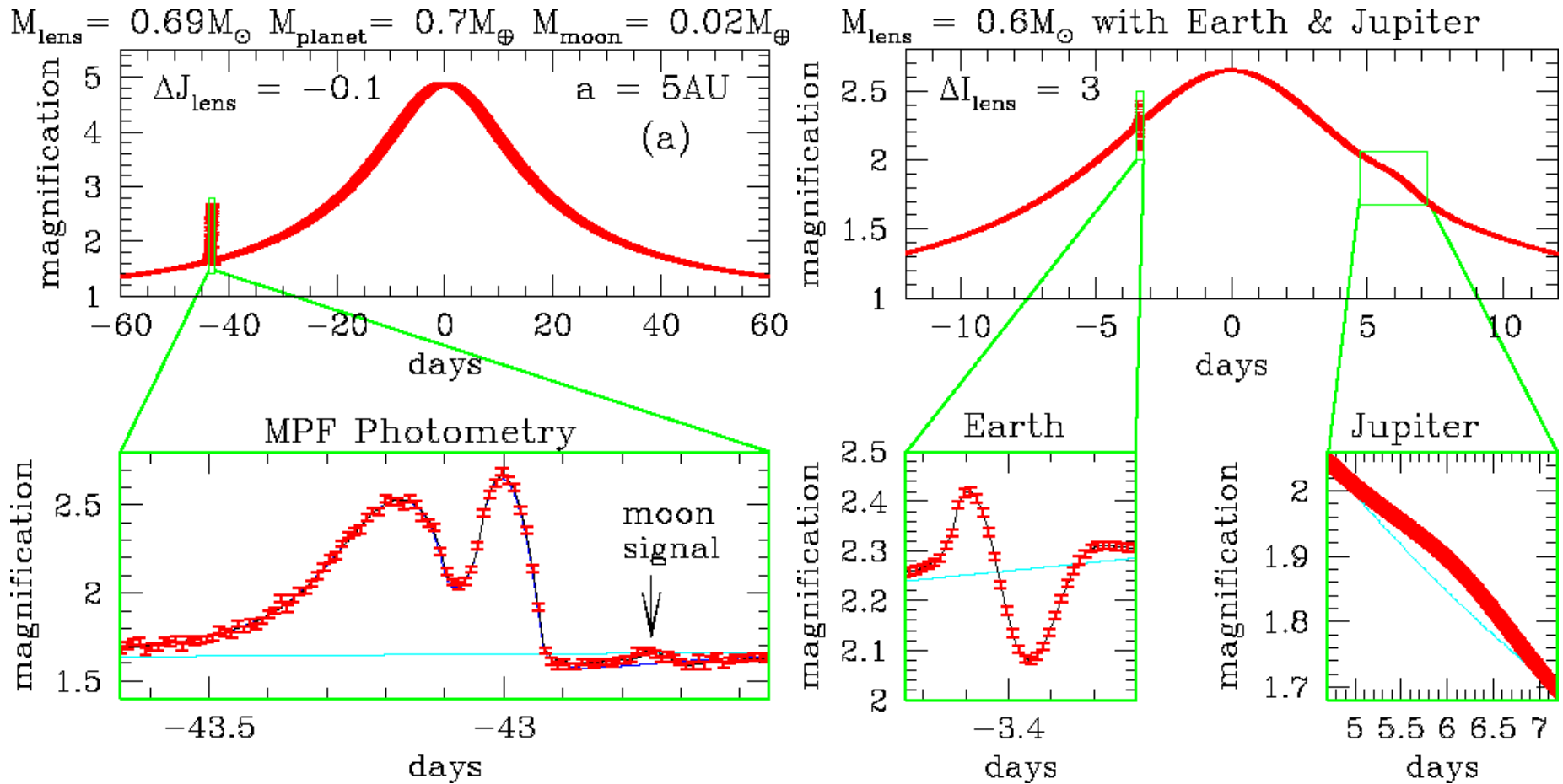


# OGLE-2006-BLG-109Lb,c Caustics

Nested caustics  
in realistic triple  
lens events are  
quite small.

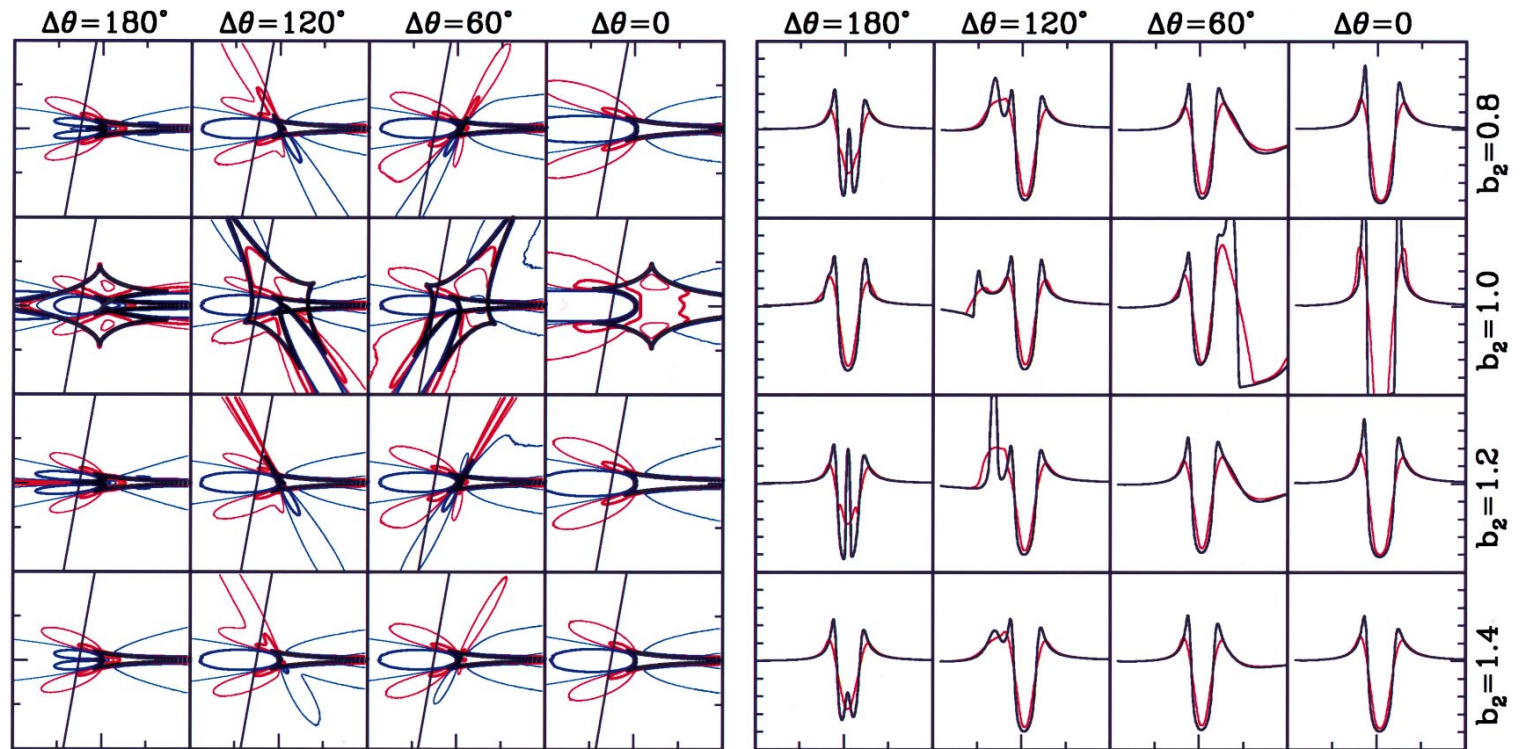


# WFIRST Will See > 2 Lens Systems in Low Magnification Events

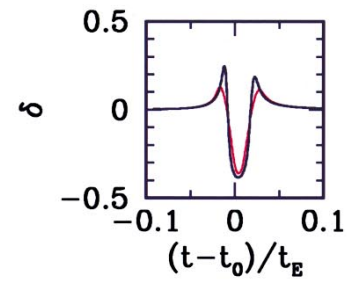
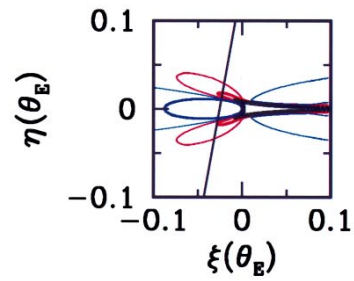


Planet + moon and 2-planet events from space-based microlensing simulations

# >2 Lens Events Are Easy to See in High-Mag Events



Planets (or stars) at a wide variety of positions influence the central caustic, and are therefore detectable.



Gaudi, Naber & Sackett (1998)

# Planetary Light Curve Calculations

- Lens Equation for point masses: 
$$w = z - \sum_{i=1}^n \frac{\epsilon_i}{\bar{z}_i - \bar{x}_i}$$
  - $w$ ,  $z$ , and  $x_i$  are the complex positions of the source, image, and lens masses
  - the inverse solution is simple: find the source position corresponding to an image position
- Binary lens solution (Schneider & Weiss 1986):
  - 2-mass equation can be converted to a 5th order complex polynomial, which has 5 solutions
  - 3 or 5 of these solutions are also solutions to the original lens equation
  - can be solved with an efficient numerical method
- Triple lens solution (Rhie 2002: astro-ph/0202294)
  - 3-mass equation can be converted to a 10th order complex polynomial with 10 solutions
  - 4, 6, 8, or 10 of these are also solutions of the lens equation
- Quadruple lens solution (Rhie, unpublished; Sullivan, unpublished)
  - 4-mass equation should be converted into a 17th order complex polynomial

# Triple Lens Equation

$$0 = \sum_{k=1}^{10} \text{cff}(k) z^k$$

$$\begin{aligned} \text{cff}(k) = & ( H_{0k-1} + H_{1k-1} a_\omega + H_{2k-1} b_\omega + H_{3k-1} c_\omega ) \\ & - ( H_{0k} \omega + H_{1k} (\omega a_\omega - 1) + H_{2k} (\omega b_\omega + a_\omega - \bar{\omega}) + H_{3k} (\omega c_\omega + b_\omega) ) \end{aligned}$$

$$H_{39} = 1; H_{38} = 3a; H_{37} = 3b + 3a^2; H_{36} = 3c + 6ab + a^3; H_{35} = 6ac + 3b^2 + 3a^2b; H_{34} = 6bc + 3a^2c + 3ab^2; H_{33} = 3c^2 + 6abc + b^3; H_{32} = 3ac^2 + 3b^2c; H_{31} = 3bc^2; H_{30} = c^3.$$

$$H_{28} = 1; H_{27} = 3a; H_{26} = d + 2b + 3a^2; H_{25} = 2ad + 4ab + a^3 + 2c; H_{24} = 2db + da^2 + 4ac + 2a^2b + b^2; H_{23} = 2dc + 2dab + 2a^2c + ab^2 + 2bc; H_{22} = 2cad + db^2 + 2abc + c^2; H_{21} = 2bcd + ac^2; H_{20} = c^2d$$

$$H_{17} = 1; H_{16} = 3a; H_{15} = 2d + 3a^2 + b; H_{14} = 4ad + a^3 + 2ab + c; H_{13} = d^2 + 2a^2d + 2bd + ba^2 + 2ac; H_{12} = ad^2 + 2abd + 2cd + ca^2; H_{11} = bd^2 + 2acd; H_{10} = cd^2$$

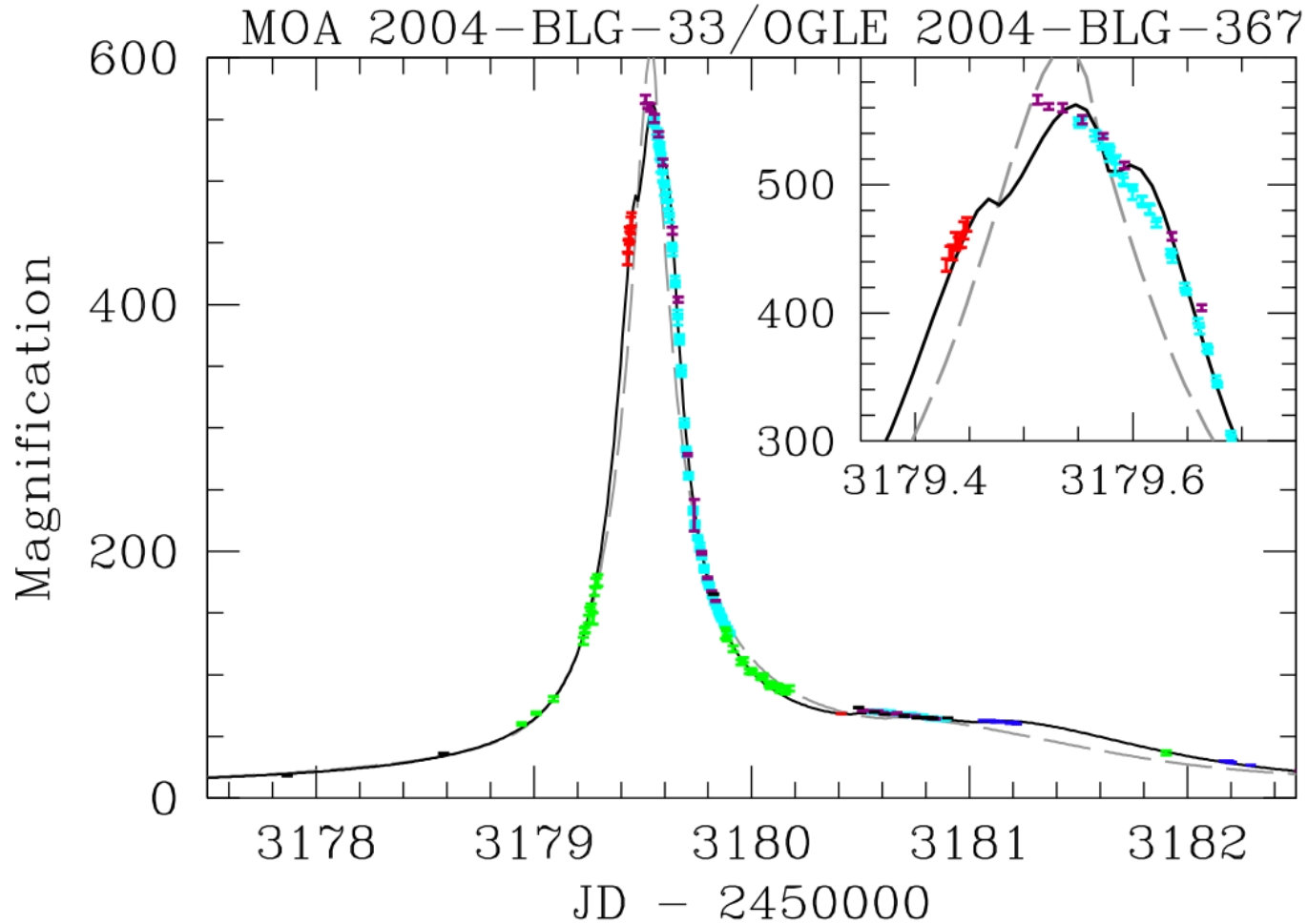
$$H_{06} = 1; H_{05} = 3a; H_{04} = 3d + 3a^2; H_{03} = 6ad + a^3; H_{02} = 3d^2 + 3a^2d^2; H_{01} = 3ad^2; H_{00} = d^3$$

- Rhie (2002) – 10<sup>th</sup> order polynomial equation
  - Equation solution sometimes requires quadruple (128-bit) precision
- Enables image centered ray shooting and hexadecapole

# Modeling Events with Higher Order Effects

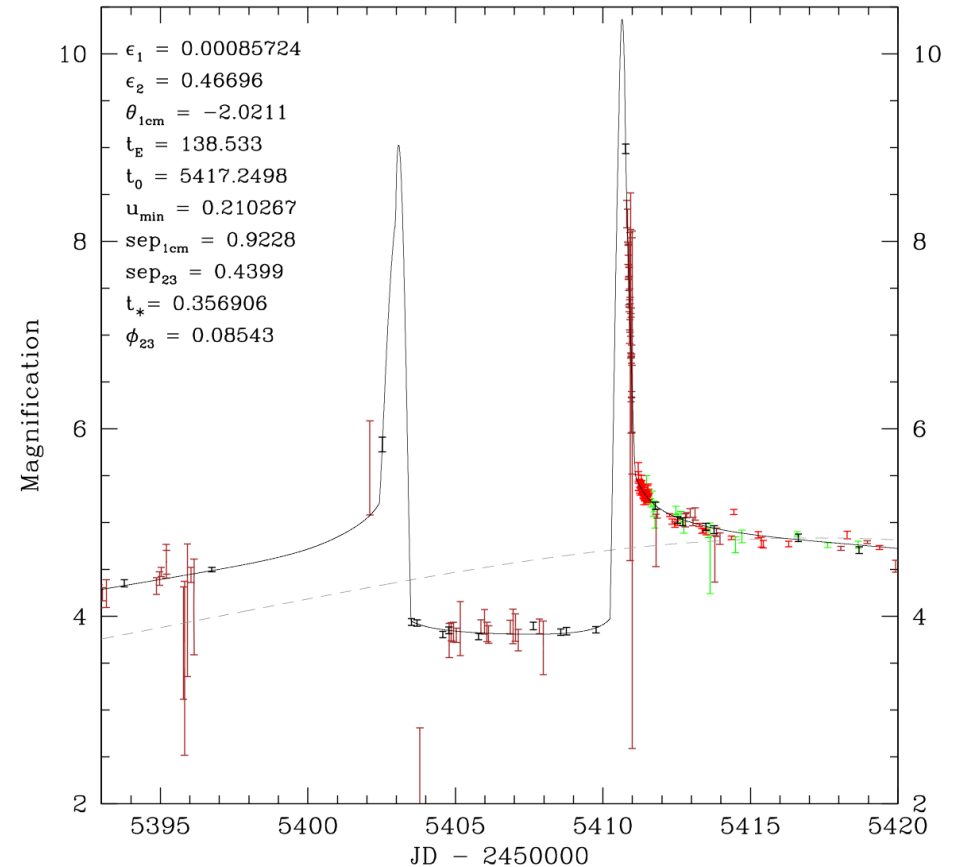
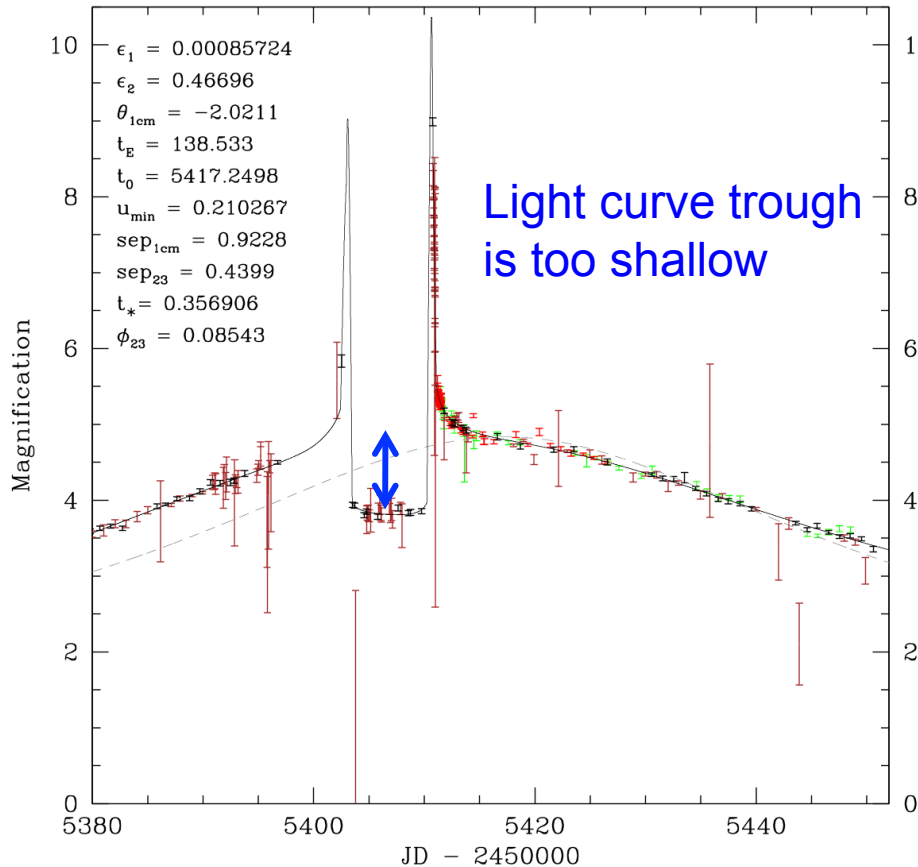
1. Investigate simplest models first, even if they don't seem so likely
  - They are easier to investigate, and you will need to exclude them to argue for a more complicated model.
2. Identify characteristic features such as caustics and cusp crossings
  - This can allow relatively easy identification of the correct caustic geometry in events like OGLE-2006-BLG-109
  - Cross-calibrate and combine data sets to avoid models with incorrect relative normalizations
3. Consider all possible models that might explain the data
  - Use your “internal” catalog of events
  - It will often be unclear which higher order effects are important
4. When possible, try perturbative approach – adding higher order effect sequentially in order of their importance.
5. If perturbative approach doesn't work, then a blind search over a high dimensional parameter space is needed
  - Use all possible tricks to speed up your light curve calculations

# Example: MOA-2004-BLG-33



- Triple-lens, circumbinary planet models provide an approximate fit, but do not match the detailed light curve shape – caustic features in model but not data
- Joe Ling found a much simpler Xallarap model (without a planet)

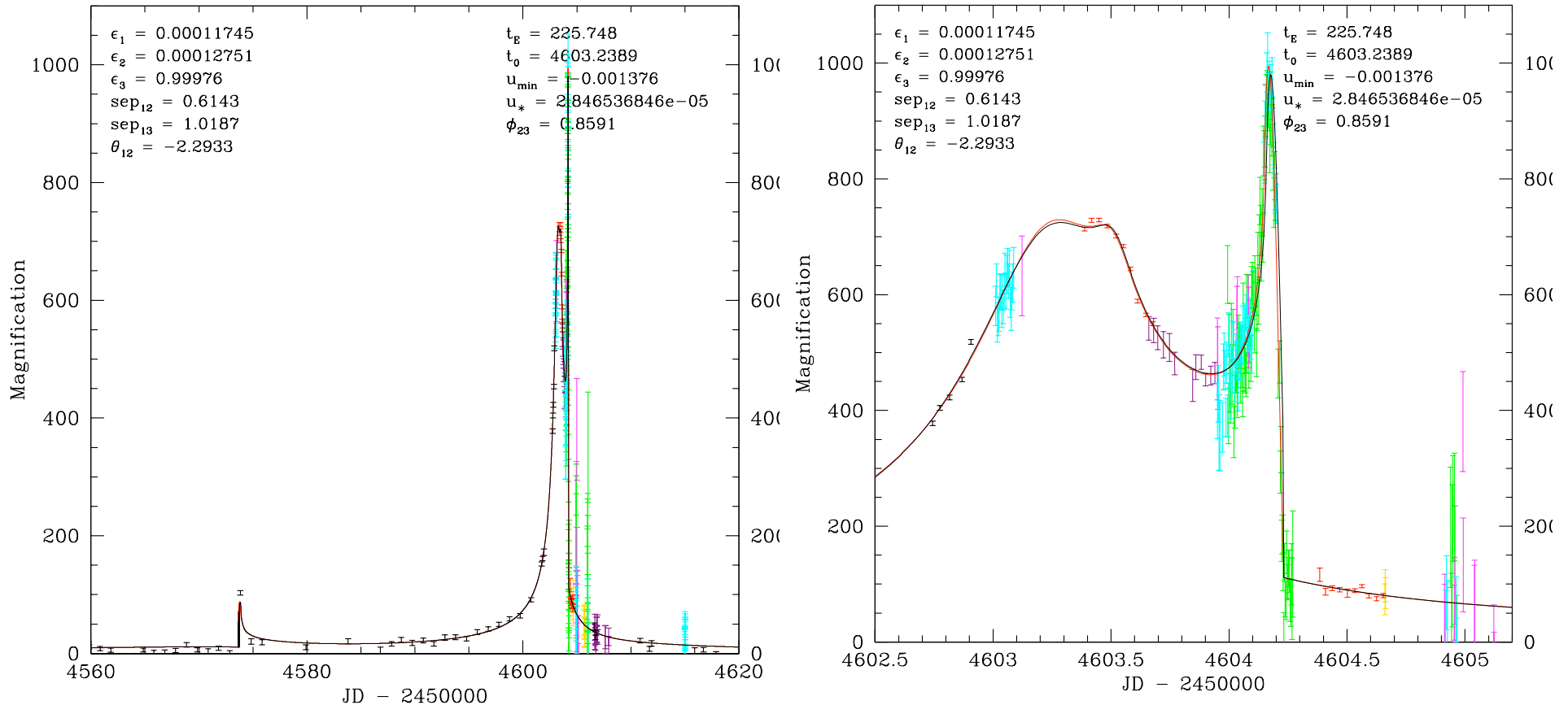
# Example: MOA-2010-BLG-117



MOA-2010-BLG-117 deviation looks like a minor image caustic perturbation, but the depth of the trough is too shallow.

- A circumbinary model is shown
- An alternative model is a binary source model, where the magnification of the 2<sup>nd</sup> lens helps to fill in the trough

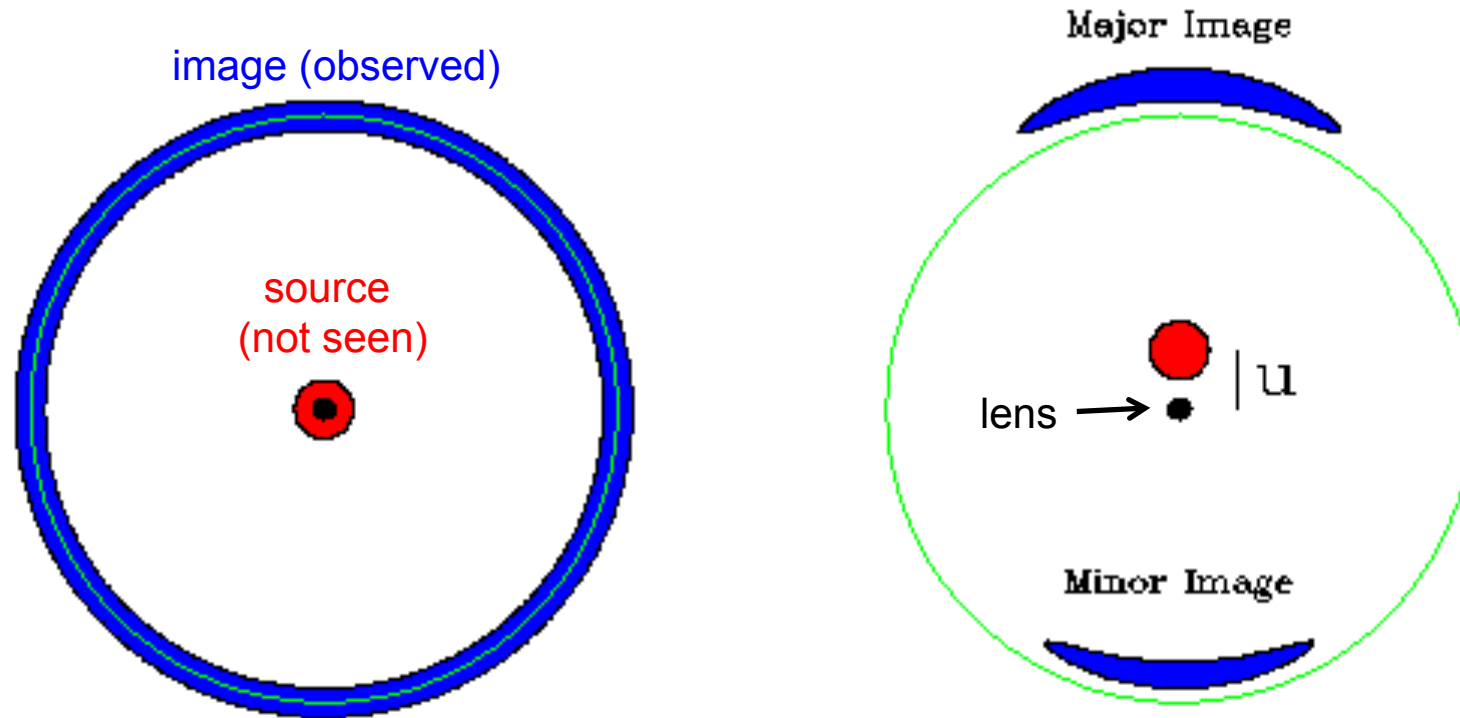
# Example: OGLE-2008-BLG-270



Incomplete light curve sampling, and somewhat noisy data from small telescopes make this event challenging

- a 1<sup>st</sup> attempt at a perturbative solution doesn't seem to work
- Nearly 30 days from caustic entrance to exit -> orbital motion important
- A high dimensional parameter-space search may be needed.

# High-Mag Modeling => Almost Einstein Ring



Images are squished in radial direction by a factor of 2, but stretched in the angular direction by a factor of  $A$ , so the angular to radial dimension of the image is  $\sim 2A$ , which is usually  $> 200$

# Microlensing Modeling Challenges

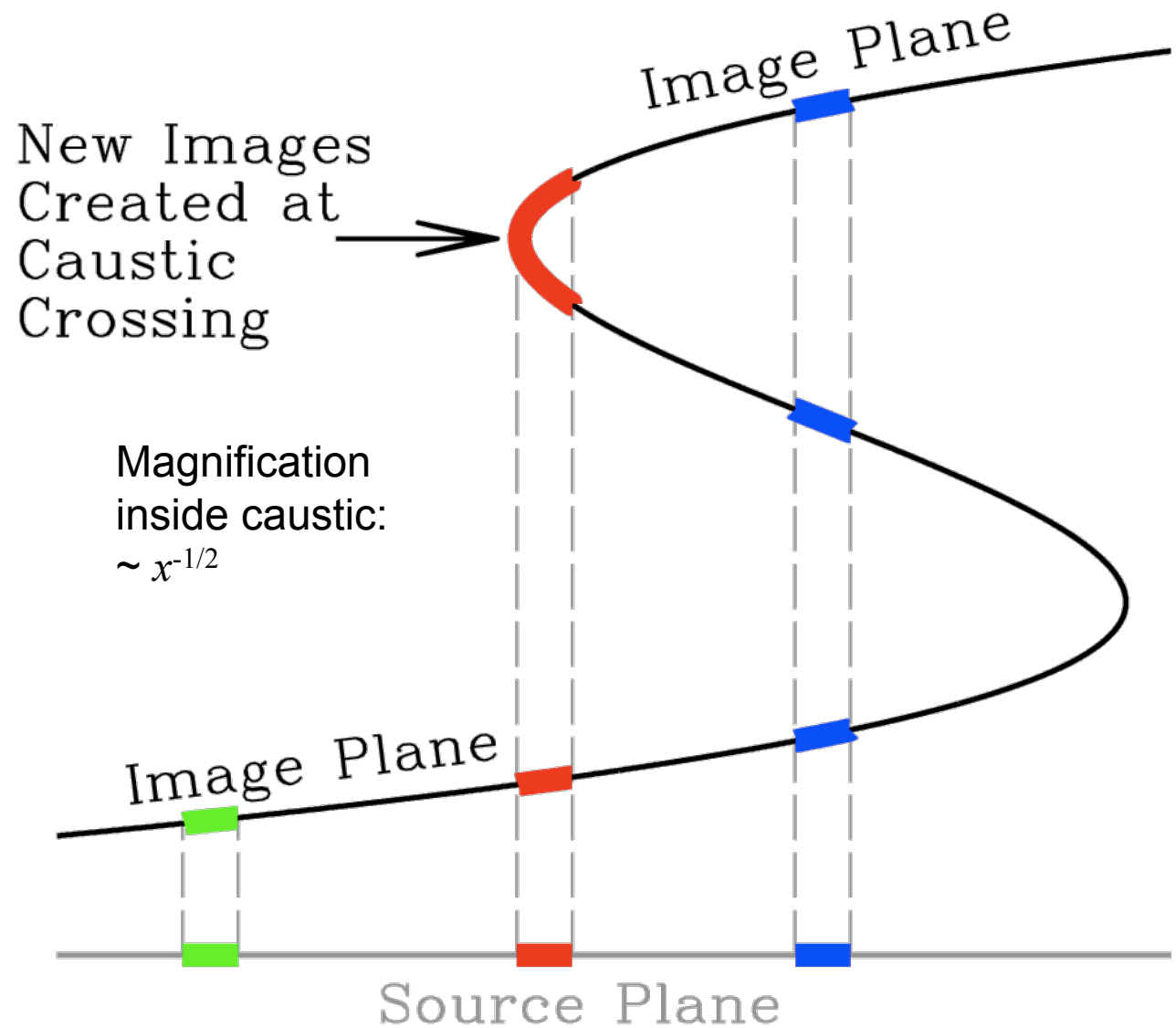
- High Magnification events
  - extreme image distortion implies cpu-intensive magnification calculations
  - high sensitivity means multi-planet sensitivity
    - higher dimensional parameter space
  - “resonant” caustic events
    - large caustic => orbital motion  $\sim 0.001 R_E/\text{day}$
- Standard modeling methods may fail
- Method designed to handle multi-planet events with orbital motion
  - Based on the method used to solve OGLE-2006-BLG-109Lb,c
  - can be used for any event, but optimized for high-mag

# The Need for Precision

- When systematic errors can be controlled, we can get photometry good to a few mmag for high-mag events
- But, stellar limb darkening profiles are not known to better than 1%
  - this implies light curve errors of up to a few mmag because limb darkening models are imperfect
- Nevertheless, it is useful to have light curve calculations precise to  $\sim 0.01\%$  or better
  - Low precision implies rough  $\chi^2$  surface
  - Markov Chain-like modeling methods optimize the numerical errors to minimize  $\chi^2$
  - Low precision calculations tend to get “stuck” at (spurious) local  $\chi^2$  minima
- In practice, linear limb darkening is usually sufficient

# New Lens Image Pairs Appear on Caustics

- Image plane = what we would see if there was no lens
- Source plane = what we really see
- The lensing event can be described as the mapping from the source plane to the image plane.
- Highest magnification occurs at caustic crossings



# Magnification from Lens Equation

- The magnification for a point source can be derived from the Jacobian determinant of the lens equation:

$$J = \frac{\partial w}{\partial z} \frac{\partial \bar{w}}{\partial \bar{z}} - \frac{\partial w}{\partial \bar{z}} \frac{\partial \bar{w}}{\partial z} = 1 - \left| \frac{\partial w}{\partial \bar{z}} \right|^2$$

- Where

$$\frac{\partial w}{\partial \bar{z}} = \sum_i \frac{\varepsilon_i}{(\bar{z} - \bar{x}_i)^2}$$

- This is the Jacobian determinant of the inverse mapping from the image to the source plane, so the magnification for each image is given by

$$A = \frac{1}{|J|}$$

evaluated at the position of each image

- Critical curves are image locations where  $|J| = 0$
- Caustics are the corresponding source locations

# Beyond the Point-Source Approximation

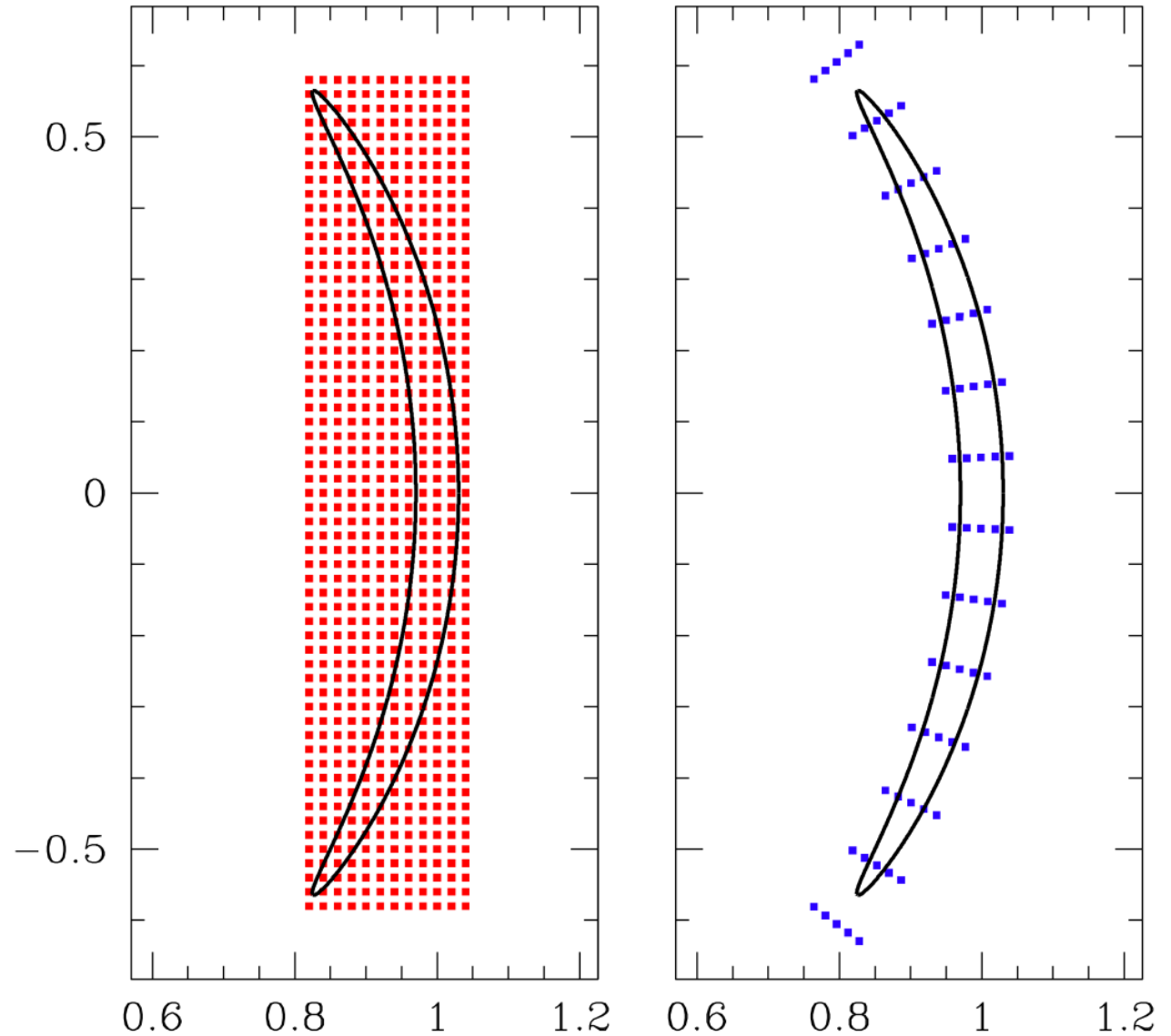
- Hexadecapole approx. (Pejcha & Heyrovsky 2009, Gould 2008)
  - Uses 13 point “grid” in the source plane
  - Cannot be used during caustic crossings
  - Not general, but fast
  - Best when combined with more general method
- Brute force ray-shooting (i.e. Wambsganss 1997)
  - Can be used for complicated static systems
    - i.e. many masses or continuous mass distribution
  - Becomes extremely slow for an orbiting lens system

# Beyond the Point-Source Approximation 2

- Image Centered Ray-Shooting (Bennett & Rhie 1996)
  - First general method for binary lens systems with finite sources
  - Used to show that microlensing can detect exo-Earths
  - use point source approximation except when the source is close to a caustic or image is close to a caustic curve
  - Shoot rays from point-source image centers plus any partial images where the disk (but not the center of the source) crosses a caustic
    - grids grow until the grid boundary is outside the image
  - For a high magnification static lens system, we can save the rays shot close to the Einstein ring.
  - Polar coordinate and limb-darkening integration improvement
    - (Bennett 2010) – presented here
  - This method was used for all planetary microlensing discoveries
    - Primary or back-up analysis
- Stokes or Green's Theorem (Gould & Gaucherel 1997; Bozza 2010)
  - Very fast for uniform source
  - Competitive for realistic limb darkened sources

# Ray-Shooting Grids

- High magnification events are the most time consuming to calculate due to highly elongated images
- Polar coordinates can sample the long image axis with  $< 1/16$  of the grid points of a Cartesian coordinate system.



# High Precision: 2<sup>nd</sup> Order Numerical Integration

Building blocks of 2<sup>nd</sup> order schemes (Numerical Recipes, Press et al.)

Trapezoidal rule: 
$$\int_{x_1}^{x_2} f(x) dx = h \left( \frac{1}{2} f_1 + \frac{1}{2} f_2 \right) + O(h^3 f'')$$

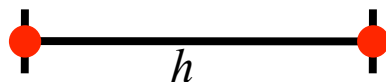
Mid-point rule:

$$\int_{x_{1/2}}^{x_{3/2}} f(x) dx = hf_1 + O(h^3 f'')$$

# Numerical Integration of Limb-darkened Images

Building blocks of 1-dimensional 2<sup>nd</sup> order numerical integration schemes

trapezoidal rule



$$\int_{x_1}^{x_2} f(x) dx = h \left( \frac{1}{2} f_1 + \frac{1}{2} f_2 \right) + O(h^3 f'')$$

midpoint rule



$$\int_{x_{1/2}}^{x_{3/2}} f(x) dx = h f_1 + O(h^3 f'')$$

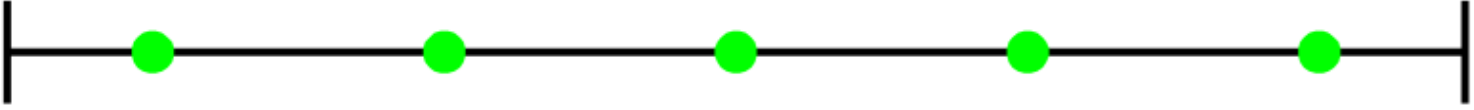
Standard 1-dimensional integration schemes can be built from these simple formulae (see e.g. *Numerical Recipes* by Press et al.)  
Build a scheme of 2<sup>nd</sup> order or higher accuracy

# Numerical Integration of Limb-darkened Images



extended trapezoidal rule

$$\int_{x_1}^{x_N} f(x) dx = h \left[ \frac{1}{2} f_1 + f_2 + f_3 + \dots + f_{N-1} + \frac{1}{2} f_N \right] + O\left(\frac{(x_N - x_1)^3 f''}{N^2}\right)$$



extended midpoint rule

$$\int_{x_{1/2}}^{x_{N+1/2}} f(x) dx = h [f_1 + f_2 + f_3 + \dots + f_{N-1} + f_N] + O\left(\frac{(x_{N+1/2} - x_{1/2})^3 f''}{N^2}\right)$$

For lensing calculations, we must calculate the grid points before we find the boundaries



$$\int_{x_a}^{x_b} f(x) dx = h_1 f_1 + h [f_2 + f_3 + \dots + f_{N-1}] + h_N f_N + O\left(\frac{(x_b - x_a)^3 f''}{N^2}\right)$$

$$h_1 = x_{3/2} - x_a \quad h_N = x_b - x_{N-1/2}$$

modifying the boundary step size would seem to restore 2nd order accuracy

# 1-Dimensional Integral of Limb Darkened Source

- Normally, we assume that the integrand is approximated by a power law in  $(x - x_L)$  where  $x_L$  is the position of the limb
- But, a limb darkened source is better approximated by a power law in  $\sqrt{x - x_L}$
- Require that the difference scheme is exact for low order power law functions in  $\sqrt{x - x_L}$  instead of  $(x - x_L)$
- Standard 2<sup>nd</sup> order schemes have error terms that scale as  $\sim h^{3/2}$  and are actually order 1.5
- A relatively simple scheme works best
- Formally higher order schemes are sometimes worse

# Integrating Over Limb-darkened Images

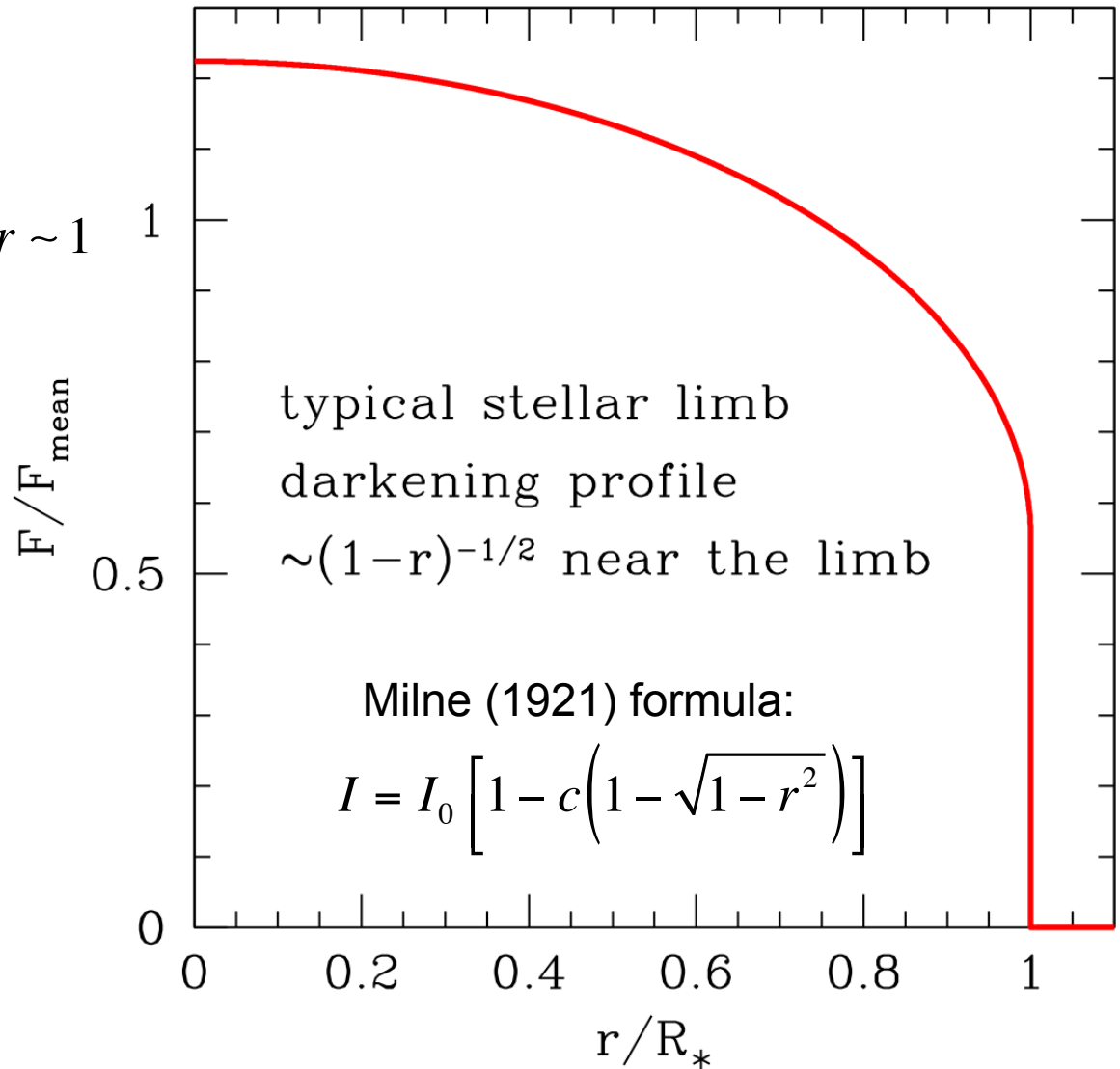
- But

$$\left( \frac{(x_{\max} - x_{\min})^3 f''}{N^2} \right) = \infty$$

both  $f'$  and  $f''$  diverge at  $r \sim 1$

for  $f \sim (1-r)^{1/2}$

- This ruins the 2nd order accuracy of the differencing scheme
- Of course, we integrate in the image plane where the stellar profile is distorted, but the  $(1-r)^{1/2}$  behavior remains near the limb



# An Attempt at a 2<sup>nd</sup> Order Scheme

This is formally 2<sup>nd</sup> order accurate for a “linear” limb darkening profile:

$$\int_{x_L}^{x_{3/2}} f(x) dx = h \left( \frac{1}{2} + \delta \right) \left[ (1 - b) f_L + b f_1 \right] ,$$

where  $\delta = (x_1 - x_L) / h$  , and

$$b = \frac{2}{3} \sqrt{\frac{\delta + \frac{1}{2}}{\delta}}$$

but the  $b$  gets very large for  $\delta \sim 0$ , so this formula is applied only for  $b \geq b_c$  where  $b_c \sim 0.15$  has been determined to be optimal empirically

This method does turn out to be 2<sup>nd</sup> order in some cases, but in other cases  $\sigma \sim h^{3/2}$ , but precision is improved by a factor of  $\sim 10$

Computational overhead of finding the boundary is a factor of 1.5-2

# 2<sup>nd</sup> Order Integration Scheme for Limb Darkened Sources

- A relatively simple scheme cancels

$$\int_{x_L}^{x_{3/2}} f(x) dx = h \left( \frac{1}{2} + \delta \right) [(1 - b)f_L + bf_1]$$

where

$$b = \frac{2}{3} \sqrt{\frac{\delta + \frac{1}{2}}{\delta}}$$

- But  $b$  can get very large when  $\delta \rightarrow 0$
- Small  $\delta$  values can lead to large numerical errors
  - presumably due to large coefficients for higher order error terms

# Implement a Cut-Off

- For  $\delta < \delta_c$  use a lower order integration scheme

$$\int_{x_{L1}}^{x_{L2}} f(x) dx = h (A_1 f_{L1} + B_1 f_1 + f_2 + \dots + f_{N-1} + B_2 f_N + A_2 f_{L2})$$

with coefficients given by

$$A_i = \left( \frac{1}{2} + \delta_i \right) (1 - b_i) \Theta(\delta_i - \delta_c) + \frac{\delta_i}{3} \Theta(\delta_c - \delta_i)$$

$$B_i = \left( \frac{1}{2} + \delta_i \right) b_i \Theta(\delta_i - \delta_c) + \left( \frac{2}{3} \delta + \frac{1}{2} \right) \Theta(\delta_c - \delta_i)$$

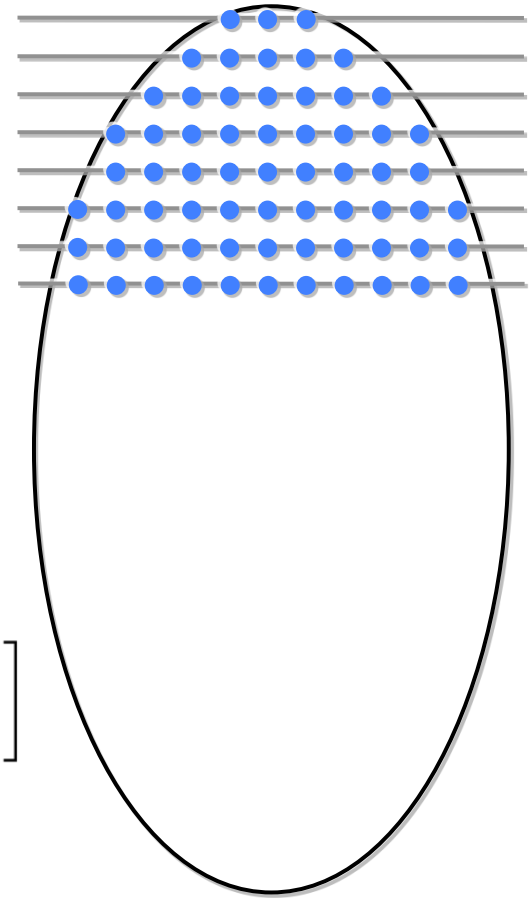
- The cut-off means that the differencing method is formally only order 1.5 accurate, but empirically, this works best.

# 2<sup>nd</sup> Dimensional Integration

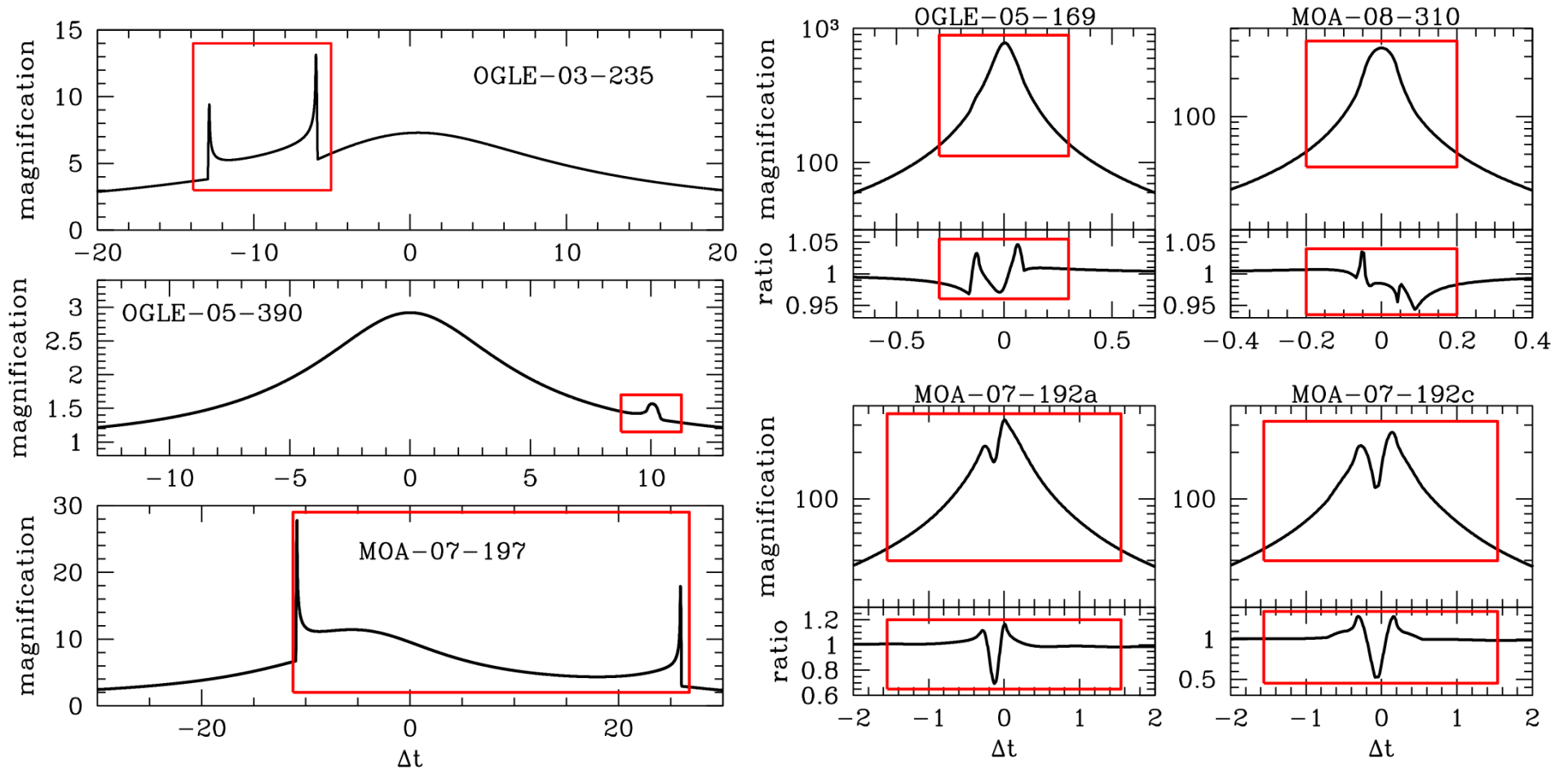
- $y$  – direction
- Integrate over rows
- Integration over  $x$  removes the derivative singularity due to  $\sqrt{y - y_L}$  terms
- If  $F_i$  indicates the integral of the  $i$ -th row, the formula

$$\int_{y_L}^{y_{5/2}} F(y) dy = h \left[ \left( \frac{3}{8} + \eta + \frac{\eta^2}{2} \right) F_1 + \left( \frac{9}{8} - \frac{\eta^2}{2} \right) F_2 \right]$$

makes the  $y$  – direction integral 2<sup>nd</sup> order accurate

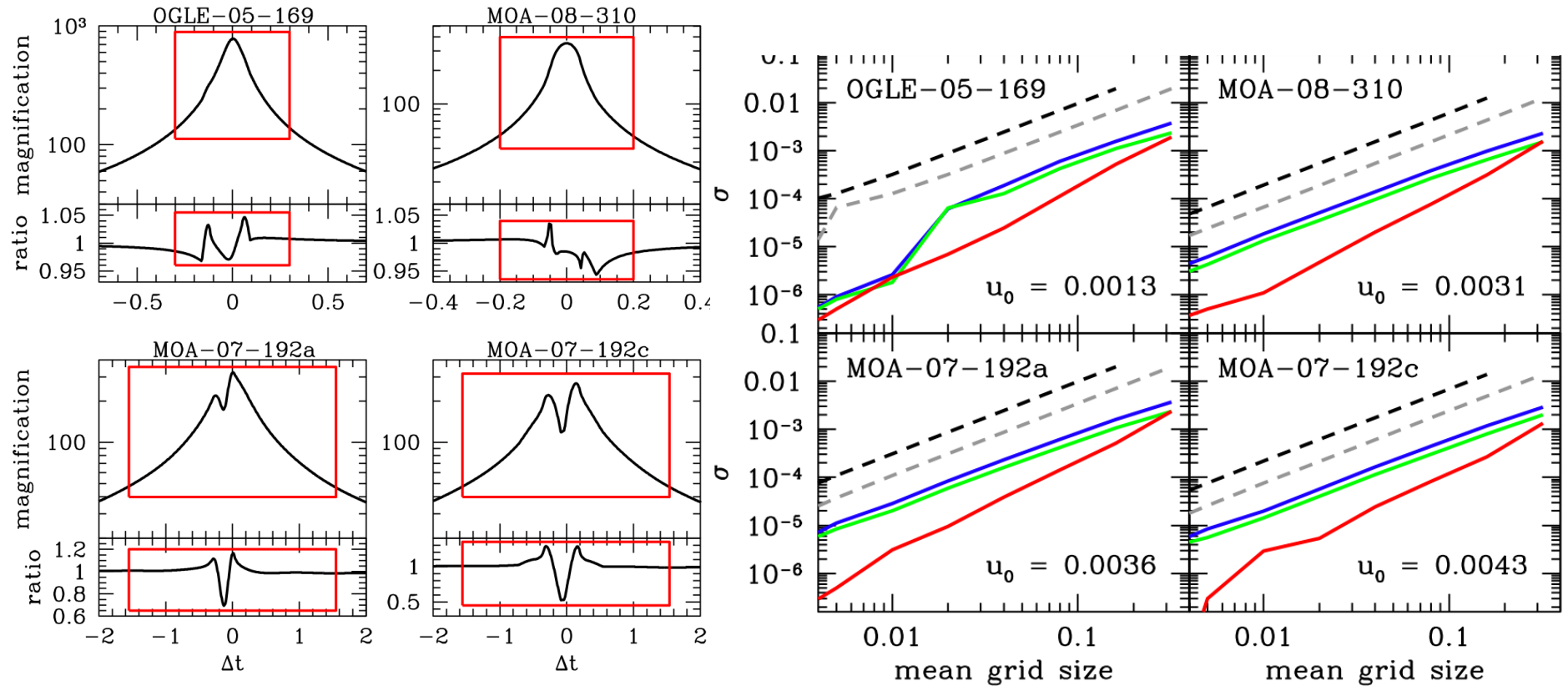


# Lightcurve Calculation Tests



Low-magnification and high-magnification light curve examples.  
**Red boxes** indicate the regions used for light curve precision tests.

# Integration Scheme Tests

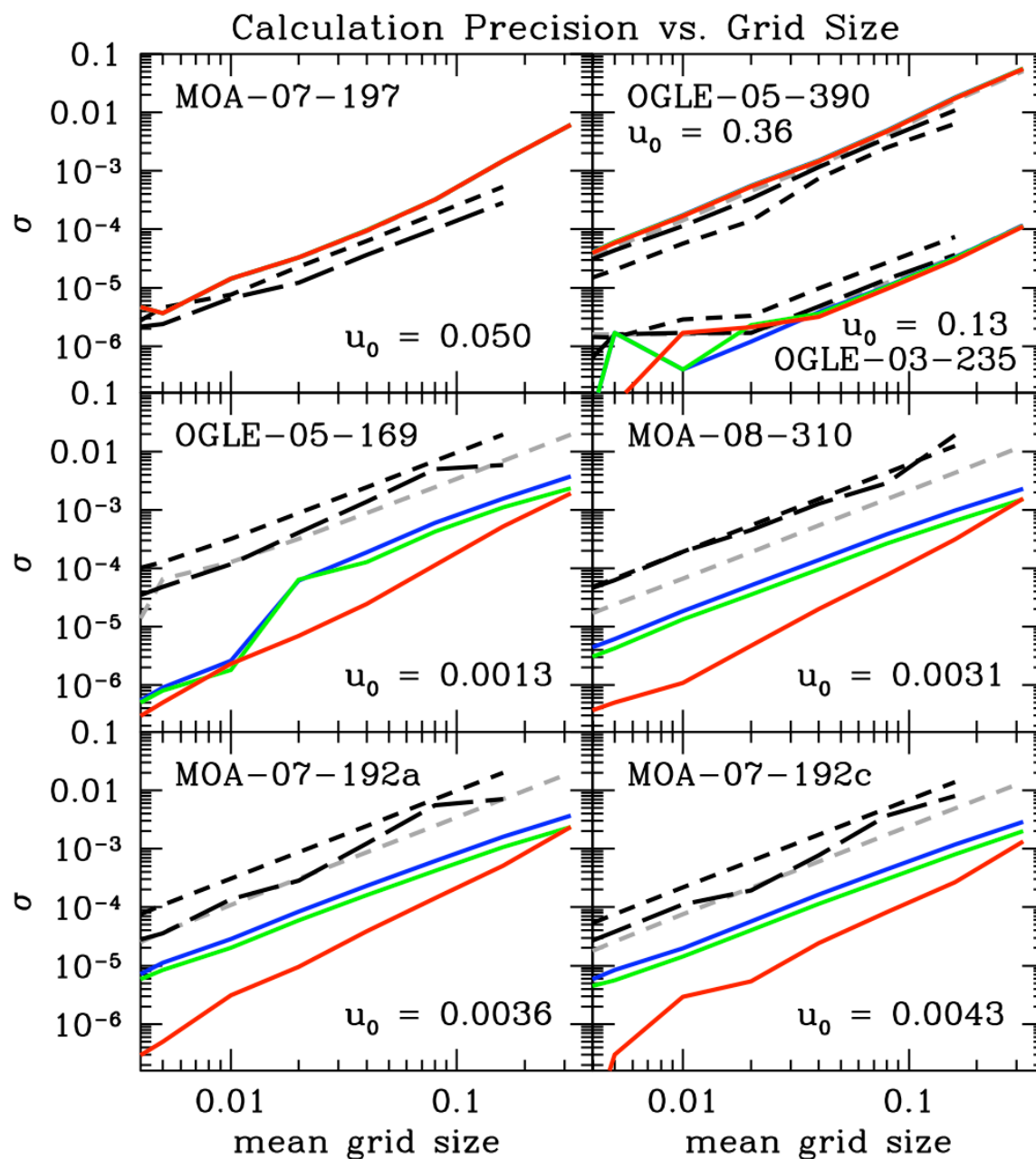


Precision tests based on 4 high mag event models (for 3 events). Right: RMS precision,  $\sigma$ , of the light calculations vs. mean grid size (in  $R_{\text{source}}$  units). Blue, green, red, and grey-dashed curves are for  $\delta_c = 0.017, 0.05, 0.15$ , and 1.00, respectively. Angular grid spacing is  $4\times$  the radial grid spacing (at  $R_E$ ). The black-dashed curve has  $\delta_c = 1.00$ , with angular = radial grid spacing.

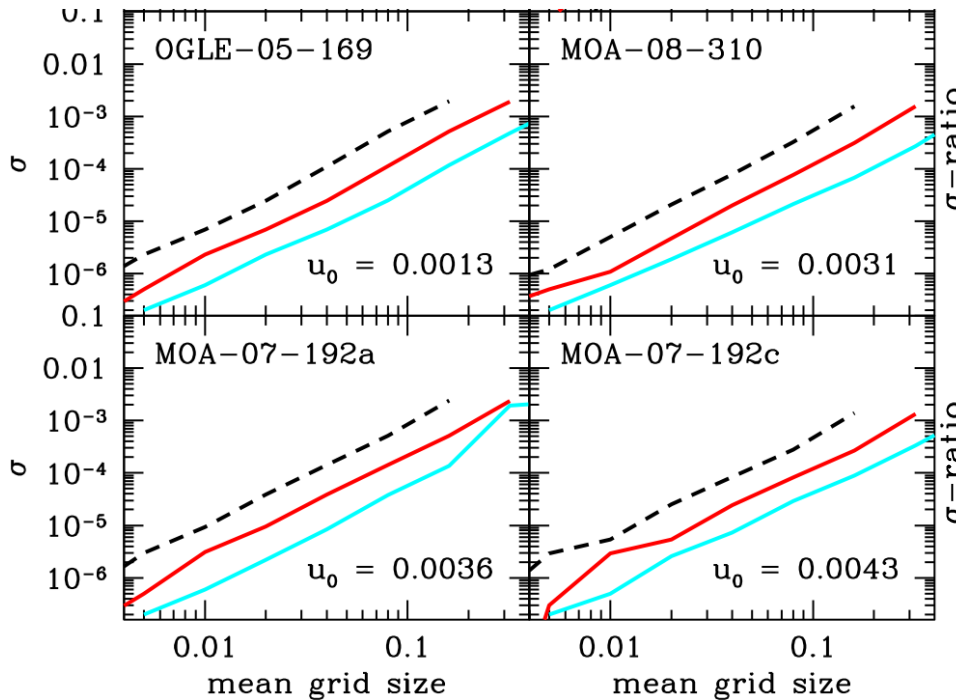
# Precision vs. Grid Size

RMS precision,  $\sigma$ , vs. mean grid size. The blue, green, red, and gray dashed curves are for  $\delta_c = 0.017$ , 0.05, 0.15, and 1.00, respectively. The angular grid spacing is  $4 \times$  times the radial grid spacing (at the Einstein ring radius). The black short-dashed curve is for  $\delta_c = 1.00$ , with equal angular and radial grid spacing. The black long-dashed curve represents a first-order integration scheme with no 2<sup>nd</sup> order corrections.

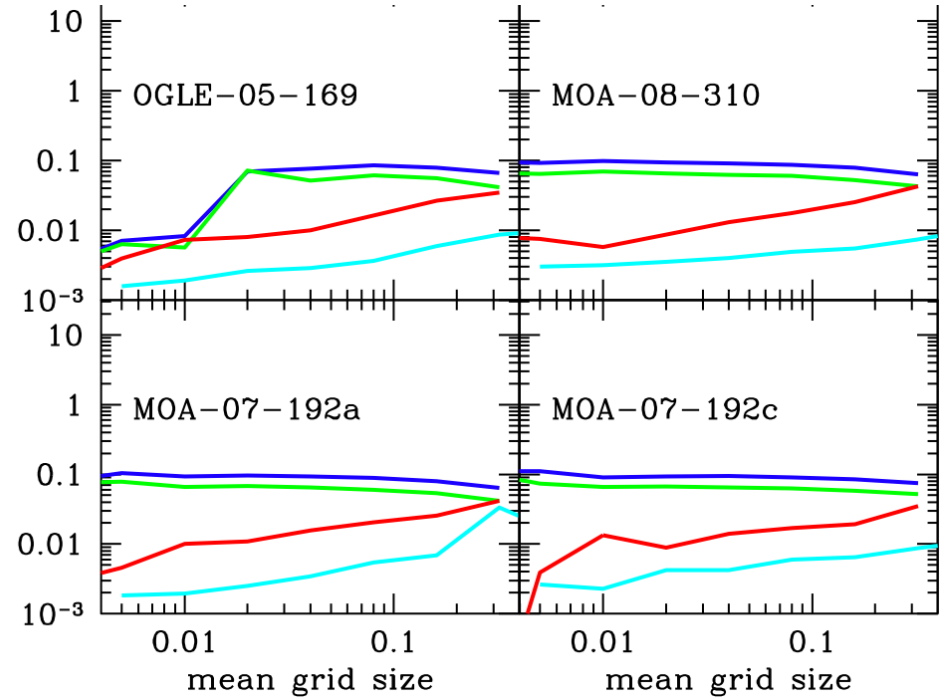
$\delta_c = 0.15$  yields 2<sup>nd</sup> order accuracy for high mag events



# Integration Scheme Tests



RMS precision,  $\sigma$ , as a function of the geometric mean grid size (in  $R_{\text{source}}$  units). The cyan, red, and black-dashed curves have an angular grid spacing of 16, 4, and  $1 \times$  larger than the radial spacing.  $\delta_c = 0.15$  is used in all cases.

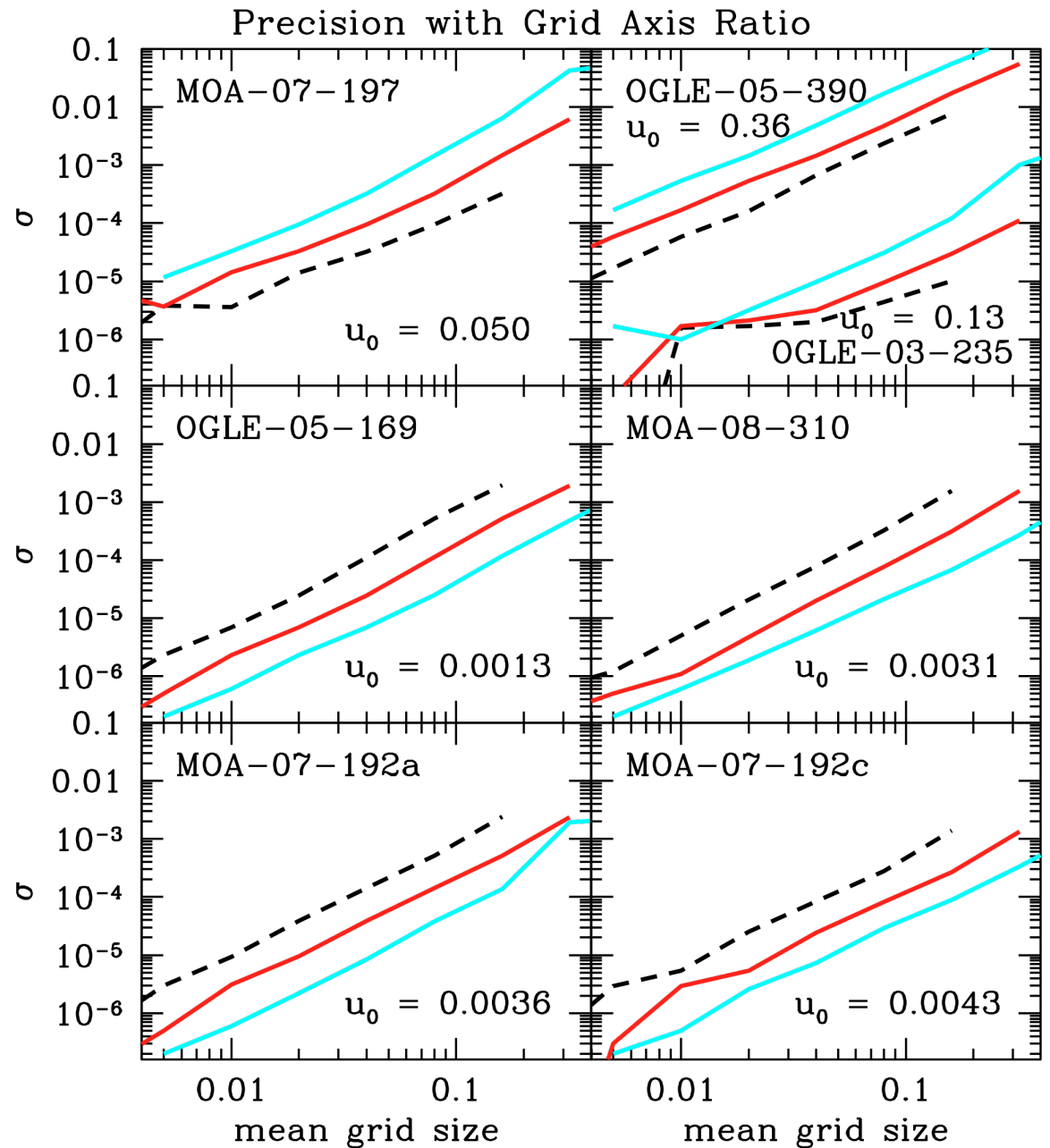


Improvement in the RMS precision,  $\sigma$ , over the “standard 2<sup>nd</sup> order” calculation case (with  $\delta_c = 1.00$  and radial = angular grid spaces) vs. mean grid size. The blue, green, and red curves have  $\delta_c = 0.017, 0.05, 0.15$ , with an angular grid spacing  $4 \times$  the radial spacing. The cyan curve has  $\delta_c = 0.15$  and angular grid spacing  $16 \times$  radial spacing.

# Precision vs. Grid Axis Ratio

RMS precision,  $\sigma$ , as a function of the geometric mean grid size (in source star radius units). The cyan, red, and black dashed curves have an angular grid spacing of 16, 4, and 1 times larger than the radial spacing, respectively.  $\delta_c = 0.15$  is used in all cases.

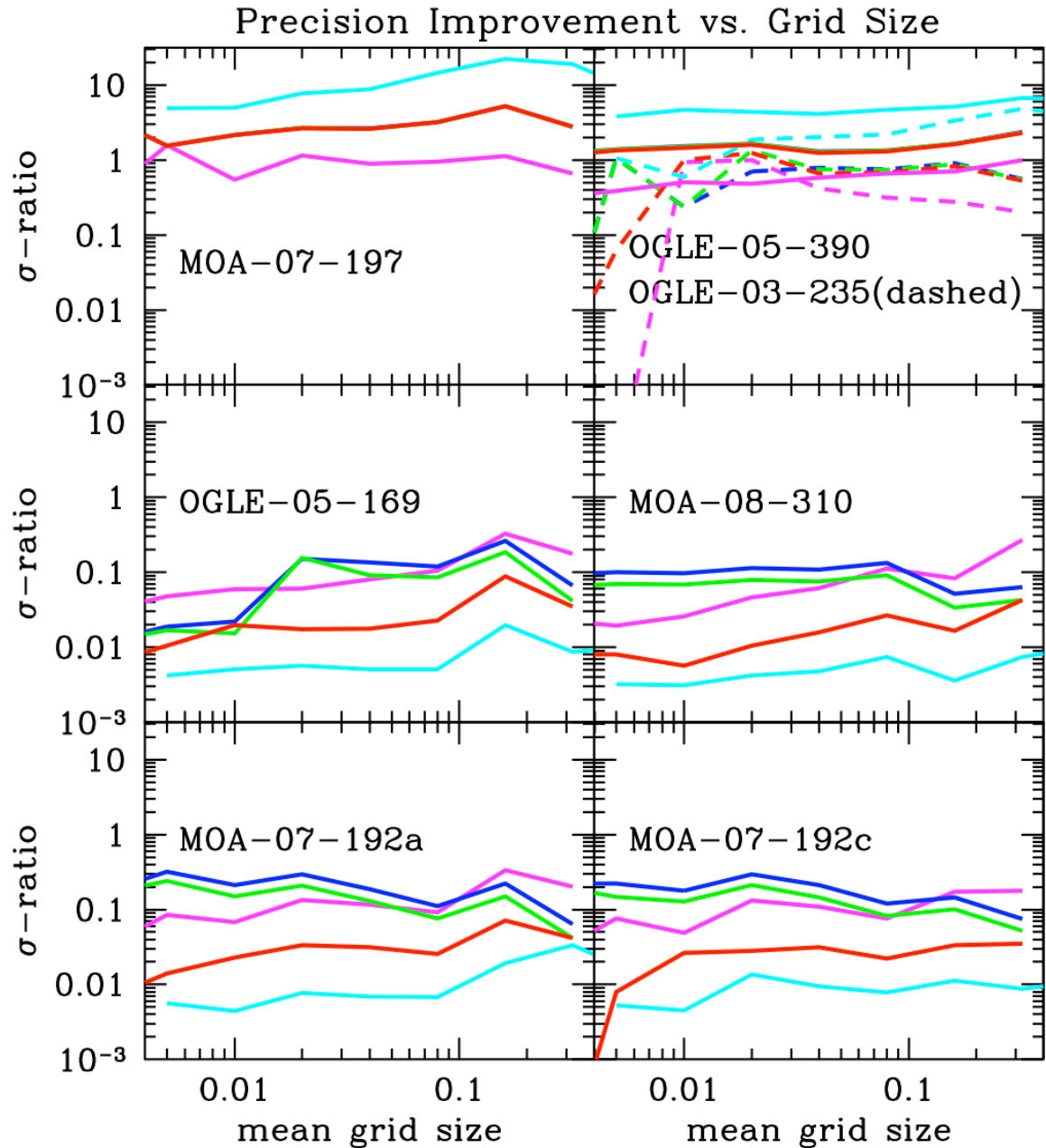
Grid ratio = 16 is better for high mag events, but only ~1.5 order accurate



# Precision Improvement vs. Grid Size

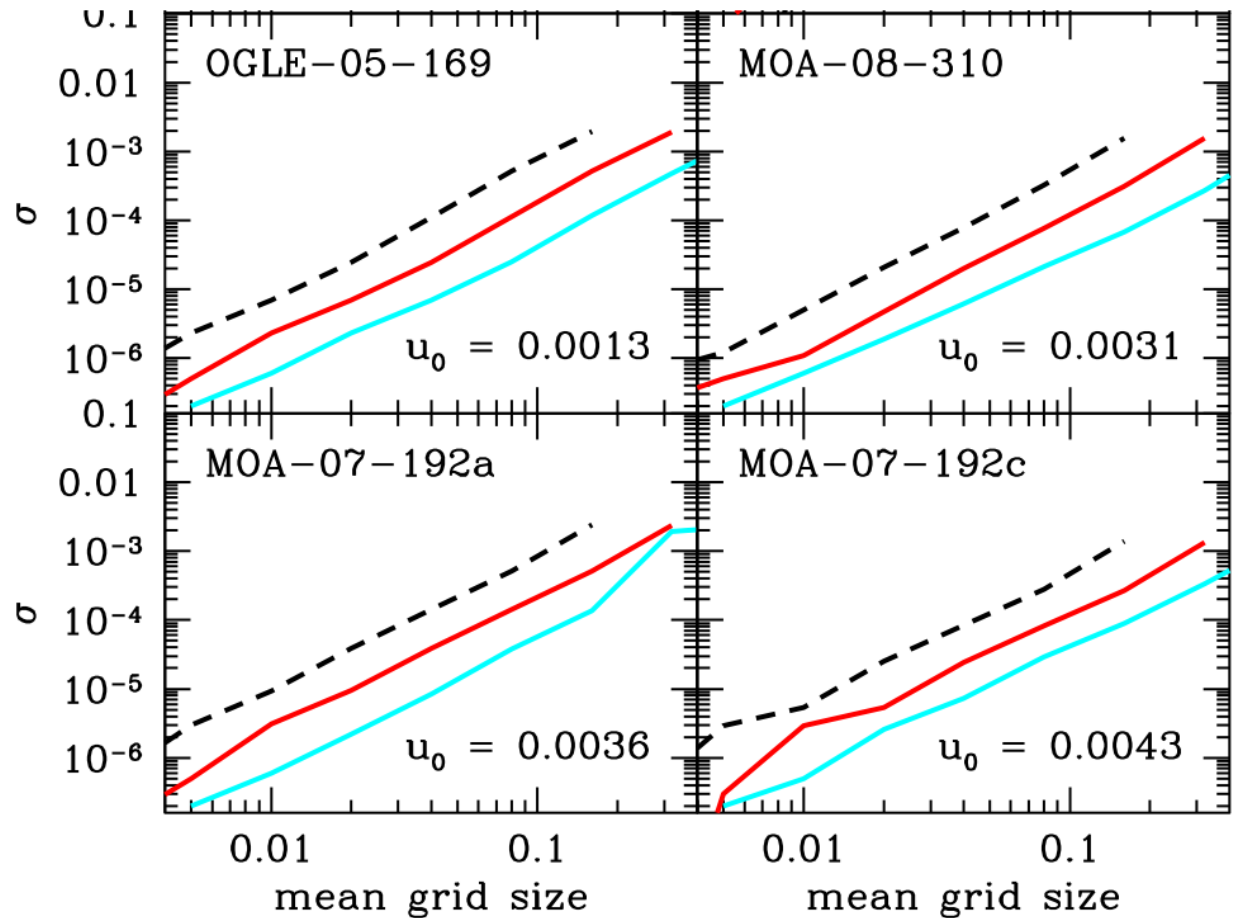
Improvement in RMS precision,  $\sigma$ , over the 1<sup>st</sup> order integration case (with equal spacing for the angular and radial grids) vs. the geometric mean grid size. Blue, green, red, and gray dashed curves are for  $\delta_c = 0.017$ , 0.05, 0.15, and 1.00, respectively, with an angular grid spacing 4 $\times$  larger than the radial spacing. The magenta and cyan curves have  $\delta_c = 0.15$  and angular grid spacings that are 1 $\times$  and 16 $\times$  larger than the radial grid spacing.

**1000 $\times$  speed improvement for high mag events!**



# Precision vs. Grid Axis Ratio

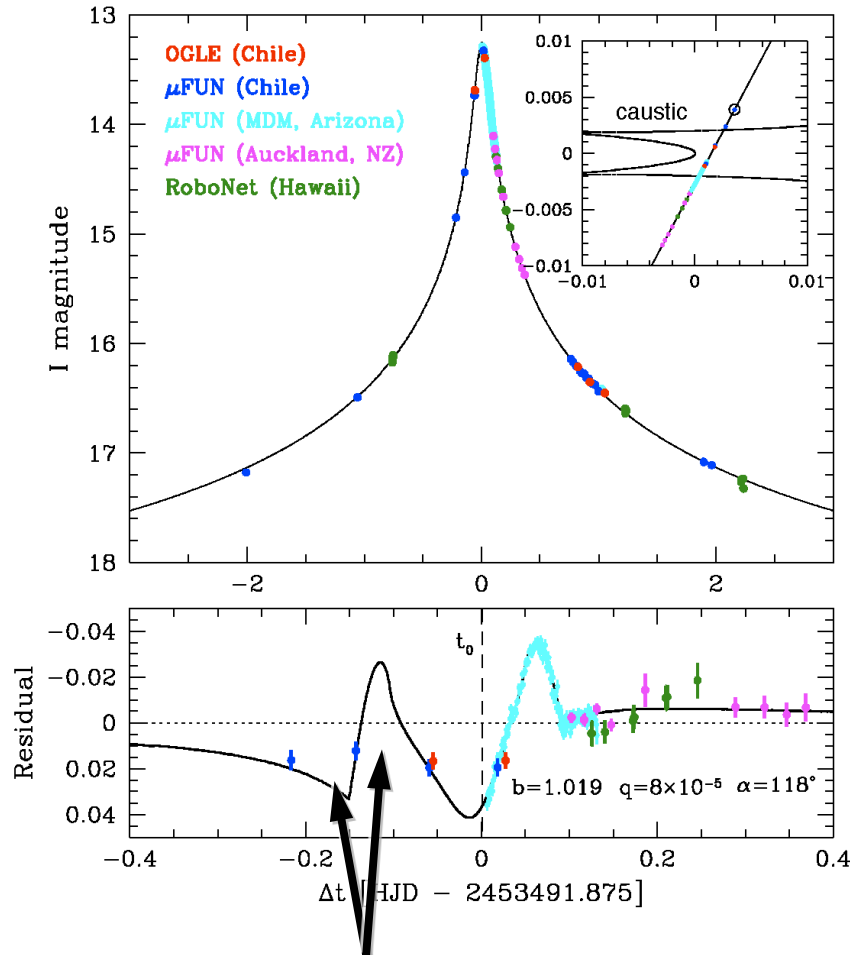
RMS precision,  $\sigma$ , for the 7 example light curves as a function of the geometric mean grid size (in source star radius units). The cyan, red, and black dashed curves have an angular grid spacing of 16, 4, and 1 times larger than the radial spacing, respectively.  $\delta_c = 0.15$  is used in all cases.



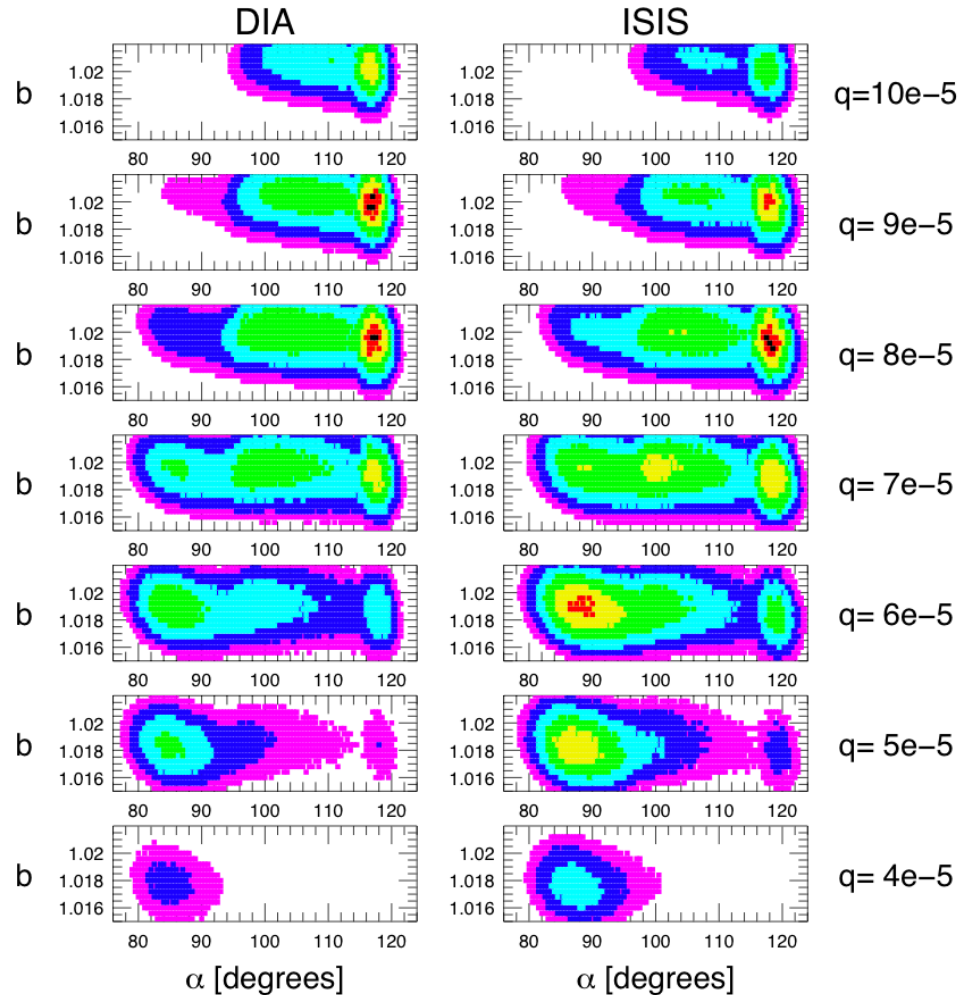
# Grid Search Global Fit Procedure

- For events with incomplete sampling and some high magnification events, the “inspection” method is not convincing
- Grid Search - fix some (typically 2) parameters and allow the others to vary – find  $\chi^2$  minima with some parameters fixed
  - Ray-shooting codes allow efficient calculation of many light curves with fixed mass ratios and separations
  - Primarily of use for high magnification events, where light curve calculation is relatively slow
- If we fix the mass ratio,  $q$ , and separation,  $d$ , then we can use ray-shooting to generate a magnification map, which enables a quick calculation of many  $\chi^2$  values
  - but  $q$  and  $d$  are not the optimum parameters for the grid from a physical point of view
  - there is a curve in  $\chi^2$  space that keeps the size of the central caustic fixed.
  - Physically, a better grid would be  $q$  or  $d$  and  $\theta$ , the angle between the source trajectory and the lens axis
- Method works well for single planet events, but events with more parameters are more tricky

# OGLE-2005-BLG-169Lb Grid Search

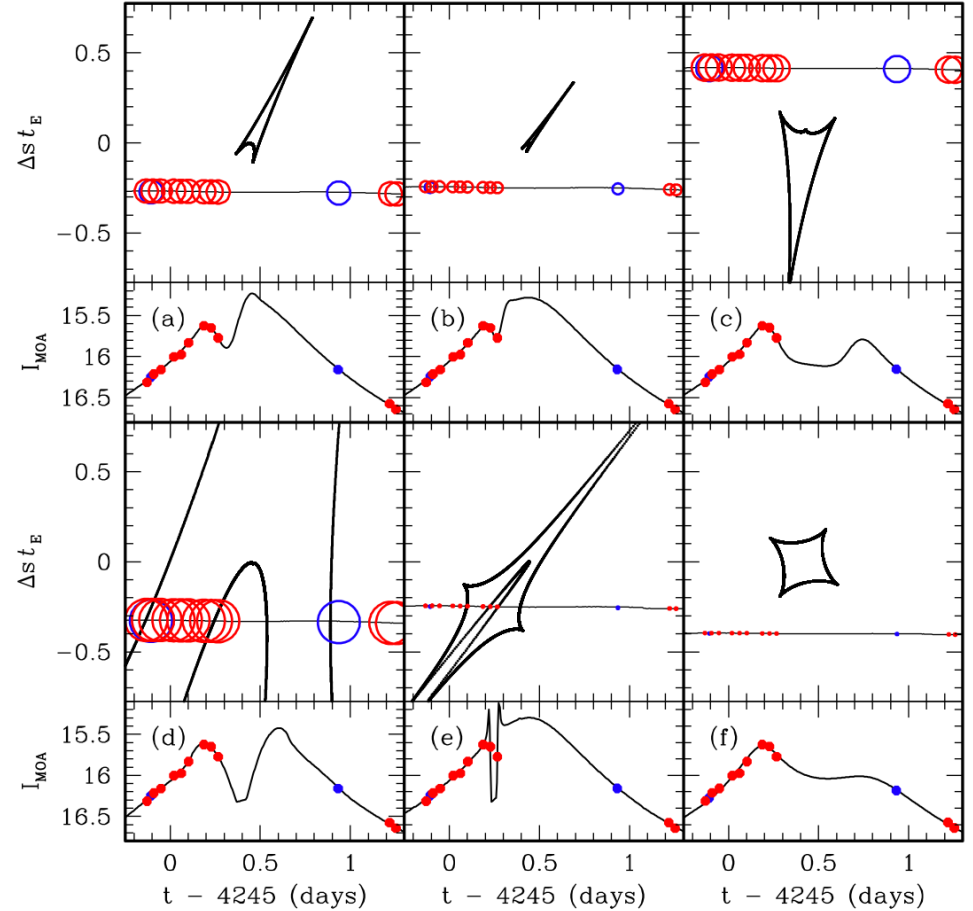
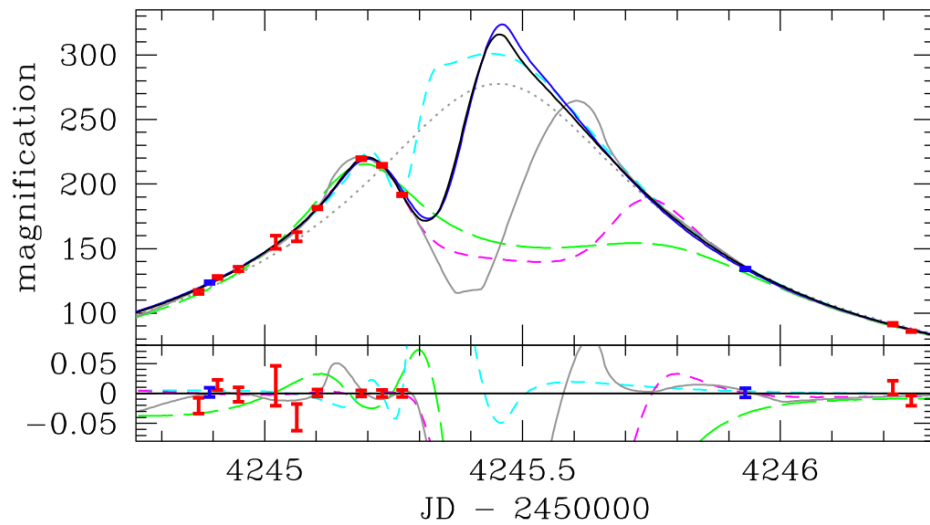
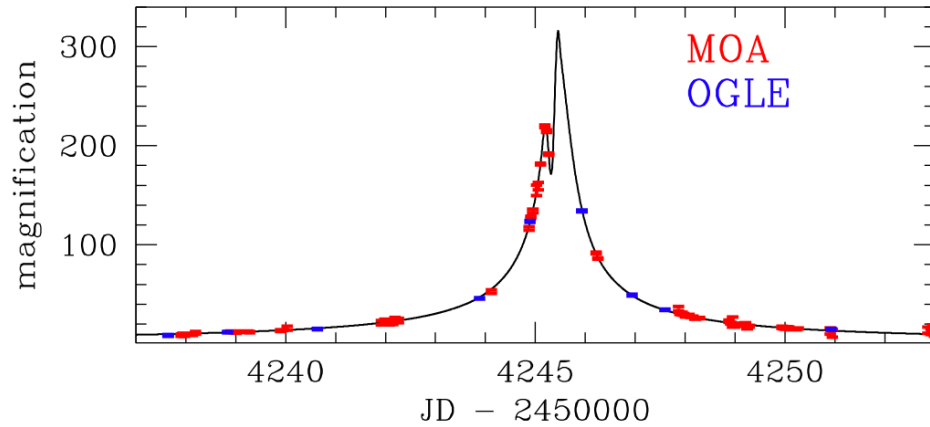


sparse sampling allows us to move light curve bump between data points



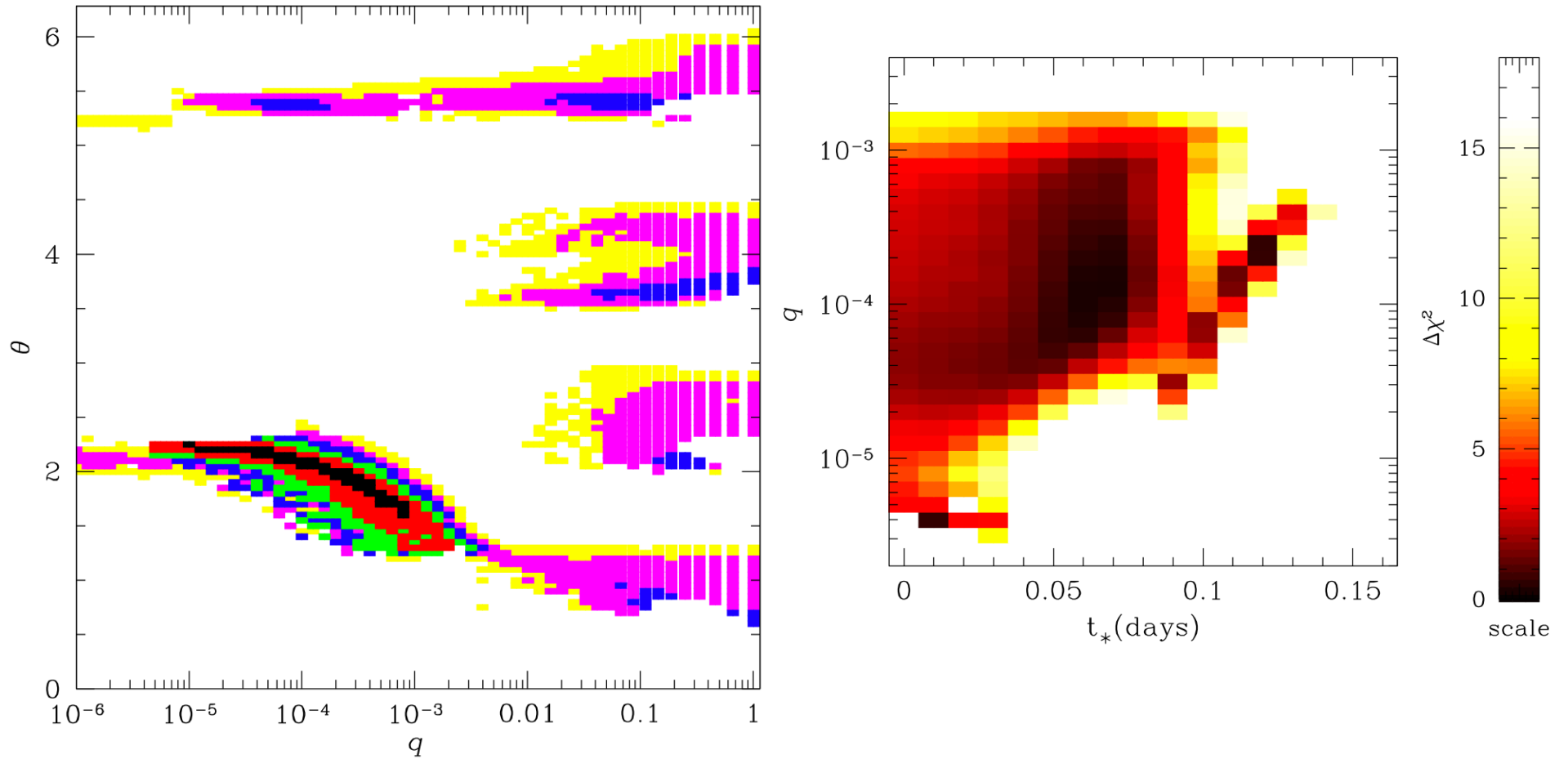
3-d grid:  $d, q, \theta$  covers a small fraction of parameter space, because the caustic crossing is obvious

# MOA-2007-BLG-192 Grid Search



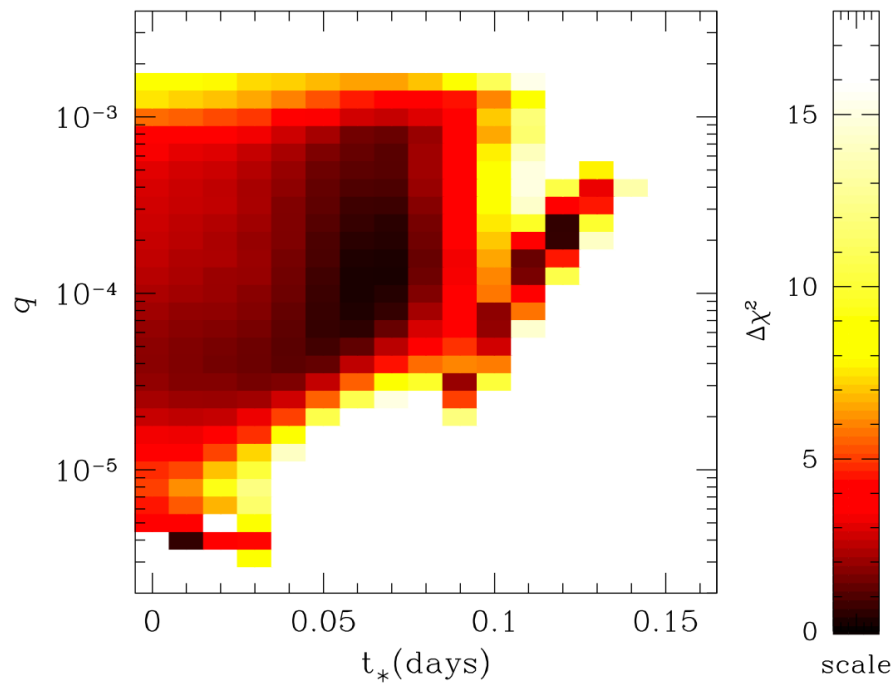
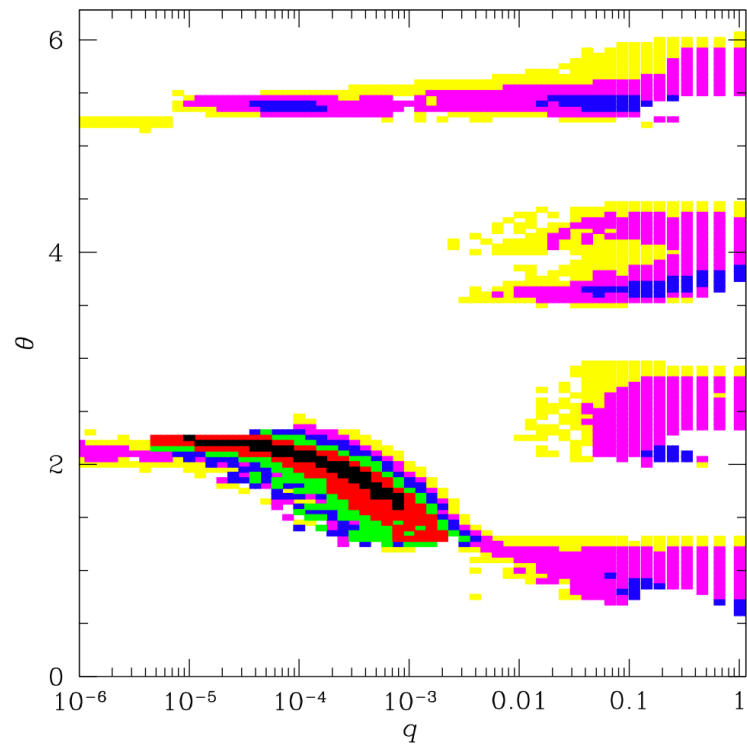
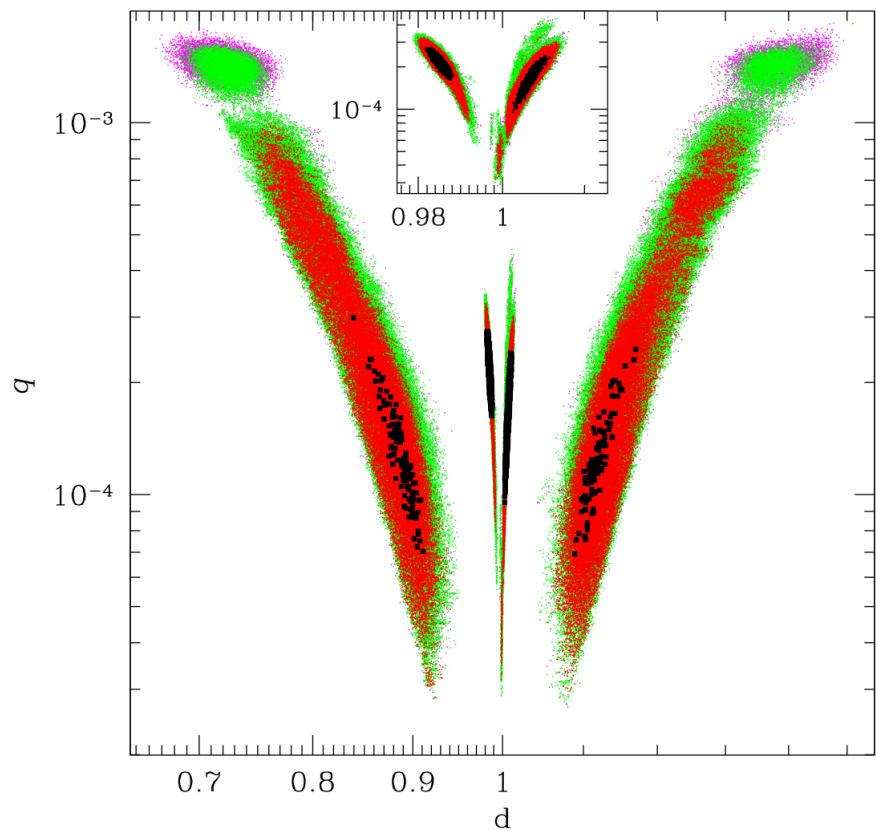
Sparsely sampled light curve allows different solutions

# MOA-2007-BLG-192 Grid Search



A grid in  $d$ ,  $q$ , and  $\theta$  can miss the degenerate solutions in  $t_*$ , the source radius crossing time.

# Grid Search



# Grid Search Complications

- Static planetary events are generally easy to characterize
- Computational efficiency demands that  $d$ ,  $q$  be grid parameters, but a full exploration of a grid in other parameters is often more useful
- Care is required with poorly sampled events
- Additional parameters may be important
  - Microlensing parallax
  - Additional planets or stellar companions
  - Orbital motion
- Full grid search can become impractical for events with more than two masses
  - unless 3<sup>rd</sup> mass is a small perturbation on the 1<sup>st</sup> 2
  - or ...

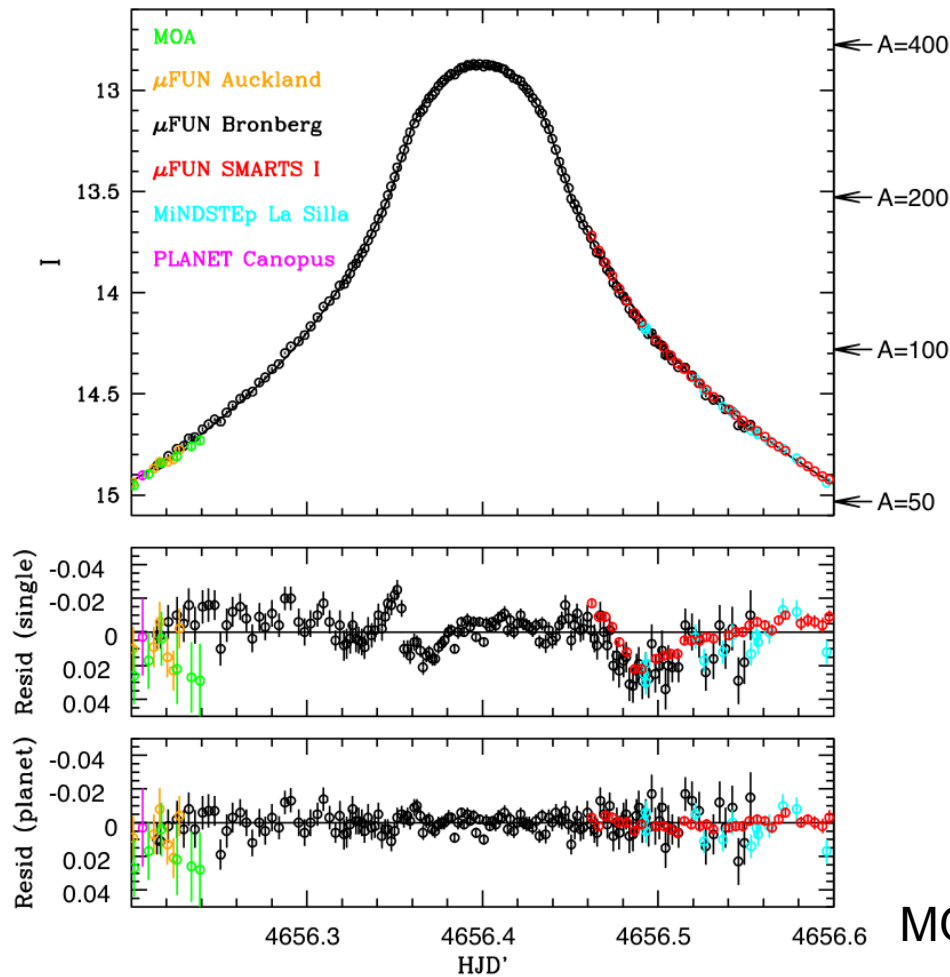
# Initial Condition Grid Search

- Advantage: the grid is a small fraction of the total calculation, so higher dimensional grids can be used
- Fix parameters that can be determined by simpler fits
  - For events with strong caustic crossings, change variables: from  $\{ t_0, t_E \}$  to two caustic crossing times  $\{ t_{cc1}, t_{cc2} \}$
  - Usually: single lens parameters  $\{ t_0, t_E, u_0 \}$  or  $\{ t_{cc1}, t_{cc2}, u_0 \}$
- Calculate  $\chi^2$  for an initial condition grid over the other parameters
- Select the initial conditions with the best  $\chi^2$  values and find the best fit with these initial conditions

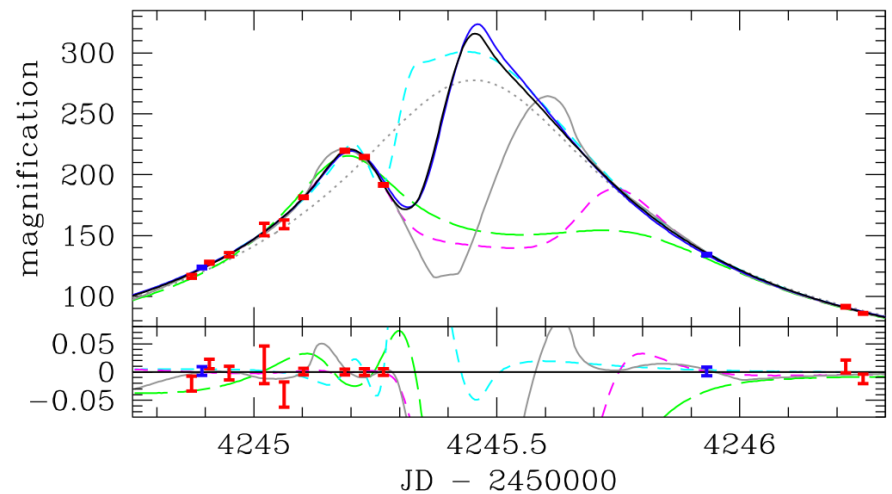
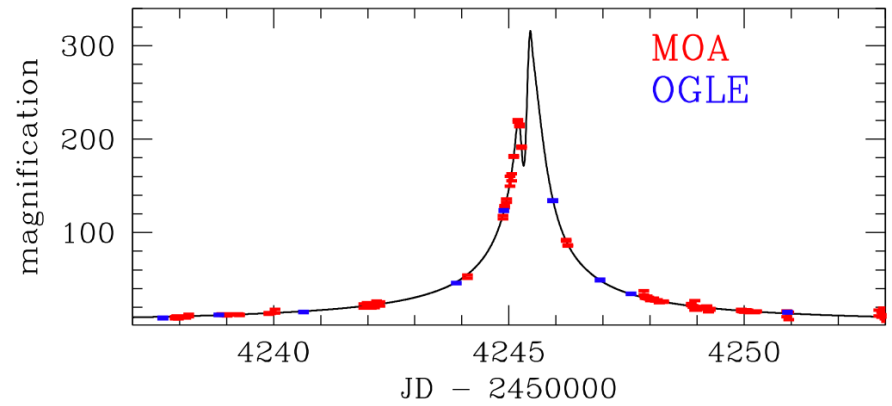
# Initial Condition Grid Search 2

- Do runs with different initial conditions lead to the same solutions?
  - If yes, we are done
  - If no, try one or both of:
    - Select the parameter sets from the grid with the next best  $\chi^2$  values, and minimize  $\chi^2$  from these initial conditions
    - Run a denser grid of initial conditions
- Tested on all published planetary events and most events in progress
  - But the real test is finding solutions when the grid search fails

# Initial Condition Grid Search Examples



MOA-2008-BLG-310: sparse grid on  $d$ ,  $q$ , and  $\theta$ ; solutions in a few cpu hours (18,000 ICs checked)



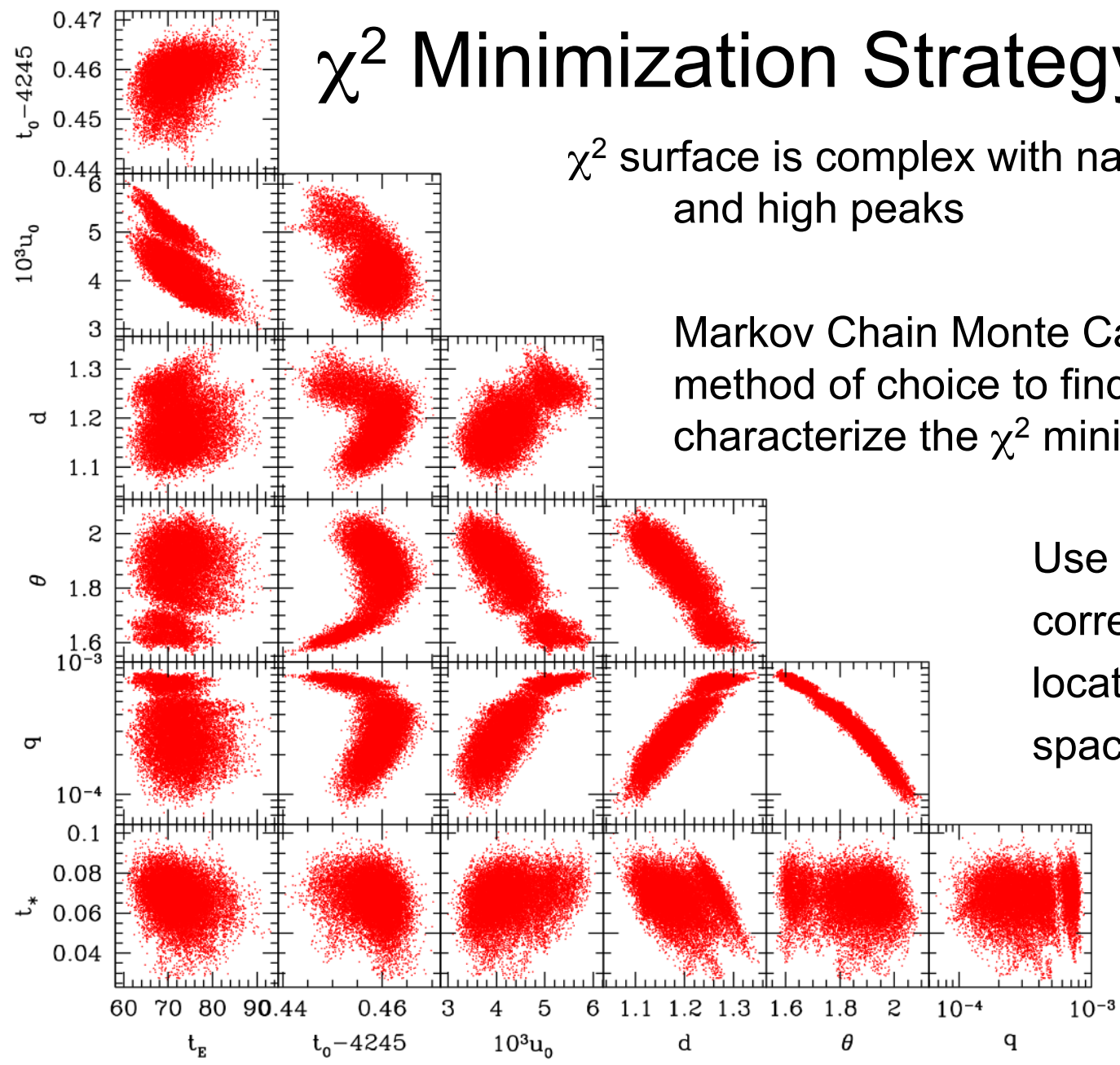
MOA-2007-BLG-192:  $\theta = 0, 356^\circ$  at  $4^\circ$  interval,  
 $q = 10^{-5}, 3 \times 10^{-5}, 10^{-4}, 3 \times 10^{-4}$   
 $d = 0.5, 0.6, 0.7, 0.75, 0.8, 0.85, 0.9, 0.95, 0.96,$   
 $0.97, 0.98, 0.99, 1.00, 1.01, 1.02, 1.03, 1.04$   
 $t_* = 0.013, 0.03, 0.047, 0.064, 0.081, 0.099,$   
 $0.116, 0.133, 0.15$  days (55,000 ICs checked)

# $\chi^2$ Minimization Strategy

$\chi^2$  surface is complex with narrow valleys and high peaks

Markov Chain Monte Carlo is the method of choice to find and characterize the  $\chi^2$  minimum.

Use the parameter correlation matrix to locate parameter space valleys.



# Markov Chain Monte Carlo (MCMC)

- Metropolis algorithm: accept or reject new solution (i.e. a set of model parameters) to add to the chain based on  $\Delta\chi^2 = \chi^2(\text{new}) - \chi^2(\text{old})$ 
  - accept if  $\Delta\chi^2 < 0$
  - accept with Probability =  $\exp(-\Delta\chi^2/2T)$  where the “temperature” is a parameter of the MCMC method
  - use  $T = 1$  to find the general location of the  $\chi^2$  minimum and to determine parameter uncertainties
  - use  $T \ll 1$  to find the best solution
- Jump function selects the new trial solution from the last accepted solution
  - We want to efficiently move through parameter space taking “large” steps, that remain in the  $\Delta\chi^2$  valley, so that a significant fraction of steps are accepted (both during the descent to the  $\chi^2$  minimum and once we’ve converged).
  - Use the parameter correlation matrix
  - Change the parameter correlation matrix frequently when searching for the best solution, but not when calculating error bars.

# Parameter Correlation Matrix

$$C_{ij} = \langle p_i p_j \rangle = \frac{1}{N} \sum_{k=1}^N p_i p_j \text{ for } N \text{ chain links}$$

- Optimize the jump function by diagonalizing  $C_{ij}$  to give the “principle axes” of shape of the local minima at our current position in  $\chi^2$  space. parameter set.
- Select new parameters with a Gaussian variance given by the  $C_{ij}$  values from the old parameter values.
- Convert back to old parameter basis with  $(C_{ij})^{-1}$  to give the new parameters in the original basis to calculate  $\chi^2$ .
- While descending toward the minimum in  $\chi^2$  space, remember only a relatively small number of chain links in order to calculate  $C_{ij}$ 
  - Possibly forget  $C_{ij}$  and start over if we become stuck for many steps with no  $\chi^2$  improvement.
- When the chain has converged to the vicinity of the  $\chi^2$  minimum, remember a larger number of chain links to estimate  $C_{ij}$ , but do not continue to update  $C_{ij}$  after the initial part of the chain.

# $\chi^2$ Minimization Recipe

## Metropolis Algorithm w/ adaptive correlation matrix

- Initial Jump function: specify uncertainty ranges for each parameter, and select new parameters with uniform probability within these ranges
- Once we have  $N_{\text{save}} \geq 20$  (or  $2N_{\text{par}}$ ) accepted Metropolis steps, calculate and diagonalize  $C_{ij}$  and use it for the Jump function
  - Select new parameters in a Gaussian distribution along the principle axes in parameter space, and use  $(C_{ij})^{-1}$  to convert back to the normal parameters.
- Recalculate  $C_{ij}$  whenever  $N_{\text{save}} \geq$  increases by 4.
- When  $N_{\text{save}}$  reaches 100, drop the oldest parameter set from list to be used to calculate  $C_{ij}$ . Continue to update  $C_{ij}$  every 4 accepted steps.
- If we do 40 consecutive  $\chi^2$  calculations without accepting one, then forget the oldest 37.5% of parameter sets so that  $N_{\text{save}} \rightarrow 0.625 N_{\text{save}}$  and recalculate  $C_{ij}$ .
  - If  $N_{\text{save}} < 20$  (or  $2N_{\text{par}}$ ), then use the initial procedure for the jump function
- When we have done 2000-3000 consecutive  $\chi^2$  calculations without improving the best value, stop. Take  $T \rightarrow T/10$ , and repeat procedure.

# Initial Condition Grid with $\chi^2$ Minimization Recipe

- Successfully tested on all published and some unpublished planetary microlensing events
- Test on OGLE-2008-BLG-270 predicted an early caustic crossing that was subsequently discovered in the OGLE data.
- Soon to be run on 2+ planet events without an acceptable light curve model.



# Homework Problem

$$w = z - \sum_{i=1}^n \frac{\varepsilon_i}{\bar{z}_i - \bar{x}_i}$$

- Solve the lens equation for the  $n = 4$  case
- Hint: don't do the algebra by hand - use a symbolic algebra program like Mathematica or Maple instead
  - Get the result in machine readable form
- Publish the result
- Likely co-authorship on the first microlensing 3-planet event!
  
- Extra-credit: get the  $n = 5$  solution